University of Stavanger

Faculty of Science and Technology

MASTER'S THESIS

Study program/ Specialization: Petroleum Technology/Drilling	Spring semester, 2018 Restricted access
Writer: Goran Jafr	………………………………………… (Writer's signature)
Faculty supervisor: Mesfin Belayneh Agonafin External supervisor(s): Ola M. Vestavik	
Thesis title: Study of the mixing zone between two drilling fluids with large density difference, when using the Heavy Over Light (HOL) solution for terrestrial drilling	
Credits (ECTS): 30	
Key words: Reelwell Drilling Method (RDM) Dual Drill String (DDS) Extended Reach drilling (ERD) Equivalent Circulating Density (ECD) Heavy Over Light (HOL) Solution Density Diffeence $\Delta\rho(\rho_{heavy} - \rho_{light})$ Rheological Characteristics Mixing zone at the interface	Pages: …111……………… + enclosure: …35……… Stavanger, 14th of July 2018

Abstract

This study is based on the use of an innovative drilling technology, called Reelwell Drilling Method (RDM), recently developed and tested to solve various issues related to conventional drilling methods. These include extended reach horizontal drilling (ERD) limitations, control of downhole pressure, hole cleaning and overcoming challenges related to equivalent circulation density (ECD). The RDM can be used to utilize a unique fluid configuration called heavy over light (HOL) solution. The HOL solution allows a heavy fluid in well annulus to control well pressure, while an active light fluid circulates through a dual channel drill string and transports cutting up to the surface. Such combination provides increasing buoyancy of the drillstring and hence reducing torque and drag, which in turn leads to overcoming ERD-limitations. Other advantages are increasing weight on bit (WOB), better hole cleaning in horizontal section, and managing downhole pressure and ECD issues.

A challenge with the RDM-technology is the control of the mixing zone between the fluids in the HOL-configuration. During this thesis, a series of experiments were performed using water-based muds with different densities and rheological properties. The purpose of the experiments was to study the effect of these properties as well as the impact of the rotation speed (*rpm*) of the drillstring on the mixing zone between the fluids. A simple small-scale experimental rig was built, where an aluminum rod, representing the drill string, was rotated in an acrylic cylinder, representing the wellbore. The light fluid was placed in the lower part of the acrylic cylinder with the heavy fluid on the top. Two different color indicators, green for the light and red for the heavy fluid, were used. Photos of the mixing zone were taken at an interval of 30 sec. The height of the mixing zone was determined by analyzing the photos visually, and by an image analysis tools in MATLAB.

The results from the experiments indicated that rotation of the rod was important to avoid channeling effects. However, high *rpm* did not have a significant effect on the further development of the mixing zone. The rheological properties such as yield point and gel strength were found to be determining factors of controlling the stability of the mixing zone.

The results have shown that the HOL-arrangement with a density difference of about 0.70 sg between the fluids was controllable. Further investigations with larger well dimensions are still needed to be representative for field use of the results.

Acknowledgments

I would like to send my great thanks and acknowledge to the following persons for their contribution to this master thesis.

- My supervisor, Dr. Mesfin Belayneh Agonafir at the University of Stavanger, for his support and academic guidance.
- My external supervisor, Mr. Ola M. Vestavik at Reelwell AS, who stands behind this brilliant and promising drilling technology, for the opportunity to attend the project and for his useful and excellent feedbacks.
- Professor Time Rune, at UIS for attending our regular meetings and his valuable feedbacks.
- The company, Schlumberger for providing drilling fluid components.

Last but not least, I would like to send my gratitude and appreciation to the University of Stavanger for allowing me to use the labs, providing with drilling fluid materials and for offering an excellent study atmosphere during the past five years.

Table of Content

List of Abbreviations

BHA	Bottom Hole Assembly
BHP	Bottom Hole Pressure
CMC	Carboxymethylcellulose
CSG	Casing
CTP	Cutting Transport Performance
DFV	Dual Float Valve
DDS	Dual Drill String
DDM	Directional Drilling Method
DP	Drill Pipe
ECD	Equivalent Circulating Density
ERD	Extended Reach Drilling
FCU	Flow Control Unit
HOL	Heavy Over Light
HSE	Health, Safety and Environment
ID	Inner Diameter
IPV	Inner Pipe Valve
LSYS	Low Shear Yield Stress
MPD	Managed Pressure Drilling
NTP	Non-Productive Time
OBD	Overbalanced Drilling
OBM	Oil Based Mud
OD	Outer Diameter
PAC	Poly Anionic Cellulose
POOH	Pull Out Of Hole
PV	Plastic Viscosity
RCD	Rotary Control Device
RDM	Reelwell Drilling Method
RT-instability	Rayleigh-Taylot Instability
ROP	Rate Of Penetration
RPM	Rotation Per Minute
sg	Specific Gravity
TDA	Top Drive Adapter
UBD	Underbalanced Drilling
WBM	Water Based Mud
WOB	Weight On Bit
XC-polymer	Xanthan Campestris Polymer
XG-polymer	Xanthan Gum Polymer
YP	Yield Point

1. Introduction

An innovation drilling technology, called Reelwell Drilling Method (RDM) has been developed and tested in the purpose of solving problems related to drilling operations when using conventional drilling that has been used since the start of the development of petroleum industry. These issues include proper hole cleaning, management of the downhole pressure, equivalent circulation density (ECD), and increased friction-induced torque and drag, which in turn limit extended reach drilling (ERD) engineering.

Reelwell AS developed the idea in 2004, where a unique flow configuration called heavy over light (HOL) solution is used in a dual conduit drill string (DDS). This solution allows using two drilling fluids with different densities in the hole at the same time when performing the drilling operation. The heavy fluid in the well annulus controls the well pressure and provides buoyancy, while the light fluid circulates inside the DDS and transport cuttings up to the surface [1].

The known problem related to HOL-solution is the development of a mixing zone between the heavy and the fluids. Therefore, this Master thesis deals with performing a series of experiments to discover the critical factors of controlling the stability at the interface between the fluids and predicting the growth of the mixing zone.

1.1   Background

Cost reduction and enhance efficiency and safety are of great needs for oil & gas industry to ensure their continuity and long-term growth, which can be possible by focusing on the development of smart technologies to solve issues related to conventional drilling methods. These issues include drilling through unconsolidated and fractured formations and formations with narrow drilling operation window, high-pressure zones, and depleted reservoirs. The mentioned problems may, in turn, result in consequences such as fracturing the formation, lost circulation, gas kick, formation collapse, poor hole cleaning and well instability. Crossing the ERD-boundaries is another challenge for the oil & gas industry to overcome [2]. Despite all these challenges and risks mentioned above, conventional drilling method or overbalanced drilling (OBD) has been used since the start of the development of petroleum industry. The reasons to still use this type of drilling method are its low technology demands and low operation cost. Overbalanced drilling is best suited for non-fractured formations with a wide margin between fracture and formation pressure. Using OBD for drilling the formations with narrow drilling operation window leads to lost circulation or differential sticking of the drill pipe [3].

Selection of a correct mud weight when applying OBD-method is the determining factor to reduce occurring the mentioned problems. Too low mud weight can cause some severe issues including fluid formation inflow, due to underbalanced condition, wellbore collapse, fill and thereby mechanical sticking. Too high mud weight leads to fracturing the formation, which in turn results in lost circulation. Another problem related to too high mud weight is differential sticking, which is the most observed source of nonproduction time (NPT) in the drilling operation and often leads to sidetracking the borehole [4]. Therefore it is essential to select a mud with a density that gives a borehole pressure higher than pore pressure (*lower boundary*) and less than fracturing pressure (*upper boundary*). This concept is called "midline principle" that is illustrated in figure 1-1. According to this principle, the mud weight should be selected close to the in-situ stress field in a surrounding rock in the formation. Designing the mud weight according to the midline principle will minimize the risk of differential sticking and lost circulation[5].
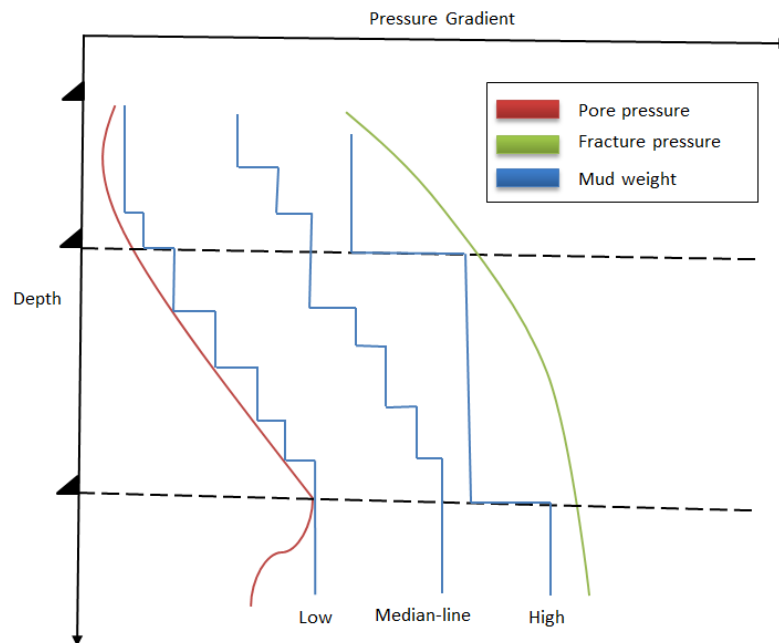
Figure 1-1: Median line principle. [3]

1.2   Equivalent Circulating Density (ECD)

Deploying conventional drilling/overbalanced drilling (*figure 1-2, green*), the bottom hole pressure (BHP), under static condition, is equivalent to the hydrostatic pressure created by the mud weight. However, in the dynamic condition, the circulating drilling fluid against the formation will cause pressure-drop in the annulus due to friction, which in turn causes an increased BHP. The total pressure exerted by the hydrostatic fluid column and friction pressure loss in the annulus is now

called Equivalent Circulating Density (ECD). Equivalent downhole pressure under dynamic conditions can then be expressed as follow:

$$BHP_{dynamic} = \rho_m gh + \Delta P_{friction} \qquad (1.1)$$

Where:

ρ_m = the density of the mud

g = Gravitational constant (9.81 m/s^2)

h = True vertical depth of the well (TVD, *measured in ft or m*)

$\Delta P_{friction}$ = Pressure loss due to friction

Circulation stoppages are a natural part of all drilling processes, for instance during connection of new drill pipes. Then the hydrodynamic pressure will disappear, and only hydrostatic pressure remains to keep the well under control.

$$BHP_{static} = \rho_m gh \qquad (1.2)$$

Change in bottom hole pressure is a common problem when drilling a wellbore with conventional drilling, which often leads to wellbore instability. ECD is a more severe challenge when drilling through a narrow operational envelope, because it will easily exceed the formation fracture pressure, and thus fracturing the formation. The two significant fracturing consequences of formation are unintentional formation breakdown and lost circulation. Since the fluid in the wellbore is open to atmospheric pressure, it is not possible to overcome these issues using conventional drilling method. Another problem is predicting ECD-fluctuation, which is not possible with traditional simulation tools [6]. To mitigate or solve such drilling hazards, deploying managed pressure drilling (MPD) or underbalanced drilling (UBD) has been an alternative[6].

1.3 Managed Pressure Drilling

Managed pressure drilling is an adaptive drilling method developed to control the annular pressure profile in the wellbore and hence overcoming ECD-related problems. The technology is based on compensating the friction pressure loss by adding backpressure from the surface. During static condition, e.g., when connecting a new pipe, the backpressure is increased to compensate for the friction pressure loss, which is now zero. During a drilling operation, the surface pressure is adjusted in such way that the downhole pressure stays within the desired interval (figure 1-2, yellow), which is equivalent or higher than formation pressure. Thus, the bottom hole pressure is

maintained relatively constant to prevent formation inflow into the wellbore. Using MPD technology, the BHP can, therefore, be expressed as follow:

$$BHP = \rho_m gh + \Delta P_{friction} + P_{back} \tag{1.3}$$

Thus, applying MPD technology for drilling operation results in limiting kick occurrence and decreasing the risk of occurrence of the lost circulation and differential pressure sticking. Another advantage with MPD is reducing the number of required casing strings since it may allow drilling for more extended open-hole sections.
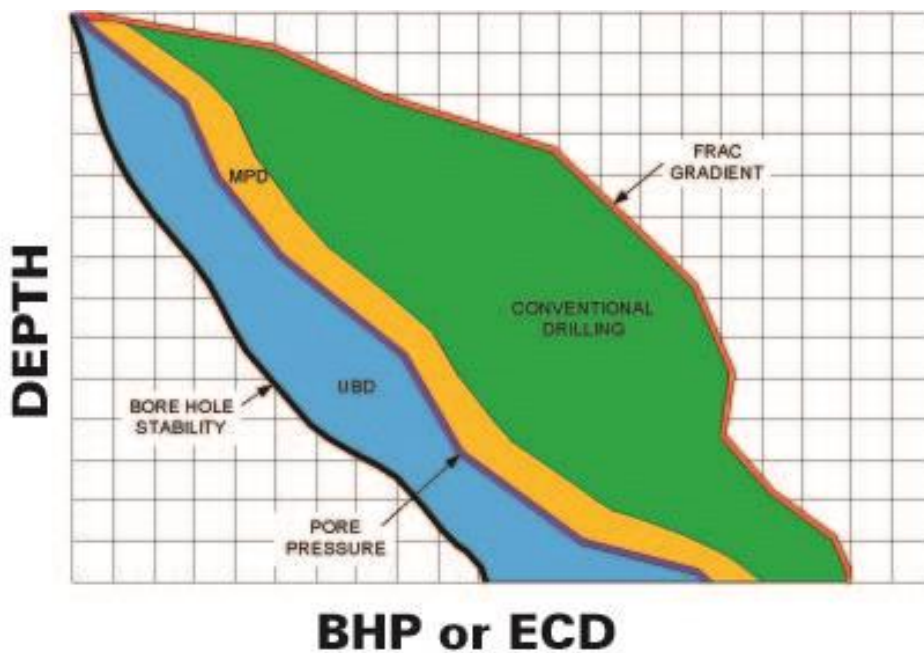
Figure 1-2: A pore pressure graph of UBD, MPD and (OBD). [7]

Another advantage with MPD is reducing the number of required casing strings since it may allow drilling for more extended open-hole sections. However, MPD, like other drilling techniques, has disadvantages such as high operational cost, complexity, need for well-trained expertise and it doesn't have a well-established standard [2, 8].

1.4 Underbalanced Drilling

Underbalanced drilling is a procedure where the drilling operation is performed with a wellbore pressure lower than formation/ pore pressure (figure 1-2, blue). A lower wellbore pressure can be reached by either using a low-density drilling mud or by injecting gas (usually Nitrogen) into the drilling mud. The injected gas reduces the hydrostatic pressure, and hence ECD in the wellbore. Drilling a well with UBD-method, the formation fluids usually flow into the wellbore. It is opposite

4

to conventional drilling where the downhole pressure is kept above the formation pressure to prevent fluid formation inflow. During the second mentioned method, the inflow of formation fluids is considered as kick, which may lead to a blowout if the well is not shut-in at the right time. However, during the UBD-method using a rotating head at the surface can control the inflow of the formation fluid. This device is essential to seal and divert the produced fluid to a separator while allowing the drilling string to continue drilling.

The advantages of UBD over conventional drilling include elimination formation damage, increasing rate of penetration (ROP), reduction of the lost circulation and elimination of differential sticking [9, 10].

When drilling with UBD-method, there are also some disadvantages including:

- High operation cost, because this method requires directional drilling tools.
- Safety issues; technically the well is all the time in a blowout condition.
- MWD tools cannot work since these tools require an incompressible fluid to work. [10]

1.5 Directional drilling Method

Directional drilling Method (DDM) is a technique used for controlling the direction and deviation of a wellpath to a predetermined target. This method has been applied to oil & gas industry since the late 1920s. Directional drilling allows drilling wells at multiple angles, which makes it possible to reach longer extend, and hence increasing the production from the oil & gas reserves. Other important applications of DDM include drilling multilateral wells from the same vertical wellbore, sidetracking, fault drilling, salt-dome exploration, and relief-well drilling. Thus, utilizing DDM minimizes the operational cost, decreases the environmental impact and increases efficiency.

Directional drilling method has been vastly improved due to the development of drilling sensors and global positioning technology. Another important technique that improved DDM is real-time technology, which can control the angle of a drill bit.

The essential tools utilizing in achieving directional drilling includes bottom hole assembly (BHA) configuration, whipstocks, mud motors, 3D-measuring device and specialized drill bits [9].

1.6 Extended Reach Drilling

Extended Reach Drilling (ERD) is basically directional drilling of very long horizontal wells. The main purpose of these technologies is covering a larger drainage area through a reservoir from a single well, which means to maximize productivity and producing the reservoir from a remote location to avoid risks. Of these reasons, differences types of ERD-technologies have been used for more than 50 years. Drilling a long horizontal well from one surface drilling location results in reducing the number of rigs, which in turn leads to drastically reduction of the drilling operation as

well as completion and production costs. Additionally, ERD-technology reduces other offshore structures, pipelines, and other infrastructure facilities, which means reducing environmental impact due to smaller drilling and production footprint [5].

A prospect can be defined as an extended reach well when the inclination of the wellbore is larger than 60^0-70^0 from the vertical and has a horizontal displacement of about 10,000 ft. With the help of a single-bend or a surface steerable motor such wells can be drilled. The technology has evolved from such simple directional drilling to horizontal, lateral and multilateral step-outs through employing both directional and horizontal drilling techniques. These techniques include geosteering, ability to apply weight on bit, efficient hole cleaning, running casing successfully to the bottom of the well and reducing torsional force [11]. Geosteering is the combination of DDM with the geological model of the subsurface. It involves gathering petrophysical data at or near the bit and transmitting the information in real time to the surface. The drilling team will then use the collected data in order to direct the drill bit to the targeted location through the pay zone [12]. Applying Geosteering incorporated with DDM, the world´s longest horizontal well was drilled in Sakhalin in Russian and was completed in 2011. The well has a measured depth (MD) of 41667 ft (12683 m and its horizontal departure is of 38514 ft (11739m) [13]. Tens of other wells with notable extended reach achievements, with the horizontal offsets from 30,000 ft. to 40,000 ft., have been drilled worldwide (figure 1-3) [15].
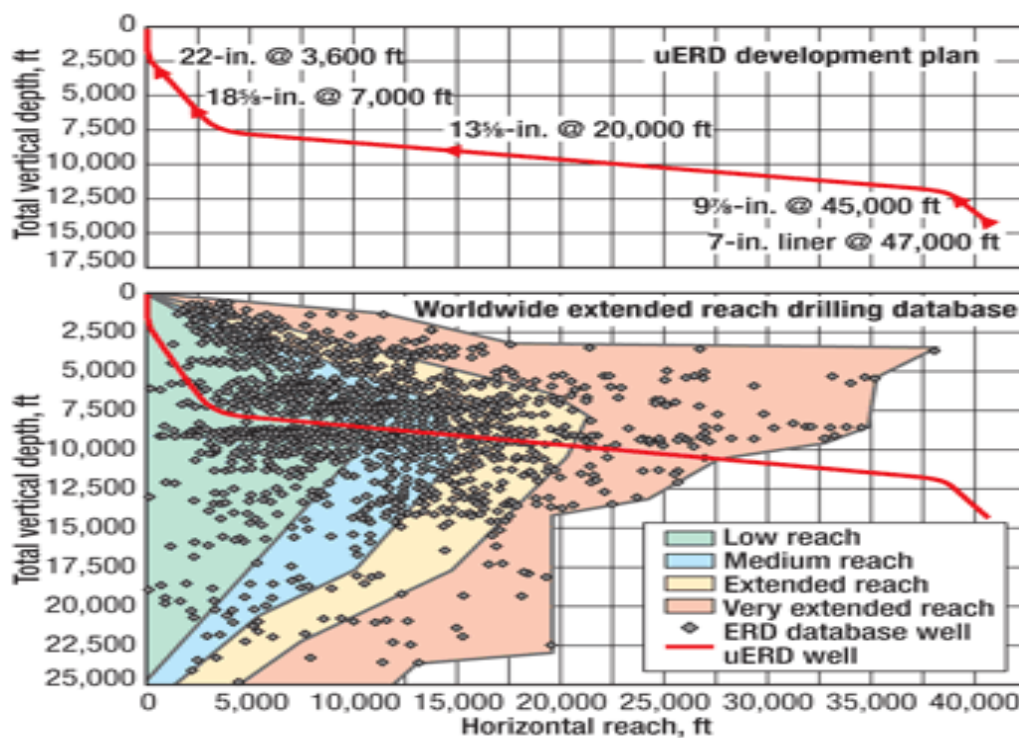

Figure 1-3: A map of the Worldwide ERD wells [14].

Despite the continuous development of new technologies, there are still several limits and challenges related to ERD to overcome. These include high operation cost, complexity and need for advanced tools for lowering and mobilize equipment into higher inclination sections ($> 40^0$). Other limiting factors to ERD-technique are mechanical loads, especially increasing torque and drag due to high friction. Other challenges are, pipe sticking due to poor hole cleaning, increased borehole instability and managing downhole pressure and too law weight on bit (WOB), which leads to the reduction of the rate of penetration. Increased borehole instability occurs due to several factors including, increased exposure time, pressure fluctuation, geotechnical interaction and drilling fluid incompatibility. Increasing torque and drag is then prevents the drill string from traveling to the bottom of the hole [15].

A wide range of measures using advanced and expensive technologies has continued to be performed in order to overcome ERD-related problems. Some of those techniques have shown promising results and progressed. Rotary steerable systems (RSS), logging-while-drilling (LWD) tools and measurement while drilling (MWD) are among those technologies that made longer ERD possible. However, some studies have shown that when the well step-out ratios increase, these conventional practical measures are not adequate to drill ERD wells in a cost-efficient way. ERD is an integrated process that requires an optimum well path profile regarding torque and drag. Controlling downhole pressure and minimizing torque and drag are two main principles that should be obeyed when planning an ERD-well. Therefore, ERD-challenges limit the capability of the conventional drilling methods to further step-out in the horizontal direction [12, 15, 16].

The most important purposes of development of the new drilling technology are lowering the operating costs and improving drilling efficiency and safety. Such goals can be approached by overcoming challenges related to ECD, better hole cleaning and breaking the ERD-barriers. According to the ReelwellTM, deploying HOL-solution can solve the mentioned issues. The main goal of the company is making it possible to double the world´s record ERD [1].

In chapter 2, this technology will be presented more in detail.

1.7 Problem formulation

The fluids used in the HOL-solution perform different functions. Therefore, they have to be separated throughout the drilling operation. Since they have different densities, the development of a mixing zone at the interface between the fluids is a natural process, which is affected by several factors. These include density differences between the fluids ($\Delta\rho = \rho_{heavy}-\rho_{light}$), the Earth´s gravity as well as the fluids´ ability to be mixed. Therefore, the main challenge with this solution is the instability at the interface between the fluids and hence controlling the growth of the mixing zone, which is more severe in vertical and high inclined wells.

1.8 Objectives

This Master thesis is an experimental study that performed for the purpose of:

➢ Defining the effect of the rotation speed of the pipe (*rpm*) on the further development of the mixing zone.

➢ Determining the impact of the rheological characteristics such as plastic viscosity (PV), gel strength and the yield point (YP) of on the growth of the mixing zone

➢ Determining the minimum limits of these rheological parameters as well as the maximum density difference, where the mixing zone can be controlled at the laboratory scale.

At the end of the work, the effect of increasing the annular gap between the pipe and the wellbore wall was studied by deploying a new pipe/well combination. This was not a part of the main focus during this work, but it was performed to obtain a better clarification of the results.

2   Reelwell Drilling Technology

Reelwell is an innovative company established by Ola M. Vestavik in Norway in 2004. The company introduced a new drilling technology called Reelwell Drilling Method (RDM). The goals of RDM-technology are solving the problems related to well drilling operations such as, Extended Reach Drilling (ERD), Equivalent Circulating Density (ECD), well instability, managing downhole pressure and hole cleaning [17]. RDM-drilling solution is based on using a unique flow arrangement called heavy over light (HOL) combined with a dual channel drill string (DDS). This combination forms a dual conduit of fluids in a closed-loop circulation system. The active fluid (light fluid) is pumped down through the outer channel to the bit and returning through the inner channel back to the surface (figure 2-1). The technology allows the return of the drilling fluid containing drill cutting, to be isolated from the casings and wellbore wall. This means that RDM enables screening out the dynamic ECD-gradient due to isolating the active fluid from wellbore wall. Thus, the active fluid is used for drilling and hole cleaning, while the passive heavy fluid is pumped down into the annulus between the DDS and the wellbore wall to control the downhole pressure in the well. According to Reelwell, using two fluids with different densities enables flotation of the drill string due to buoyancy. This mechanism leads to a significant reducing friction-induced torque and drag, thereby pushing the existing boundaries of ERD beyond conventional reach [1].

Since the fluid in the well annulus (heavy fluid) is not normally flowing, it is then possible to monitor the downhole pressure directly by controlling the pressure in well annulus during the drilling operation. Such information and measurements may be critical in case of low mud weight window or low rock strength environments. Using RDM allows gathering downhole data simply and reliably at the surface, which in turn leads to reducing the need for downhole measurement tools [1].

2.1   Reelwell technology equipment

In order to make RDM-technology adapted to a standard drilling rig the following special tools have to be installed: [1, 18]

➢ Dual Drill String (DDS)
➢ Top Drive Adapter (TDA)
➢ Dual Float Valve (DFV)
➢ Flow Control Unit (FCU)
➢ An optional piston to provide WOB

2.1.1 Dual Drill String

A dual drill string (DDS) is a dual wall drill string with an outer and an inner conduit. The outer channel is for the flow of the light drilling fluid down to the bit, while the inner channel is for flowing the flow, caring cuttings, back bottom to the surface. The DDS-pipes (figure 2-1) are currently delivered in steel and aluminum and are available in different pipe diameters include 5-7/8 and 6-5/8-in. steel and 5-7/8 to 7-1/2 in. aluminum.[1, 18]

Figure 2-1: illustrates the inner geometry of a DDS [19].

2.1.2 A Top Drive Adapter

The top drive adapter (TDA) is a swivel that directs the returned fluid through a second standpipe and mud hose (figure 2-2). This device is used to connect the DDS to the top driver on the rig that provide rotation [1, 18].
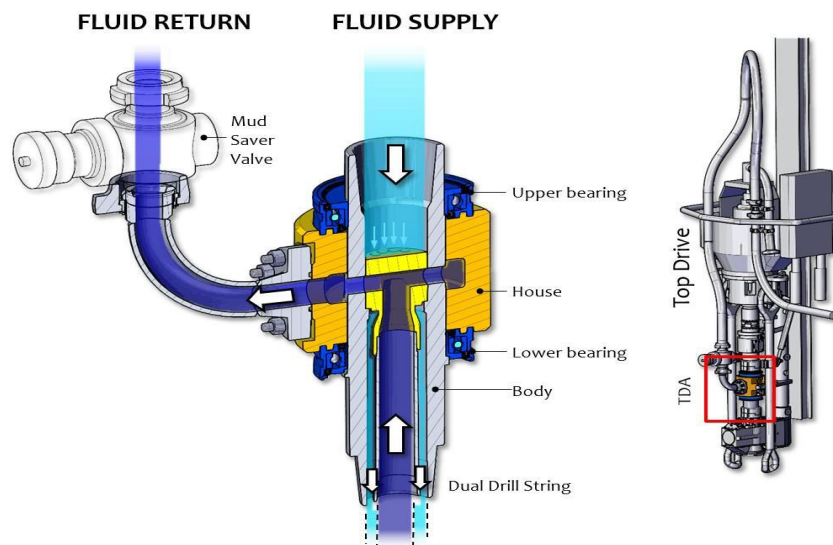
Figure 2-2: Shows a TDA [20].

2.1.3 Dual-Float Valve

In the bottom, the lower part of the dual drill string is connected to a standard bottom hole assembly (BHA) through an inner pipe valve called Dual-Float Valve (DFV). The return flow with cuttings sucks into the inner channel through entrance ports, which are a part of the valve, and transports up to the surface (*figure 2-3*) [1, 18].
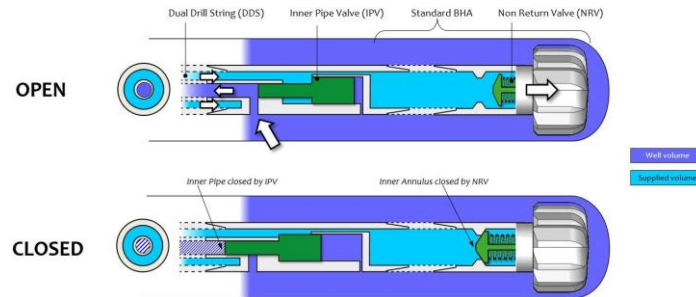
Figure 2-3: Illustrates a DFV connecting a DDS to a standard BHA [20].

2.1.4 Flow Control Unit

The Flow Control Unit (FCU) is a control system consists of a valve arrangement that is equipped with pressure and flow sensors. Through these sensors, the whole RDM-system's flow and pressure can be regulated (*figure 2-4*) [1, 18].
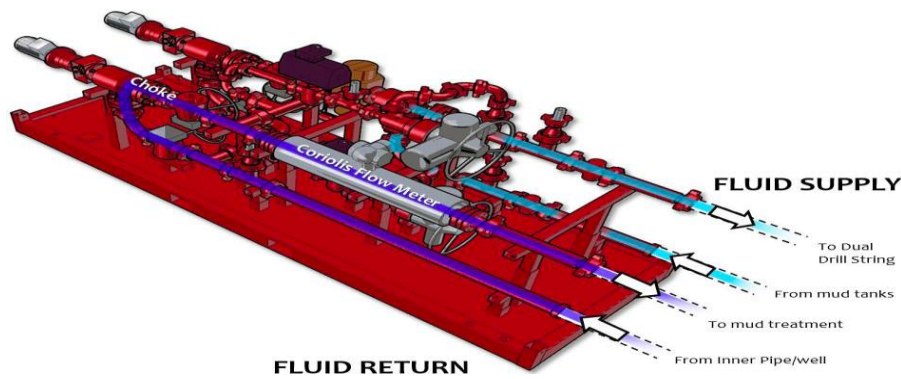
Figure 2-4: A schematic figure of a FCU [19].

2.1.5 Piston

Using the piston is an optional tool inserted at the DDS for preventing loss of the fluid from the well annulus and provides hydraulic WOB, and hence increasing horizontal reach. It is designed to slide inside the casing, allows drill pipe rotation and isolates the well annulus. It enables pressurizing of the well annulus between the sliding piston and the rotary control device (RCD) but allows flow upward in the well annulus. This mechanism can generate the WOB when required [1, 18].

2.2   Heavy Over Light-Solution

Heavy Over Light-solution (HOL-solution) is the denotation of the situation when a heavy passive fluid is placed in the annular well, while the light fluid is performing the drilling operation inside the DDS. Hence, the drilling fluids will be used for different purposes. The active circulated light, the blue colored in figure 2-5, is pumped down through the outer channel to the bit. The return fluid, caring drill cuttings from the bottom of the well, is transported back to the surface through the separate concentric inner channel, as described before. Thus, the light fluid is circulated inside the dual drill string and around the bottom hole assembly. When using RDM, the BHA should be adapted for reduced flow. The adapting that has to be performed includes MWD mud pulse, the downhole motor and the drill-bit nozzles [18]. Another function the light fluid is providing power to downhole tools. With the help of controlling the flow rate and by choking on the surface, the downhole pressure of the light fluid can be controlled at the surface. On the other hand, the heavy fluid, the red colored in figure 2-5, is used to control the pressure in the well annulus. Thus, the stationary heavy fluid provides stability of the well as well as creates the buoyancy of the drill string [1, 19]. To ensure proper seal during the drilling operation, the Rotary Control Device (RCD) is placed on the top of the BOP. The downhole piston at the drill string provided hydraulic WOB, which increases horizontal reach.

a)   **b)**
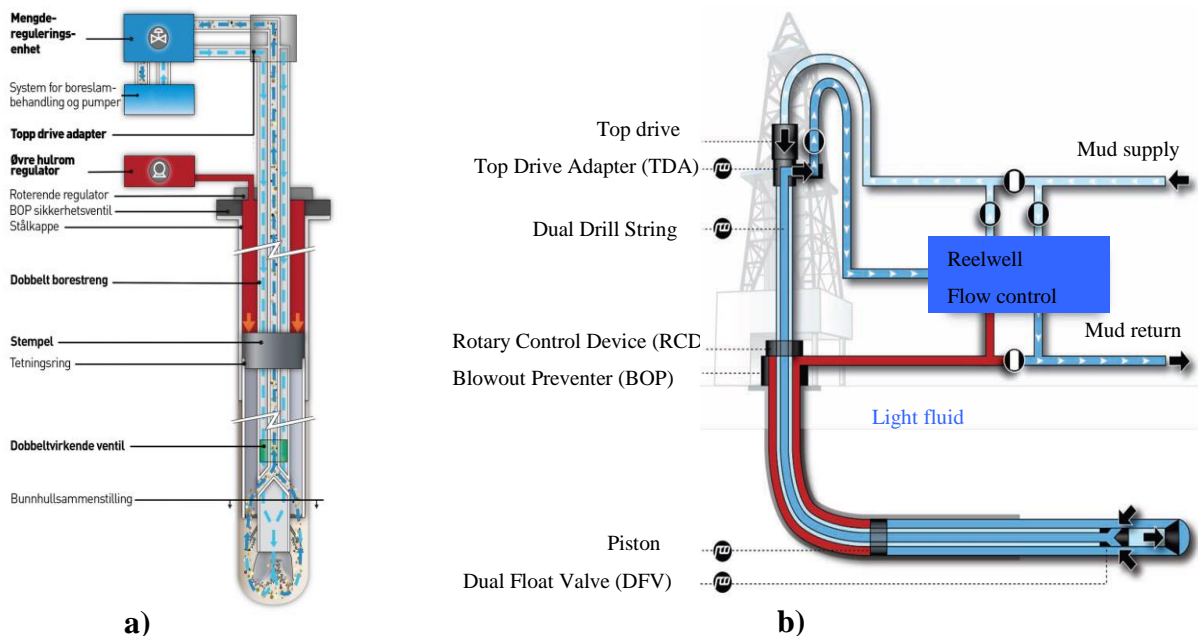
Figure 2-5: A schematic figure of RDM in a) vertical and b) horizontal section [18]

According to RDM drilling, the technology has a promising potential to increase the envelope of ERD due to the following reasons: [1, 17]

- Using a floating technique of the drill string (buoyant drill string) leads to the reduction of the mechanical loads, torque and drag.

- Avoiding issues related to dynamic Equivalent Circulating Density (ECD), since ECD is screened from the formation.

- Using a piston type arrangement at the drill string makes hydraulic weight on bit (WOB) possible.

2.2.1 Reducing Torque and Drag Applying HOL-solution

In an ERD-well, the torque and drag increase due to several factors including hole instability, ineffective hole cleaning, differential sticking, high friction, and increasing the effective weight of the drill string [21]. Employing HOL-solution, the density of the outer fluid (heavy) is higher than the density of the inner fluid (light). Therefore using RDM, the buoyancy factor (β) will be much smaller compared to conventional drilling where the inner and outer fluid has the same density. The effective weight of a buoyant drill pipe is its weight in air multiply by buoyancy factor (β), which is usually < 1. This results in increasing buoyancy force and decreasing effective weight. The higher the difference in the densities of the fluids the greater the buoyant force.

According to a simulation study performed by Reelwell, a density difference between heavy and light fluid of about 0.60 sg (ρ_{heavy} - ρ_{light}) make it possible to approach a full buoyancy (figure 2-6). Using a fully buoyant aluminum DDS, with a specific density of 2.70 sg, provides a reduction of rotary surface torque from about 65 kNm at no buoyancy to about 9 kNm at full buoyancy [1].

Well annulus Heavy fluid density [sg]	Outer channel (DDS) Light fluid density [sg]	Δρ (ρ_h-ρ_l) [sg]	Buoyancy
1.2	1.2	0	No buoyancy
1.56	1.2	0.36	Partly buoyancy
1.75	1.15	0.60	Full buoyancy
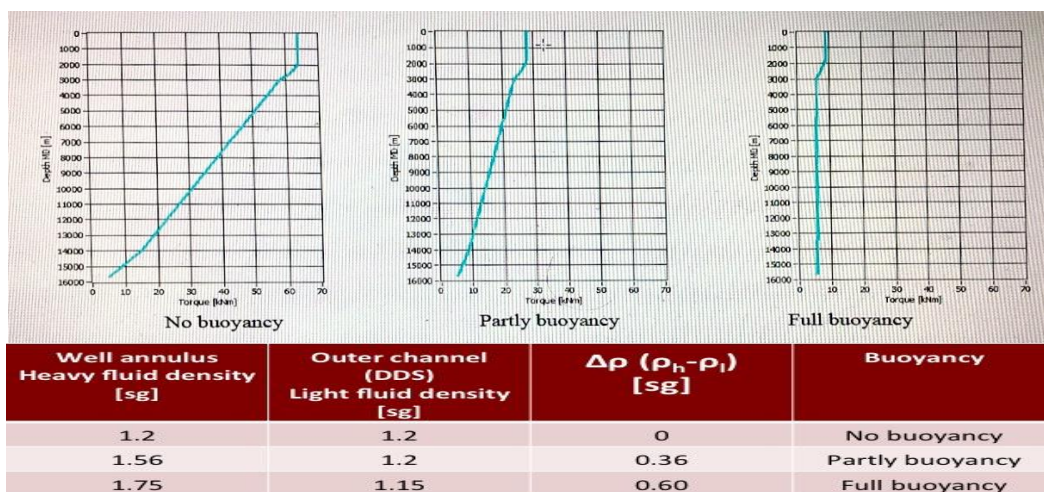
Figure 2-6: Change in torque profile of the DDS as function of buoyancy [1].

In addition to the reducing surface rotary torque, the maximum hookload, when pooling out of the hole (POOH), was reduced from 120 tons to about 3 tons (*figure 2-7)*. The maximum string compression load decreased from about 70 tons at no buoyancy to about 10 tons at full buoyancy of the drill string [1].

Well annulus Heavy fluid density [sg]	Outer channel (DDS) Light fluid density [sg]	$\Delta\rho\ (\rho_h - \rho_l)$ [sg]	Buoyancy
1.2	1.2	0	No buoyancy
1.56	1.2	0.36	Partly buoyancy
1.75	1.15	0.60	Full buoyancy
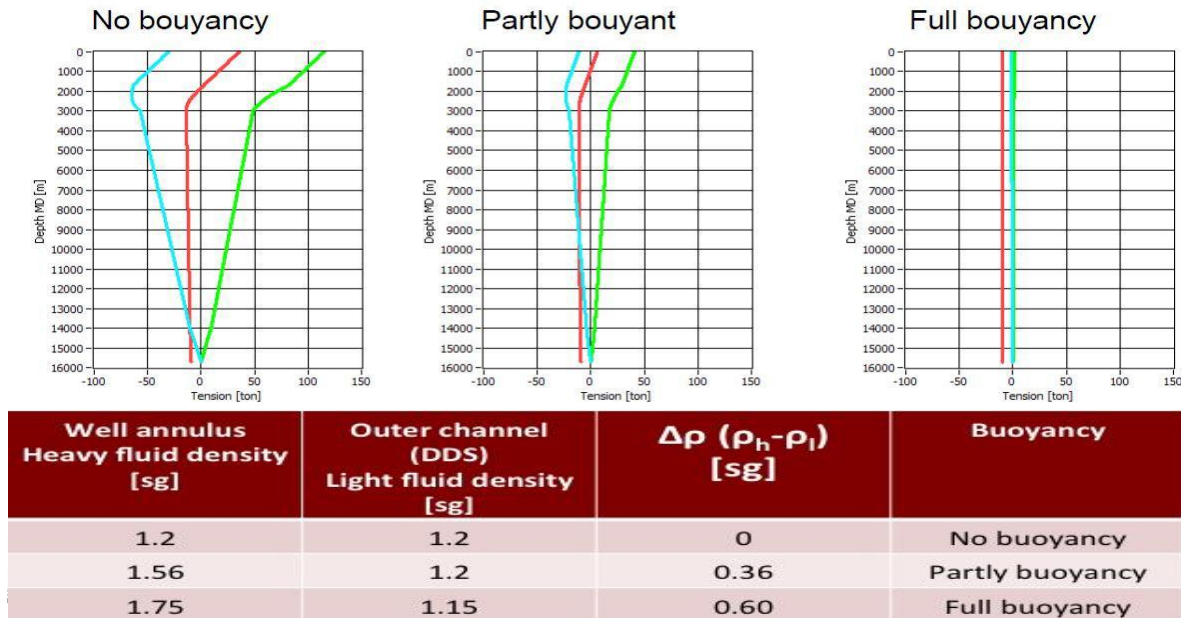
Figure 2-7: Torsion profile of DDS as function of buoyancy [1].

Additionally, increasing buoyancy results in significant reduction of the friction between the drillstring and the wellbore wall due to the floating condition of the drill string. According to the study, the coefficient of friction has less effect, due to the overall low friction resistance at high buoyancy effects. A lower effective weight and smaller friction resistance lead to significant reduction of the mechanical loads torque and drag [1]. Reducing torque and drag makes it possible in the doubling of the length of the world´s record ERD, which at the moment is about 12 km [22].

2.2.2 Elimination the Effect of the Dynamic ECD

As mentioned above, the DDS used in RDM-system has one outer annulus for pumping down the light fluid and the inner channel to transport the drilling fluid and cuttings back to the surface. At the same time, the heavy fluid is in a static condition between DDS and the wellbore wall. Compared to the conventional drilling (figure 2-8), circulation of the fluids in such path reduces the amount of the active fluid that interacts with the wellbore wall, thereby overcoming ECD-related issues [1].
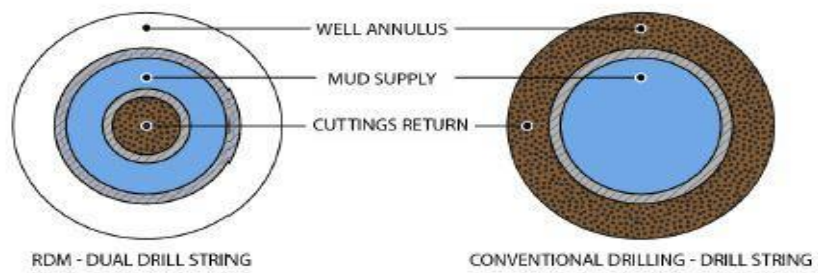
Figure 2-8: Illustrates DDS versus conventional DS [20].

2.2.3 Providing Hydraulic Weight On Bit

Providing hydraulic WOB in HOL-arrangement, where the drill string is partly or completely buoyant, is based on the deploying of a piston at the drill string that allows rotation of the DDS and bypasses the flow upward in the well annulus. This mechanism pressurizes the heavy fluid in the well annulus between the sliding piston and the rotary control device (RCD) on top of the BOP, thereby generating additional hydraulic weight on the bit when required. [1, 17, 18].

3. Theory

Drilling mud plays a critical role in drilling operations regarding efficiency, safety, and environmental issues. Therefore it is essential to balance the properties of the muds so that they will fit particular wells with the circumstances in depth and the formation drilled through. Drilling fluid is a complex liquid with specific properties that make it possible to drill deep wells in different formations. It consists of a base fluid, to which various substances and chemicals are added to control the density, viscosity, and other rheological characteristics. Drilling muds are categorized into two main groups; water-based muds (WBMs) and oil-based muds (OBMs). The base fluid in WBM consists of salt water (*brine based*) or fresh water, to which bentonite and polymers (*typically drispac or xanthan*) are added to increase viscosity and gel strength. This type of base fluid usually has a specific density of about 1.02-1.03 sg. However, OBMs mainly consist of synthetic oil, to which water is added to make an invert emulsion, and it has a specific density of about 0.80 sg [10, 23].

Low cost and less environmental impact are the main advantages of Water-based mud (WBM). For these reasons, WBM is usually used in the opening holes, where there is no return to the rig. Another advantage with WBM is its high capability to suspend solid particles, and cuttings due to its higher gel strength compared to OBMs. For further drilling operation, OBM is usually used as it has several advantages compared to WBM. It reduces friction between the wellbore wall and drill string, it does not interact with swelling clay (*reactive shale*), and it can withstand higher temperatures. Other advantages of OBM are it has minor damage to the formation/reservoir while providing a greater drilling speed compared to WBM. Some of the disadvantages of OBMs include the environmental issue, difficulty with controlling of barite sag (*it will be discussed later*), high cost, and difficult to control lost circulation [11].

Due to environmental and technical considerations, WBM was used for all experiments during this master Thesis. The rheological characteristics and some physical properties of such type of drilling fluid will, therefore, be discussed in detail in the next sections.

3.1   Water-Based Muds

WBMs are the most used drilling fluid. Approximately 80% of all oil & gas wells are drilled with WBMs. Seawater, fresh water, brine saturated brine or formation brine are conventional base fluids for preparing WBMs [23]. Selection of the type of base fluid depends on the well section to be drilled or anticipated well conditions. In offshore, shallow sections are usually drilled using seawater-based muds containing some additives, such as shale inhibitors and polymer. Bentonite plays an important role in drilling mud industry, especially in the water-based drilling mud systems.

Bentonite consists of several clay minerals; the most important one is montmorillonite. The purposes of adding bentonite include reduction of lost circulation, through the colloidal clay particles, and increasing viscosity to enhance hole cleaning efficiency [23, 24].

Once bentonite is added to water, it occurs some chemical reactions that change the properties of the fluid. It is desired that a drilling mud will affect the formation to a minimum extent as possible while keeping its primary functions. By adding salts, clay or polymers one can change the behavior of the particles in a solution. These additives determine the properties of the fluid, such as viscosity, yield point, gel strength and building filter cake. Chemical and electrical forces between particles determine the properties of the fluids. These electrochemical forces can either be repulsive or attractive, which in turn determines the condition of the drilling fluid. Clays, in general, exist in two broad categories (figure 3-1), either non-dispersed (aggregate) of dispersed [11, 23].

3.1.1 Aggregate (non-dispersed) System

In an aggregated system, the particles are bound together in aggregates. The sheet structure of the clay is assembled and packed together. Non-hydrated clay usually exists in this state, where the platelets are arranged parallel to each other via attractive forces. The clay sheets may separate from each other due to a hydration process or a mechanical influence. Thus, the aggregated system can become flocculated or deflocculated. Generally, a flocculated bentonite mud system will go over to an aggregated state by time. This, in turn, results in a system with less free particles and thus smaller total particle surface. A typical non-dispersed system is simple gel-and-water systems used for drilling shallow sections. Disadvantages with such system are including low viscosity and high fluid-loss, which leads to a reduced ability for cutting transport and higher operating cost [10, 11].

3.1.2 Dispersed System

A dispersed system occurs in a solution of suspended particles when the aggregates are completely broken. In such clay system, the particles can have both positive and negative charges on the edges depending on the pH-level, while the surface of the particles can have pH-dependent negative charges. This allows a dispersed system to become either flocculated or deflocculated. When bentonite hydrates in fresh water the clay minerals may become relatively dispersed. A proper bentonite mud system should be dispersed and deflocculated.

A dispersed drilling fluid system can be prepared by adding chemicals and dispersants to the mud system. It is necessary to make the drilling fluid dispersed, especially when higher density muds are desired. Dispersing process improves rheology of the fluid and making more tolerant for solids, and hence it allows making a drilling mud with a density of up to 20.0 ppg (*about 2.40 sg*) [10, 11, 23].

The most commonly used dispersant is lignosulfonate because of its low cost and efficiency. It is also well-known to students, most operators, and rig personnel. Lignosulfonate perform its function usually at higher pH-level, pH >10 [11, 23]. A disadvantage with a dispersed system is it can significantly decrease the rate of penetration and contribute to the erosion of the hole [23].

Figure 3-1: Shows behavior of clay minerals in a drilling mud system [11].

3.1.3   Flocculated System

A flocculated system occurs when the clay platelets have net attractive forces to each other. In this system, the particles are connected surface-to-surface or end-to-end and form clusters. Changes in the electrolyte concentration, temperature and solids crowding are the mechanism behind flocculation of the system. In a flocculated system the viscosity, gel strength, yield point, and fluid-loss will increase significantly. Both dispersed and non-dispersed (aggregated) systems can be flocculated [11].

3.1.4   Deflocculated System

A deflocculated mud system occurs when the clay particles have the same electrical charge, which results in a repulsive net force between the particles. A mud system can be deflocculated under alkaline condition, where the net charge of the particles is negative. Adding deflocculants or diluting fluids to a fluid system, a completely deflocculated system can be achieved. The deflocculants are thought to be adsorbed on the edges of the clays, thereby neutralizing the positive charge on the ends of the clay particles. This reaction results in net negative charges on their side surfaces, which makes the particles to separate. Since there are no any electrical attractive forces between the particles, therefore the fluid-loss and yield point will decrease in a deflocculated mud system [11].

3.2 Bentonite

As an industrial material, bentonite is defined as clay consisting of Smectite group minerals. These minerals were earlier referred to as Montmorillonite, and the name is still used in the petroleum industry today. The name of bentonite was first proposed by Knight in 1898 and is named after Benton Shale where the clay was thought to have occurred. There are two types of Bentonite include swelling (sodium) and non-swelling (calcium) bentonite. The swelling type is very high water-soluble and provides the fluid with a proper viscosity and contributes with particle suspending capacity [25]. Bentonite is not considered as weighting material, as it does not increase the fluid density significantly. Of these reasons, Bentonite has traditionally been used to give drilling muds viscosity and gel strengths. Due to availability in large quantities, low cost and little polluting, it has been used for drilling of the top sections of wells. During drilling of the top holes, in many cases, there will not be return paths up to the platform, and the drilling mud is usually released on the seabed. During drilling the smaller sections further down in the well, after a return path (riser) has been created, polymers are added to achieve higher viscosity and gel strength. In some cases, the drilling fluid shall have higher viscosity to be able to transport the drill cutting up to the surface. In order to increase viscosity, relatively large amounts of bentonite must be added, which means that it requires large storage space on the platform and high transport cost. Therefore adding polymer is a smarter alternative [25, 26].

3.3 Polymers

The history of using polymers as an additive in drilling fluid formulations goes as far back as to the 1930s when cornstarch was added to a formulation in the purpose of the fluid-loss control. Thereby polymers have been applicable in nearly every water-based drilling mud system, and still, some systems are especially dependent on polymers. Adding polymers to clay suspensions is of great interest in the petroleum industry due to the polymer's capacity to modify the drilling fluid's colloidal and rheological properties. Polymers are more expensive than bentonite, but the same viscosity can be achieved by adding a much smaller volume compared to bentonite [27].

Polymers consist of large molecules that are composed of a chain of monomers. The way the polymers are put together determines their properties. The polymer additives in water-based muds may be classified according to their chemistry and functions. Regarding their chemical properties, they are occurring as anionic and nonionic polymers. The main function of the anionic polymers is increasing the viscosity of the fluids while the function of the nonionic polymer is providing filtration control in the drilling mud. The most types of polymers that are used to increase viscosity in drilling mud consist of long chains. This construction provides the drilling muds a good particle

bearing capacity. Carboxymethylcellulose (CMC), Poly Anionic Cellulose (PAC) polymer and Xanthan Campestris (Xanthan-XC) biopolymer are among the most commonly used polymer to provide drilling mud system with viscosity, filtration control, and gel strength.

There are also polymers with thinning capacity that added to drilling mud in order to reduce viscosity and gel strength, include lignosulfonate, lignite, and lignin. Lignosulfonate is the most commonly used polymer to control viscosity and fluid loss of the drilling muds. It is used in both saline and fresh water, and it is stable at temperatures of over 200 $^{\circ}$C. It performs its function at pH levels between 10-11. Of this reason, caustic soda (NaOH) is added to the drilling mud systems to increase the pH of the fluid. However, polymers can be destroyed at high pH, therefore it is important to keep the pH-level of the drilling mud between 10 and 11[11, 27, 28].

3.4   Barite

Barite is the most used weighting material in the drilling fluid industry due to its low cost, high specific density, and it doesn't react with other substances. The density of the mineral is typically between 4.20-4.30 g/cm^3. It consists mainly of barium sulfate ($BaSO_4$), but it also contains $BaSO_3$ and other minerals and heavy metals. China, India, and the USA are the world´s leading producer of Barite. Barite that is used in Norway comes from Spain and Morocco, but it is crushed in Norway and consist of more than 85% $BaSO_4$ [25]. Barite is also used for preparing barite plug for killing underground blowouts. The barite plug seals the wellbore through increasing the hydrostatic head on the active zone and hence prevents the additional influx of formation fluid. Another mechanism behind sealing capability of the barite is its high fluid loss- and dehydrating capacity, which enhances forming a solid plug in the hole [11].

3.4.1   Barite Sag

Barite sag occurs when heavy minerals in the barite and other solid particles, such as cuttings, falls into the bottom of the wellbore due to gravity. Barite sag happens when circulation is stopped in vertical wells, whereas, in deviated and horizontal wells, it occurs due to a complex setting mechanism called "Boyocott settling." This mechanism states that heavier particles settle quickly at the low side of the wellbore, while the lighter fluids are at the high side. Due to this mechanism, barite sag is a more severe issue in deviated than in vertical section. At angles as high as 75°, significant barite sag was measured, and 60°-75° was the most critical range [29, 30].

Barite Sag causes variation of the mud weight in a borehole. In the shallow depth, the density of the mud becomes lower compared to the mud weight in the deeper section of the well. This situation can lead to pressure control issues, and hence well control incident. At the shallow section of the well, there will not be sufficient mud weight to balance formation pressure, which can lead to

wellbore collapse. In the deeper section, the higher mud weight may cause formation fracturing and hence lost circulation. Thus barite sag can lead to both economic and safety related issues during drilling operation [9].

Utilizing drilling muds with higher gel properties, such as gel strength and low shear yield stress, can minimize the risk of occurring barite sag issues. It has been shown that barite sag occurs 10 times faster in drilling fluid with a yield stress of 5 lb/100ft^2 compared to the same type of fluid with a yield stress of 12 lb/100ft^2 [29].

Due to the differences in their chemical and physical properties as well as rheological characteristics, barite sag is a more severe problem in OBMs compared to WBMs. In OBMs, which are usually an invert-emulsion drilling fluid, gel strength will not develop to the same extent as in WBMs [31]. Another reason is the density differences between the base fluids that are used to prepare the water-based and oil-based muds. Mineral oil with a density of about 0.80 sg is usually used as the base fluid in OBMs while brine with the density of 1.025 sg is used for preparing the WBMs. For this reason, a higher amount of barite is required to make an OBM with a specific density than a WBM with the same density. The higher amount of weighting material the higher risk of occurring barite sag [30, 32].

3.5   The Main Functions of a Drilling Mud

Regulations put many requirements on the properties and capacity of the drilling mud. Transport the cuttings from borehole up to surface and controlling the downhole pressure to prevent blowouts were historically the first use of the drilling mud. Due to the multifunction and complexity of the drilling fluid, it is difficult to assign a specific function. Priority of one or more functions over the others varies depending on the phase of the drilling operation.

Following are the main functions of the drilling fluid [9, 25, 33]:

- Control of downhole pressure and prevent the inflow of the formation fluids into the well.
- Transport of cuttings from beneath the bit up to the surface.
- Suspending the solids and weighting materials during both dynamic and static condition.
- Provides mechanical and chemical stability to the uncased sections of the wellbore.
- Builds low-permeable filter-cake on the wellbore wall to reduce lost circulation.
- Reduces the friction between the drill pipe and wellbore wall and/or casing due to its lubricating property.
- Cools down the drillstring and drill bit

3.6   Rheology

Rheology is the science that deals with how materials flow as the function of the shear rate within a particular time and special direction. The rheological properties of a material can be affected by pressure, temperature and the duration of the applied shear or load. Rheology affects transport and movements of all kind of fluids in an oilfield, including drilling fluids, cement slurry, completion- and workover fluids and produced fluids. Of these reasons understanding rheological characteristics of the oilfield fluids is very important for the petroleum industry. Viscosity, gel strength and yield point of the drilling fluids are those important characteristics that will be in focus during this master thesis. Viscosity is the measurement of the resistance of a fluid to flow while both yield point and gel strength are measurements of attractive forces between the particles. Viscosity and the yield point are dynamic properties of the fluids whereas the gel strength is the measurement of electrostatic forces under static conditions varying with time. However, the yield point and gel strength are related to each other. A decrease in the one parameter will usually result in the reduction of the other. These properties can be controlled in a mud system by similar chemical treatment [11, 25, 27, 34].

Rheological characteristics can be defined using the rheological models include Bingham plastic, Power Law, and Herschel-Buckley models [11]. They will be discussed in the later sections.

3.6.1   Viscosity

The Viscosity of a fluid is its physical property that measures the resistance of the fluid to flow. The resistance to movement of the fluid occurs because of two reasons. These include friction forces between the various components in the fluid and the attractive forces between electrically charged particles or ions in the fluid (*electrostatic forces)*. Some parameters, including temperature, pressure, shear rate, shear stress, time, physical and chemical nature of the fluid affect its viscosity [25].

Shear rate (Sec^{-1}) and shear stress (N/m^2, Pa) are two terms using for describing viscosity of a liquid placed between two plates. The top plate is moved at a rate of 1m/sec, while the bottom plate is stationary. Shear stress is the amount the force required to move a given area of the fluid, while the shear rate is the velocity gradient of the fluid.

Viscosity can be calculated by plotting shear stress as a function of shear rate. Consequently, the unit of viscosity is Pa.s. Another common unit used for measuring viscosity is the Poise. Since Poise is large scale, cP, which is equal to one mPa.s, is usually used. Based on their response to the shear rate, fluids are categorized as Newtonian and non-Newtonian [11, 25, 35].

3.6.1.1 Newtonian Fluids

Newtonian fluids are shear-rate independent fluids, in which the viscosity is only a function of pressure and temperature. Thus, the viscosity for Newtonian fluids will remain constant at a particular pressure and temperature regardless of changing of the shear rate.

Typical characterization of Newtonian fluids is they start immediately to move when shear stress or a load is applied (figure 3-2). Water, gasoline, oil, alcohol, and glycerin are some examples of Newtonian fluids, which can be described by Newton´s law of viscosity [11, 25, 35].

<u>Newton´s Law of Viscosity Model for Newtonian Fluids:</u>

Newtonian´s law of viscosity describes the response of the Newtonian fluids when a shear load is applied. The model states that in such fluids shear stress between adjacent layers, the moves parallel to each other at different speeds is directly proportional to the shear rate (*velocity gradient*). Viscosity or viscosity coefficient is described as a constant ratio of the shear stress to the shear rate at a given pressure and temperature. By plotting the shear stress versus the shear rate a straight line with the start from the origin, will be produced (figure 3-2). The constant slope of the line represents the Newtonian or dynamic viscosity of this type of fluids [35].
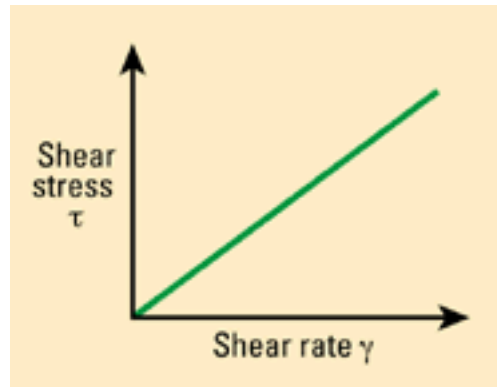

Figure 3-2: Flow curve for Newtonian fluid [11].

$$\tau \; \alpha \; \frac{du}{dy} \tag{3.1}$$

$$\tau = \mu \frac{du}{dy} = \; \mu * \gamma \tag{3.2}$$

Where;

μ = Viscosity [cP]

τ = Shear Stress = $\frac{F}{A}$, [lb/100ft^2, or Pa]

$\frac{du}{dy}$ = Shear rate (γ) = Velocity gradient of the fluid, $[Sec^{-1}]$

3.6.1.2 Non-Newtonian Fluids:

Non-Newtonian fluids are those fluids that don´t follow Newton´s law of viscosity, i.e., there is no a constant of proportionality between shear rate and shear stress for these types of fluids. Majority of fluids are classified as non-Newtonian, and their viscosity depends on the shear rate. These fluids are divided into three different subcategories (*figure 3-3*), including, Bingham plastic-, pseudoplastic (*shear thinning*)-, and dilatant (*shear thickening*) fluids [11, 35].

Most of the drilling fluids are either Bingham plastic or pseudoplastic fluids, while cement slurry is classified as dilatant fluid [10, 11].

Bingham Plastic fluids

Bingham plastic fluids are fluids that require minimum shear stress, called yield stress (yield point), to initiate flow. Such fluids are also called shear thinning since the effective viscosity decreases with increasing shear rate. Drilling muds that contain some charged particles are classified as Bingham plastic fluids, e.g., a mixture of water and bentonite [10, 27, 36].

Pseudoplastic Fluids

Pseudoplastic fluids are shear-thinning fluids that do not have any yield point. It can be difficult to see the transition between the plastic and pseudoplastic phase in these fluids. Viscosity decreases by increasing shear rate. Most invert-emulsion drilling fluids and polymer solutions can be classified as pseudoplastic fluid.

Dilatant Fluids

Dilatant fluids are shear-thickening fluids, for which the viscosity increases with increasing shear rate. They behave as dilatant only at specific shear rates. Suspensions with a high content of solid particles can be categorized as dilatant fluids, for example, cement slurry.
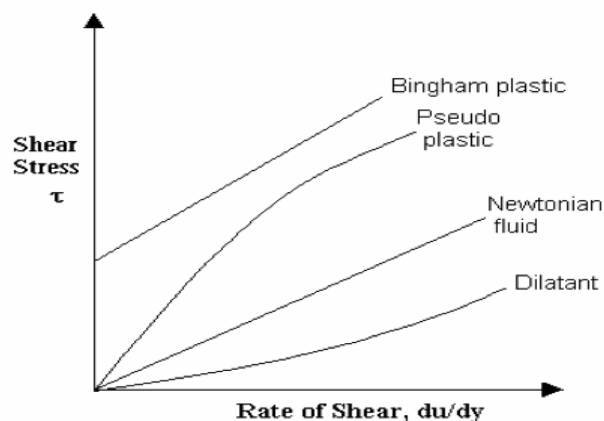

Figure 3-3: Flow curve for non-Newtonian fluids. [11]

.

3.6.2 Yield Point (YP)

Yield point (YP) or yield stress is the minimum required shear stress to initiate a Bingham plastic fluid to flow. It defines as the resistance of the fluid to flow due to the attractive forces between colloidal particles (*electrostatic forces*). It is the measurement of the attractive forces between particles under dynamic condition [26].

The oil & gas industry has recognized the yield stress of the drilling fluid as a key factor for evaluating barite sag, hole cleaning. ECD, swab/surge pressures and other issues related to drilling operations. Increasing the yield point results in increasing the ECD. The yield point also affects the carrying capacity of drilling muds during hole cleaning. The capability of the drilling fluid to transport cuttings up to the surface is indicated by the yield point (YP). A drilling mud with a high yield point can carry drill cuttings better than similar drilling mud with the same density and viscosity but with lower yield point. Therefore, using conventional drilling, the yield point should be at reasonable values for hydraulics and cutting transport performance [26, 27, 37].

Another parameter that affects the hole cleaning capacity of the drilling mud is the inner diameter of the hole. When drilling a large diameter hole, the yield point must be increased in order to improve the efficiency of the hole cleaning [33]. Based on this statement, a higher yield point is required when operating HOL-solution with larger density differences between the fluids. Therefore, the yield point may be an important parameter to be considered when preparing the drilling muds for the mentioned purpose.

The gel properties of drilling fluids can be modified with the help of adding the deflocculants or flocculants to the mud systems without significant changing of the plastic viscosity. Adding deflocculant to a clay-based mud will lower the yield point while it is increased by adding flocculants or freshly dispersed clay. Yield point has different units such as Pascal (Pa) and lb/100ft^2. It can be estimated by using rheological models that will be discussed in later sections [11, 33, 36].

Due to difficulties with quantifying of the yield point, using standard lab and field viscometers, several conventional measurements and regression-analysis techniques are usually used to predict the true value of this parameter. During a study involving direct measurements using standard viscometers and statistical analysis of 48,310 reports, it was shown that the low-shear yield point (LSYP) was the most suitable alternative for determining the yield stress of drilling fluids [37].

3.6.3 Gel Strength

Gel strength is the expression of thixotropic properties (*time-dependent shear thinning property)* of mud slurry. It is related to attractive forces between the particles in the slurry when it is at rest, and it is measured as a function of time. According to the API standard, the gel strength is defined as the shear stress measured (*using Fann viscometer*) at the shear rate of 3 *rpm* after the drilling mud has been at rest for 10 sec, 10 min, and 30 min. The dial readings can then be directly reported in *1lb/100ft²* as the gel strength of the mud at the mentioned time intervals [11, 26, 33].

The procedure of measuring gel strength is described in Appendix C.

Gel strength is an important property of drilling muds to keep particles/cuttings suspended in the wellbore annulus during static condition, e.g., when connecting new pipes. This property of the drilling muds prevents the solid particles from falling to the bottom and hence reducing the risk of occurring drilling issues such as sticking of the drill pipe and barite sag [38].

However, the gel strength of the fluids should easily be dissolved again after the mud circulation has been stagnant for a period. If the gel strengths are very high or the gels are progressive, the required pressure, which is called gel-breaking pressure, will be significant. In this case, there will be a danger of fracturing of the formation and other well control problems [11, 33].

The gel strength of drilling muds depends on temperature and time. By measuring 30 min gel strength, the time factor can be partially included for progressive gels under the condition that the fluid is stable at the bottom hole temperature. If for each section of annulus the gel-breaking pressure is higher than surge or swab pressure the first mentioned term should be used.

Gel-breaking pressure can be calculated as follow [11]:

$$P_g = \frac{4L\tau_g}{1200(ID_{well} - OD_{pipe})}$$

(3.3)

Where:

P_g = Gel breaking pressure, [psi]

L = Length of annulus section, [ft]

τ_g = 30 min gel strength, [lb/100ft²]

ID_{well} = Inner hole diameter, [in]

OD_{pipe} = Outer drill pipe diameter, [in]

3.7 Rheological Models

Rheological models are mathematical models used to describe the relationship between shear rate and shear stress for Newtonian and non-Newtonian fluids. A concentric cylinder viscometer (e.g., Fann viscometer) is usually used to accomplish the rheological evaluation of oil field fluids. These

types of instruments provide a limited number of shear rates ranging from 3 *rpm* (5.1 Sec^{-1}) up to 600 *rpm* (1022 Sec^{-1}). The generated data are analyzed, using the rheological models, in order to define the rheological properties of the fluids. The most commonly used models in drilling fluid technology for non-Newtonian fluids are Bingham plastic-, power law- and Herschel-Bulkley models (*figure 3-4*). Combination of these models is often necessary to describe rheological behavior of most types of non-Newtonian fluids [11, 26, 39].
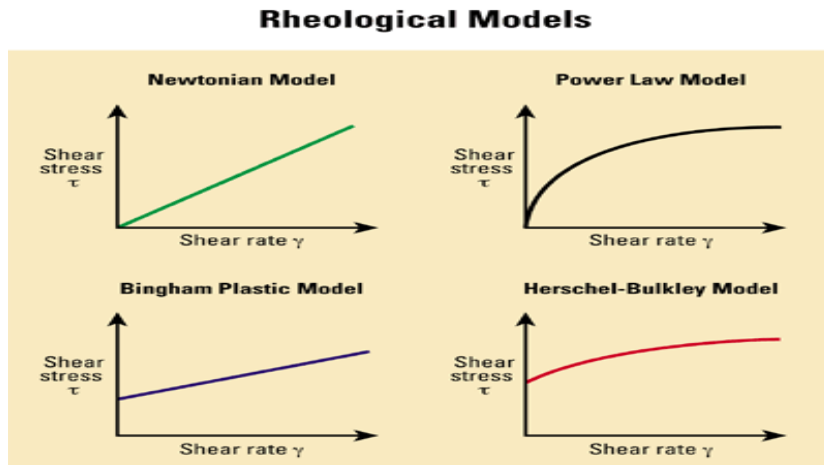
Figure 3-4: Rheological models. **[11]**

3.7.1 Bingham Plastic Model

Bingham plastic model is a rheological model that is used to describe flow characteristics of the most types of drilling fluids in the drilling mud industry. This model can suit best for describing fluids, which have yield point (YP) and plastic viscosity (PV).

Bingham plastic model is based on the higher shear rates, usually at 600- and 300 *rpm* viscometer dial reading. From these two measurements, the rheological characteristics such as effective viscosity, plastic viscosity (PV), and yield point (YP) can be determined (*figure 3-5*).
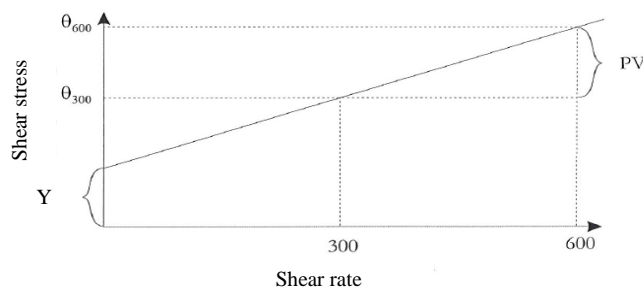
Figure 3-5: Bingham Plastic model [11].

27

From the figure, the relationship between the shear stress and shear rate in the Bingham model can be described as in the following mathematical equation [11, 25]:

$$\tau = YP + \ PV * \gamma \tag{3.4}$$

Where;

τ = shear stress, [Pa, lb/100ft^2]

YP = yield point, [Pa, lb/100ft^2]

Υ = shear rate, [rpm, Sec^{-1}]

PV = plastic viscosity, [cP]

Effective Viscosity of The Bingham fluids

For non-Newtonian fluids, the effective viscosity is defined as the ratio of the shear stress to shear rate, and it varies with the shear rate for the Bingham fluids. Unlike Newtonian fluids, the effective viscosity for non-Newtonian fluids is not constant. For most drilling fluids the effective viscosity decreases as shear rate increases. Fluids that behave in such a manner called for shear thinning fluids, as described before. Effective viscosity can be calculated directly from the dial reading and expressed as follow [11, 39]:

$$\mu \ = \frac{300 * \theta_{rpm}}{rpm}, [cP, mPa.s] \tag{3.5}$$

Where:

θ = Dial reading obtained from viscometer

μ = Effective viscosity

rpm = Rotation speed (rotation per minute)

Equation (3.5) can be simplified, and the effective viscosity of Bingham plastic fluids can then be calculated directly from 600 *rpm* dial reading as in the following mathematical formula [39]:

$$\mu = \frac{\theta_{600}}{2}, [cP = mPa.s] \tag{3.6}$$

Plastic Viscosity of The Bingham Fluids

As mentioned in the earlier section, the effective viscosity decreases with increasing the shear rate. When the shear rate approaches infinity, the effective viscosity reaches a limit called plastic viscosity (PV). Thus, the plastic viscosity is the lowest value of the effective viscosity that the fluid can have as shear rate reaches its infinite value. From the flow curve of Bingham plastic model (figure 3-5), the plastic viscosity can be defined as the slope of the curve, and it can be calculated directly from 600 and 300 *rpm* dial readings as described in the following equation [11, 25, 39]:

$$PV = 511[mPa] * \frac{\theta_{600} - \theta_{300}}{(1022 - 511)S^{-1}} \tag{3.7}$$

The equation can be simplified and expressed as follow:

$$PV = \theta_{600} - \theta_{300}, \qquad [cP, mPa.s] \tag{3.8}$$

In the drilling fluid industry, plastic viscosity is used as an indicator of the shape, size, distribution, and quantity of the solids as well as the viscosity of the liquid phase [11].

Bingham plastic Yield point

As describes before, the yield point (YP) of a fluid is the measure of the electrostatic forces between the solid particles under flowing condition. In the Bingham plastic model, the YP is extrapolated to the shear rate of zero. Thus, the intersection of the curve with the shear axis (y-axis) is the yield point of the fluid as seen in figure 3-5. The yield point of the Bingham fluids is calculated from 600 *rpm* and 300 *rpm* dial reading as following formula [11, 39]:

$$YP = \theta_{600} - PV = 2 * \theta_{300} - \theta_{600}, \left[\frac{lbs}{100ft^2}\right] \tag{3.9}$$

The yield point can be converted to Pascal by multiplying equation (3.9) by the factor of 0.511.

$$YP = 0.511 * (2 * \theta_{300} - \theta_{600}), [Pa] \tag{3.10}$$

For shear thinning plastic fluids, such as drilling muds, the yield point will decrease with increasing the shear rate [39].

3.7.2 Power-Law fluid Model

Power Law model is an alternative to the Bingham model since the second mentioned model is to describe the fluid flow properties only to a limited extent. Power-Law model gives a good description of the relationship between the shear stress and the shear rate of pseudoplastic fluids and hence for the most types of the drilling muds.

The advantage of using the power law model is that the model can be used at any values of shear rates, especially at the low one. It gives a better description of the fluid flow characteristics compared to the Bingham model.

The relationship between the shear stress and the shear rate in the power-Law model can be described as follows [11, 25, 39]:

$$\tau = K * (\gamma)^n, \left[\frac{lb}{100ft^2}\right] \tag{3.11}$$

Or

$$\log \tau = \log K + n \log(\gamma) \tag{3.12}$$

Where;

K = The flow consistency index, [lb/100ft^2.s^n]

n = The flow behavior index, [dimensionless]

$\gamma = \dfrac{du}{dy}$ = $shear\ rate\ or\ velocity\ gradient\ perpendicular\ to\ the\ plane\ of\ the\ shear, [S^{-1}]$

γ^n = Power law expression

Based on the value of the index n, the Power-law fluids can be classified into three categories (figure 3-6) namely; pseudoplastic, Newtonian and Dilatant fluids [11, 39]:

For;

n < 1 : Pseudoplastic fluid behavior

1 = 1 : Newtonian fluid

1 > 1: Dilatant fluid

a. Dilatant; **b**. Newtonian; **c**. Pseudo plastic
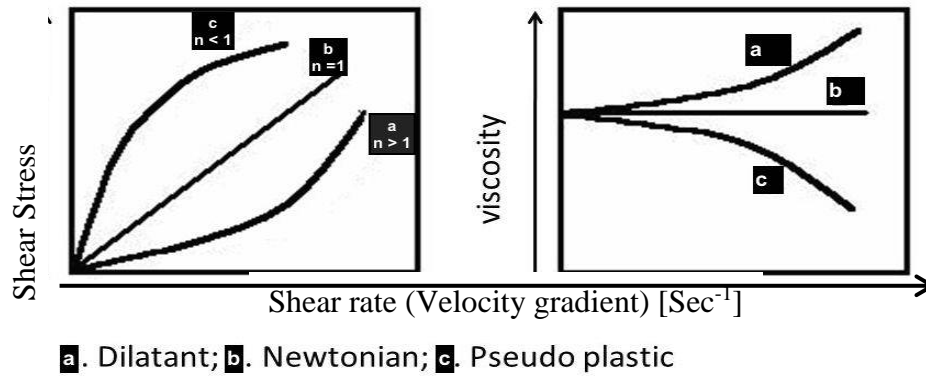
Figure 3-6: Power law fluids are categorized into three groups depending on the index *n* [25].

At shear rate $(\Upsilon) = 1 \rightarrow K = \tau$ regardless *n*-value. Therefore, *K* is related to the viscosity of the fluid for the low shear-rates. For the higher shear rates, *K* is the measure of the solid content of the fluid. The index "*n*" indicates the deviation of the fluid from being Newtonian. The lower the *n*-value, the more shear thinning is the fluid.

From equations (3.11 and 3.12), *K* and *n* can be calculated and expressed as the following mathematical models [11, 39]:

$$n = \frac{\log \frac{\tau_1}{\tau_2}}{\log \frac{\gamma_1}{\gamma_2}} \tag{3.13}$$

$$K = \frac{\tau_1}{\gamma_1^n} = \frac{\tau_2}{\gamma_2^n} = \frac{\tau}{\gamma^n} \tag{3.14}$$

The two equation (3.13) and (3.14) can be solved by measuring shear stress at two different shear rates; for instance, for measurements at 600 and 300 *rpm*, which are equivalent to 1022-and 511 s^{-1}, ***n*** and ***K*** can be expressed as follow:

$$n = \frac{log \frac{\theta_{600}}{\theta_{300}}}{\log \frac{1022}{511}} = 3.32 * \log \left(\frac{\theta_{600}}{\theta_{300}}\right) \tag{3.15}$$

$$K = \frac{\theta_{300}}{511^n} = \frac{\theta_{600}}{1022^n}, \qquad \left[\frac{lbs}{100ft^2} . s^n\right] \tag{3.16}$$

The disadvantage with the Power-low model is that the model has no yield point, and it underestimates shear stress at low shear rates [39].

3.7.3 Herschel Bulkley Model

Herschel Bulkley model is a modified version of the Power-law model. It is the best model to describe the rheological properties of fluids with a non-linear behavior and have yield stress. It fits best to measured data of the drilling fluids at lower shear rates. The yield stress and other parameters can be calculated from the measured data using the following equations [11, 25, 39]:

$$\tau = \tau_0 + K * \gamma^n \tag{3.17}$$

Or

$$\log(\tau - \tau_0) = \log K + n \log \gamma \tag{3.18}$$

Where:

τ = Shear stress

τ_0 = Low shear yield stress (LSYS)

γ^n = Power law expression

Yield stress at zero shear rate (τ_0), which is also called low shear yield point (LSYS), can be calculated using the dial readings at 6-and 3 *rpm* and expressed as follow [11].

$$\theta_0 = 2 * \theta_3 - \theta_6 \tag{3.19}$$

To express τ_0 in the unit, lb/100ft^2, equation 3.19 has to be multiplied by the factor 1.0678:

$$\tau_0 = 1.0678 * \theta_0 , \left[\frac{lb}{100ft^2}\right] \tag{3.20}$$

To report τ_0 in Pascal [Pa], θ_0 has to be multiplied by the factor 0.511:

$$\tau_0 = 0.511 * \theta_0 , [Pa] \tag{3.21}$$

From the power-law model, *K* is equal to shear stress when shear rate = 1, regardless of the value of the index *n*. Therefore, at low shear rates, *K* is necessarily related to the viscosity of the fluid. However, *K* is the measure for solid content of the slurry at higher shear rates.

To calculate shear stress (τ), using equation (3.17), the indexes, *k*, and *n,* first have to be determined. For this model, these values can be calculated as follow [11, 39]:

$$n = \frac{\log\frac{\tau_1 - \tau_y}{\tau_2 - \tau_y}}{\log\frac{\gamma_1}{\gamma_2}} \qquad (3.22)$$

$$K = \frac{\tau_1 - \tau_y}{\gamma_1^n} = \frac{\tau_2 - \tau_y}{\gamma_2^n}$$

$$k = \frac{\tau - \tau_y}{\gamma^n} \qquad (3.23)$$

Using the dial readings at 600 and 300 *rpm* (*equivalent to 1022 and 511 S^{-1} respectively*), the equations 3.23 and 3.24 can then become as follows:

$$n = \frac{\log\frac{\theta_{600} - \theta_0}{\theta_{300} - \theta_0}}{\log\frac{1022}{511}} = 3.32 * \log(\frac{\theta_{600} - \theta_0}{\theta_{300} - \theta_0}) \qquad (3.24)$$

$$K = 0.511 \left(\frac{\theta_{600} - \theta_0}{1022^n}\right) = 0.511 \left(\frac{\theta_{300} - \theta_0}{511^n}\right), [\text{Pa}. S^n] \qquad (3.25)$$

or

$$K = 1.0678 * \left(\frac{\theta_{300} - \theta_0}{511^n}\right), \left[\frac{\text{lb}}{100\text{ft}^2} . S^n\right] \qquad (3.26)$$

Then, the shear rate γ has to be stated in S^{-1}, which can be obtained by multiplying the shear rate in *rpm* with the converting factor of 1.7023 [11, 39].

Herschel Bulkley vs. Bingham Model

As seen in equation 3.17, the shear stress (τ) must be larger than yield stress (τ_0) in order to initiate fluids to flow. This is the reason that yield stress causes a sudden change in the pressure when the fluid starts to move or when it is about to stop moving. However if the shear stress (τ) is lower than or equal to the yield stress (τ_0), the fluid will behave like a solid. Therefore during a drilling operation, any activities that change the fluid status between the static and dynamic condition will cause well pressure to change abruptly if the yield stress (τ_0) of the fluid deviates from zero [11].

Using Herschel Bulkley model the obtained yield point is more accurate compared to the Bingham model. Considering equation 3.10, the measured Bingham plastic yield point (YP) will always be larger than the shear stress at 3 *rpm* dial reading. This indicates that Bingham model overestimates yield point of the fluids.

Herschel Bulkley model has yield stress, and it suits best to the measured data at low shear rates. Therefore, it is preferred to Power-law and the Bingham plastic model [11, 39].

Of these reasons, the Herschel Bulkley model was used to estimate the yield stress or LSYS and reported as the YP of the drilling fluids during this master thesis.

3.8 Gravity

Isaac Newton was the first who described gravity in 1687. He stated gravity as an attractive force that acts between all particles with mass in the universe. Assume two objects with masses; m_1 and m_2 are interacting with each other. The gravitational force between these two objects is directly proportional to the product of the bodies' masses s and inversely proportional to the square of the distance between the centers of the objects. The proportionality constant is called gravitational constant, and the relationship between these parameters are shown as follow [40, 41]:

$$F = G \frac{m_1 m_2}{r^2}, [Pa] \tag{3.27}$$

Where:

F = Gravitational force

m_1 and m_2 = The masses of the objects interacting

r = The distance between the centers of the masses

G = The gravitational constant

As every planetary body in the universe, the Earth is surrounded by its gravitational field, which can be conceptualized with Newtonian physics as utilizing an attractive force on all bodies. The strength of the gravitational field is mathematically determined to be equal to the acceleration of objects under the Earth´s influence. A standard value of the gravity of purposes of weights and measures has defined by the International Bureau of Weights and Measures. The value denoted g and it is determined to be 9.80665 m/s^2 or 32.1740 ft/s^2 [41].

According to Newton´s third law, all interaction forces between two objects are equal in magnitude but with opposite direction. Based on this statement, when the Earth exerts a force on any falling object, at the same time the Earth itself experiences a force equal in magnitude but in the opposite direction to that. This means that both the falling objects and the Earth accelerate towards each other. However, due to the Earth´s enormous mass, the acceleration imparted to the Earth by this opposite force is negligible compared to the one by the object. For a falling body near the surface of the Earth, Newton´s law of universal gravitation simplifies to the product of the mass of the falling body and the constant vector g and is expressed as follow:

$$F = mg \tag{3.28}$$

Where:

F = The weight of the falling body

m = The mass of the body

From the equation of density, mass is equal to the product of density and volume ($m = \rho * V$). The higher the density, the higher the gravitational force [41, 42].

$$F = \rho * V * g \tag{3.29}$$

Applying Newton´s theory of gravity, in the HOL-arrangement, the net gravitational force acting on the heavy fluid is larger than the one on the light fluid. This results in pulling the heavy fluid beneath the light fluid and hence mixing the fluids.

3.9 Density

Density or volumetric mass density of a substance, element or a mixture defines as its mass per unit volume [43]. The density of any drilling fluid is determined mainly by the amount and the average specific density of the solids in the system [11]. In the industry, the drilling muds are usually weighted using an instrument so-called Baroid Mud Balance. Using this device density of the drilling fluid can be determined in pound per gallon (ppg). The measured density in *ppg* is an oil field unit, and it can be converted to specific gravity "sg" by dividing the obtained value to the density of water, which is 8.33 ppg at 16 °C [39].

Mathematically the density of drilling muds can be calculated by the following equation:

$$\rho_m = \frac{M_t}{V_t} = \frac{M_L + M_s}{V_L + V_s} \tag{3.30}$$

Where:

M_t = Total mass

V_t = Total volume

M_L = Mass of liquid (water or oil)

M_S = Mass of solids

V_L = Volume of liquid (water or oil)

V_S = Volume of solids

During the drilling operation, the density of the drilling mud determines the downhole pressure in the wellbore, which has to be equal or higher than formation pressure (pore pressure) and lower than formation fracturing pressure [5, 11]. The density can be changed due to several factors including downhole pressure and temperature, lost circulation, incorporated of drill cuttings, and gas cut. Therefore, it has to be corrected to the actual pressure and temperature at any depth in the wellbore [44, 45]. In order to maintain the density of drilling mud at the desired level, it is usually measured at regular intervals after it goes through the shaker and before it pumps down again into the well [25, 26].

3.10 Torque and Drag

During any drilling operation, the rotating drill pipe bears against the side of the casing and the wellbore wall. This happens partly because of the flexibility of the drill pipe, but also because no hole is truly vertical. This mechanism leads to increasing sliding friction forces and thereby increasing torque during rotation. In addition to friction forces, the drill pipe is also targeted to loads created by its weight (tension) and compressive force from the bottom of the well (compression). Summation of these loads will cause increasing the drag force during the raising and lowering the drill pipe. Increasing torque and drag can be large enough to cause loss of power under some particular circumstances such as highly deviated holes, undergauge holes, poor drill string dynamics and holes with frequent changes in the direction [5].

As mentioned before, the most significant challenge related to ERD is managing torque and drag. Increasing these mechanical loads brings severe limitation when drilling ERD-wells. Reducing the sliding friction force is the central mechanism behind the reduction of the torque and drag. The sliding friction force, in turn, depends on two factors including the normal contact force and the friction coefficient between the surface of the drill pipe and the wellbore wall (and the casing).

The amount of the normal force is determined by several factors such as the effective weight of the drill pipe, inclination, and azimuth of the wellbore. The friction coefficient depends on the degree of lubrication at various places in the wellbore and the specific contacting materials [5, 46].

A drilling mud with a proper lubricity property can significantly reduce the friction between the surfaces. It can also reduce the normal force due to buoyancy. Thereby, the reduction of torque and drag will be the result of these two properties of the drilling fluids [5, 10, 11, 33].

To provide such lubricity to WBMs is necessary to add lubricants into the mud system. Lubricants cause reduction of friction resistance and hence the power loss may be relieved. One of the commercial water-soluble lubricants is the triglyceride mixture that is used in WBMs to reduce torque [33]. It has also been shown that micronized polymers can reduce the friction factor in

WBMs [27, 47]. Though, the environmental impacts, high cost, changing the chemical properties and affecting on the other principal functions of the drilling fluid are those limitations of using the most effective additives to the WBMs [24, 48]. On the other hand, OBMs are excellent torque and drag reducers, especially in ERD-wells, due to their high lubricity. However, because of the environmental concerns usage of OBMs is highly restricted by the regulations, and they are also more costly compared to WBMs [47, 49].

3.11 Buoyancy

Physical law of buoyancy, also known as Archimedes principle, discovered by the ancient Greek mathematician and inventor, Archimedes, for more than 2000 years ago. He suggested that any object, partially or completely is submerged in a fluid (liquid or gas), is buoyed by a buoyant (upward) force. The amount of the force, exerted by the surrounding fluid, is equal to the weight of the fluid displaced by the object. For any object partially submerged in a liquid, the volume of the displaced fluid is equal to the fraction of the volume below the surface, while the volume of the displaced fluid is equivalent to the total volume of the body if it is fully immersed in the fluid.

In petroleum engineering field, the buoyancy factor for a drill pipe with the same fluid inside and outside can be calculated by the following formula [50]:

$$\beta = 1 - \frac{\rho_f}{\rho_s} \tag{3.31}$$

Where:

β = Buoyancy factor

ρ_f = Density of the fluid

ρ_s = Density of the pipe material (*usually steel*)

If the density of the fluid outside the pipe is larger than the density of the fluid inside the pipe, the general expression for buoyancy factor (β) will be as follows [5]:

$$\beta = \frac{w_T}{w_s} = \frac{w_s + w_i + w_o}{w_s} = 1 - \frac{w_o - w_i}{w_s} = 1 - \frac{\rho_o A_o - \rho_i A_i}{\rho_s A_s} \tag{3.32}$$

$$\beta = 1 - \frac{\rho_o r_o^2 - \rho_i r_i^2}{\rho_s (r_o^2 - r_i^2)} \tag{3.33}$$

Where:

ρ_o = Density of fluid outside the pipe

ρ_i = Density of fluid inside the pipe

ρ_s = Density of fluid drill pipe material (*usually steel*)

r_o = Outer radius of drill pipe

r_i = Inner radius of drill pipe

The effective weight of the drill pipe can be calculated by multiplying the weight of the drill pipe in the air with buoyancy factor (β). From the equation (3.33) it is clear that the buoyancy force will increase when the density of the outside fluid is larger than the density of the inside fluid and thereby decreasing the effective weight of the drill pipe [5].

3.12 Theory Of The Mixture

Theory of mixture is about modeling a multiphase system using the principle of continuum mechanics. Two miscible drilling fluids with different densities (ρ_h and ρ_l) and viscosities (μ_h and μ_l) will be mixed and result in a new mixture fluid. The density and the viscosity of the new fluid will differ from the two parent fluids and mathematically can be calculated using the following formulas [51]:

Determining the Density of the Mixture:

$$\rho_{mix} = \alpha_h \rho_h + (1 - \alpha_h)\rho_l \tag{3.34}$$

Where:

ρ_{mix} = Density of the mixture fluid

ρ_l = Density of the light fluid

ρ_h = Density of the heavy fluid

α_l = Volume fraction of the light fluid

α_h = Volume fraction of the heavy fluid

Determining the Viscosity of the Mixture

Similarly to the determining ρ_{mix}, the viscosity of the mixture (μ_{mix}) can be calculated as in following equation [51]:

$$\mu_{mix} = \alpha_h \mu_h + (1 - \alpha_h)\mu_l \tag{3.35}$$

Where:

μ_{mix} = Viscosity of the mixture fluid

μ_l = Viscosity the light fluid

μ_h = viscosity of the heavy fluid

α_l = Volume fraction of the light fluid

α_h = Volume fraction of the heavy fluid

3.13 Rayleigh-Taylor Instability Newtonian Fluids

Rayleigh-Taylor instability (RT-instability) occurs when two fluids with different densities, the heavier on the top of the light, are subjected to a constant acceleration such as the Earth´s gravity. Some examples of RT-instability include mushroom clouds like those from volcanic eruptions, atmospheric nuclear explosions, instability in plasma fusion reactors and the behavior of water suspended above oil in the gravity of Earth [52-54].

Rayleigh (1900) and later Taylor (1950) performed the first experiment for studying the instability of the interface between two superposed Newtonian fluids, water, and oil. The fluids are immiscible and have different densities. During their experiments, the more dense fluid (water) was placed on top of the less dense (oil). Both fluids were subjected to the Earth´s gravity acting perpendicularly to the interface between the fluids. Since the equilibrium is unstable, any disturbances of the interface cause the heavy to fall downward as spikes, and an equal volume of the lighter fluid will rise as a bubble into the heavy fluid (*figure 3-7*) [53, 55].
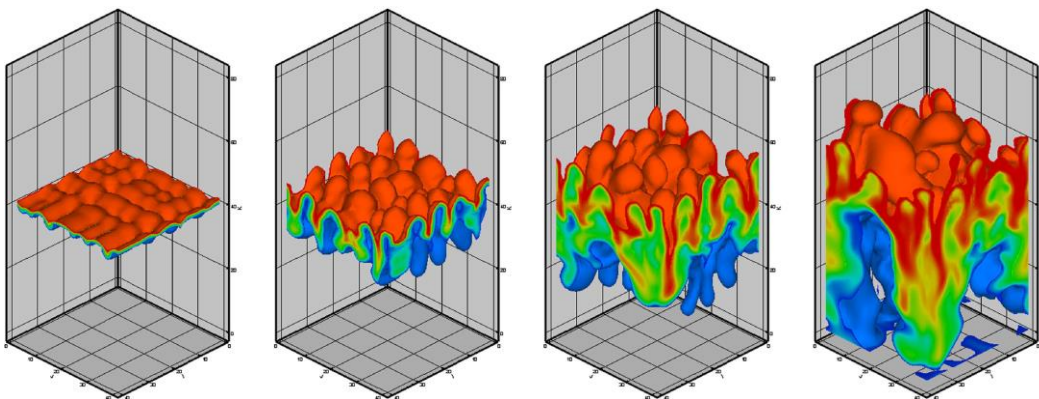
Figure 3-7: RT-instability at the interface between two Newtonian fluids at different period of time [55].

RT-instability develops at the interface as the result of so-called baroclinic torque. This torque is created by misalignment of the pressure and density gradient at the disturbed interface. The torque will, in turn, create vorticity (ω) and induce a velocity field (*figure 3-8*) that increases the baroclinic torque [56, 57].
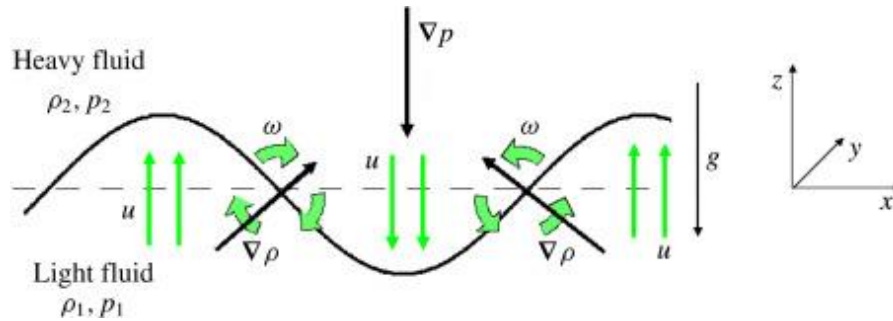
Figure 3-8: RT-instability model: A baroclinic torque at the interface creates vorticity and the induces a velocity field [57].

From the figure 3-10, one can observe two counter-rotating vorticity (ω) and velocity fields that sum at the peak and trough of the disturbed interface.

The RT-instability progress follows four main steps (figure 3-9). The first step starts with perturbations with smaller amplitude compared to their wavelength at the interface. The initial Perturbations have a sinusoidal shape in the early part of this stage. The fluid motion will follow an exponential model, which results from a linearization of the equation of motion. In the second stage, the small perturbation will grow into ubiquitous mushroom-shaped spikes and bubbles. The mushroom-shaped spikes are the structure of the heavy fluid into the light fluid, while the bubbles are the structure of the light fluid raised into the heavy fluid. The third stage is the interacting of the structures named in the second stage due to competition and bubble merging. During this stage, smaller bubbles and spikes combine to produce larger ones. The third stage results in the last stage, where a region of turbulent mixing is developed. This region assumed to be a self-similar and turbulent, where the Reynolds number is sufficiently large [52, 56, 58].
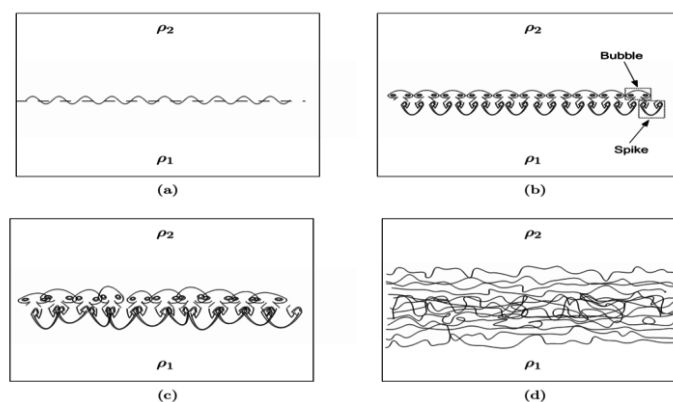
Figure 3-9: RT-instability occurs in four steps [58].

3.14 Rayleigh-Taylor Instability non-Newtonian Fluids

The similarity to Newtonian fluids, the RT-instability will occur when two non-Newtonian fluids of different density ($\rho_h > \rho_l$), are in a gravity field directed downwards. Such instability also occurs in the movement of the system with an acceleration directed from the heavier to the lighter fluid. As the instability develops, the bubble-fingering shape, as described above, will form with a constant velocity. The light fluid penetrates the heavy one in the form of bubbles, and the heavy fluid makes spikes in the light fluid [55].

3.15 Effect of The Rotational Force (γ)

When a drill string rotates, it creates a rotational force by its angular velocity. The force will, in turn, cause deformation of the fluid around the pipe. The fluid deformation will be highest at the wall of the drill pipe and will then be reduced as moving away from the pipe (see figure 3-10). The relationship between the shear rate and the angular velocity is given as follow [59]:

$$\gamma = \frac{\omega * r_{dp}}{r_w - r_{dp}} \tag{3.36}$$

Where:

γ = The shear rate

ω = The angular velocity

r_w = The inner radius of the well

r_{dp} = The out radius of the drill pipe

$r_w - r_{dp}$ = The gap between the wellbore wall and the pipe
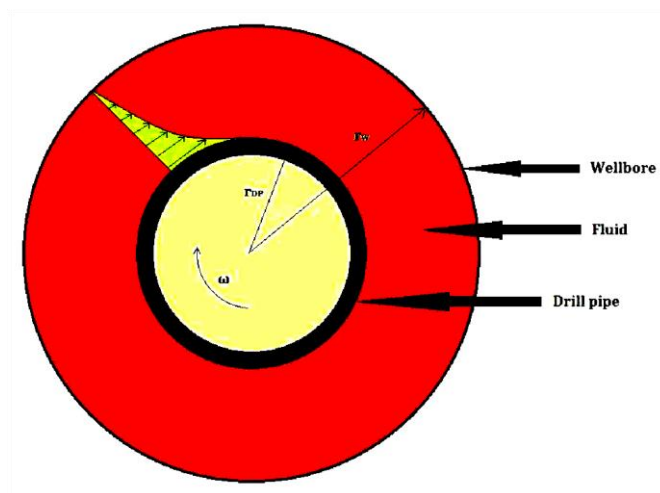
Figure 3-10: Rotation of drill pipe in the wellbore causes a rotational force [60].

41

For high rotation speed and a narrow annular gap between the wellbore and the pipe, the shear stress will increase. Considering the interface between the heavy and the light fluid in the HOL-arrangement, higher shear stresses may lead to a homogeneous mixing zone, which may probably prevent channeling. The rotational action on the mixing zone will be studied in more detail in Part I in chapter 6 and will be discussed in chapter 8.

3.16 Effect of Viscosity on The Instability at The Interface

Study of the effect of the viscosity on RT-instability has shown that these parameters have a significant impact on the interface between the fluids. In a study, it was shown that when two fluids of different rheological properties but with the same densities flowing upward in a vertical annulus, the interface stayed stable if the viscosity of the displacing fluid (*lower fluid*) was higher than the viscosity of the displaced fluid (*upper fluid*) [53].

Additionally, viscosity plays an important role in hole cleaning. It has been shown that cutting transport performance (CTP) could be improved by approximately 8% by increasing fluid viscosity as long as the flow regime remained turbulent and the velocity was kept constant. However, a further increase of viscosity leads to turn the flow regime into transient of laminar, which resulted in decreasing CTP by about 12% [61]. Therefore, in HOL-configuration using by Reelwell technology, it desired to keep the viscosity of the light fluid (active fluid) at the lowest possible level in order to provide a more efficient and optimal hole cleaning. The effect of the viscosity on the development of the mixing zone between the heavy and the light fluid will be studied as a part of this master thesis.

3.17 Stockes´s Law

Stockes´s law is an expression of the frictional force (*drag force*) that is exerted on a spherical particle (*object*), with a very small Reynolds number, settling in a viscous fluid. The Irish physicist and mathematician, George Gabriel Stokes, derived the law in 1851. The force is also known as Stocks' drag, and it acts on the interface between the fluid and the particle. Stocks' force is acting upward, i.e., on opposite direction to the Earth´s gravitational force (*figure 3-11*). The drag force can be expressed in the following equation [62]:

$$F_d = 6\pi\mu r v_t \qquad\qquad (3.37)$$

Where:

F_d = The drag force (frictional force)

μ = Dynamic viscosity of the fluid

v_t = Settling velocity (*terminal velocity*) of the falling particle

r = The radius of the spherical object

The gravitational force (F_g) that acts on the spherical object is a function of the volume of the object and the density difference (ρ_p-ρ_f) between the particle and the fluid (*due to buoyancy and weight*). F_g can be shown as follow:

$$F_g = (\rho_p - \rho_f)g\frac{4}{3}\pi r^3 \qquad (3.38)$$

Where:

F_g = Gravitational force

ρ_p = Density of the particle

ρ_f = Density of the fluid
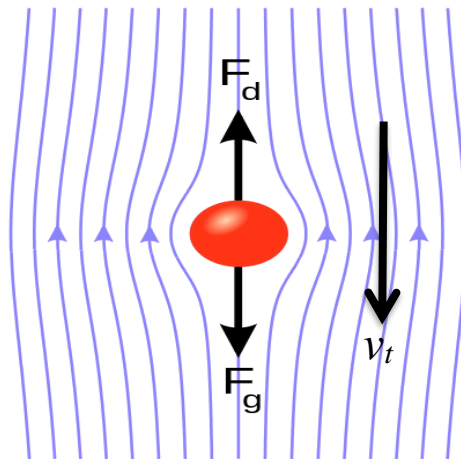
Figure 3-11: A falling particle through a viscous medium [63].

When the acting forces are in balance, i.e., $F_d = F_g$, the particle reaches a terminal velocity that can be expressed in the following equation [62]:

$$v_t = \frac{2r^2g(\rho_p - \rho_f)}{9\mu} \qquad (3.39)$$

Where:

V_t = Terminal velocity

μ = Viscosity of the fluids

r= Radius of the sphere

43

3.18 Effect Of Yield Stress On Suspending Particles

Drilling fluids, which usually are non-Newtonian Bingham fluids, introduce new factors into particle settling calculations as seen in Stokes´ law. Thus, the clay particles in a drilling mud system are subjected to surface shear forces, which occur due to the impact of the yield stress. The force acts upward in the opposite direction to the Earth´s gravitational force. Consider the clay particles as a spherical solid particle with the density (ρ_p) and a radius (r) moving in a drilling fluid. The particle is subjected to both the gravitational and surface force (*figure 3-12*).
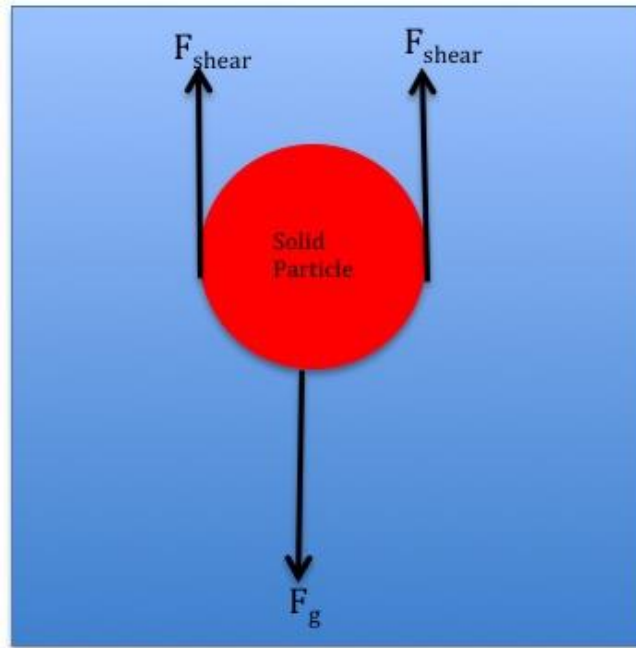
Figure 3-12: A suspended particle in a quiescent drilling mud system [60].

$$\Sigma F = F_{body} + F_{surface} \tag{3.40}$$

Where:

F_{body} = the gravitational force

$F_{surface}$ = shear stress force

The surface force consists of shear stress forces caused by yield stress from the drilling mud. This force is acting upwards, can be calculated as the product of yield stress and surface area of the particle.

$$y_s = \frac{F_y}{A_{surface}} \tag{3.41}$$

Since the yield point (YP) is the minimum yield stress required to carry the solid particle during dynamic condition the equation (3-41) can be rewritten as follow:

$$y_s = \frac{F_y}{A_{surface}} \tag{3.42}$$

$$F_{ys} = y_s * A_{surface} \tag{3.43}$$

When the gravitational force (equation 3.38) is equal to surface shear force (equation 3.43), the particle will be in equilibrium (suspended).

$$y_s * A_{surface} \geq (\rho_p - \rho_f)g\frac{4}{3}\pi r^3$$

$$y_s \geq \frac{(\rho_p - \rho_f)g\frac{4}{3}\pi r^3}{A_{surface}}$$

$$y_s \geq \frac{(\rho_p - \rho_f)g\frac{4}{3}\pi r^3}{4\pi r^2} = \frac{(\rho_p - \rho_f).r.g}{3}$$

$$y_s \geq \frac{(\rho_p - \rho_f).d_s.g}{6} \tag{3.44}$$

Where:

d_s = Diameter of the particle

ρ_p = Density of the particle

ρ_f = Density of the fluid

The suspended particles in a drilling fluid that exhibit gel properties will have a settling velocity that depends on several parameters. After including these parameters; the cross-sectional geometry, flow condition and particle concentration, the settling velocity can be expressed as follows [64]:

$$v_{sp} = \sqrt{\frac{4d_s g(\rho_s - \rho_f)}{3\rho C_D}}(1 - Y_a^{0.94}) \tag{3.45}$$

Where the parameter "Y_a" is shown in the following equation:

$$Y_a = \frac{3\tau_y}{d_s g(\rho_s - \rho_f)} \tag{3.46}$$

Where:

V_{sp} = particle settling velocity in Bingham plastic fluids

τ_y = The yield stress of the fluid

C_D = Drag coefficient of a sphere

Based on equation 3.44, it is seen that the particle will be maintained suspended when the yield stress is equal to or higher than the right term of the equation. The density difference between the solid particles (barite particles) and the medium (ρ_p-ρ_{mix}) in the mixing zone as well as in the light fluid section (ρ_p-$\rho_{light\text{-}fluid}$) is larger than $\Delta\rho$ (ρ_p-$\rho_{heavy\text{-}fluid}$) in the heavy fluid part. According to the statement in this equation, a higher yield point is probably required to keep the same particle suspended in the mentioned parts of the well compared to the heavy fluid section.

Based on the equation 3.46, the higher the yield stress of the drilling fluid the higher the parameter Y_a, which in turn slows down the settling velocity of the solid particles.

Therefore during this thesis, the main focus will be on investigation the effect of the gel properties of the fluids on the mixing zone to determine the minimum value of these properties, at which the growth of the mixing zone can be controllable.

3.19 MATLAB

MATLAB (Matrix Laboratory) is an extensive mathematical program with its scripting language based on "C" (imperative programming). Cleve Moler, who was a computer science and director at the University of New Mexico, started MATLAB's development in the late 1970s. Moler wanted to give students access to LINPACK and EISPACK without having to learn Fortran. MATLAB became requested and popular by other universities who also wanted to use MATLAB in education. MATLAB allows simple matrix manipulation, plotting of functions and data, implementation of algorithms, user interface creation and interfaces with other programming languages. MATLAB can be expanded with toolboxes. In principle, one can do everything with MATLAB as with C. The program is one of the most used mathematical software among engineers. There are tens of toolboxes that are used in MATLAB including Image processing toolbox that will be used during this master thesis to analyze the color changing of the mixing zone in a HOL-concept [65].

3.19.1 Image Processing Toolbox ^{TM}

Deploying this toolbox, one can perform a comprehensive series set of reference-standard algorithms and workflow for an image, including image analysis, processing, and algorithms development.

The photos of the development of the mixing zone between the heavy and light fluid in the column that was taken during each experiment from the start until the end of the mixing process, i.e., until the mixing zone is stabilized, will be analyzed concerning color space conversion. This procedure is based on quantitatively measuring color accuracy by analyzing pixel intensities cross-sections along line segments, a term so-called "improfile" in MATLAB [65].

3.19.2 Image Analysis of the Heavy Over Light

"Improfile" can retrieve the intensity values of pixels along a path or multiple paths and display the data on a plot. If the path is consist of a single line segment, a two-dimensional plot will be created, where the presented values on the x-axes are the distance along the line segment/segments, while the values of the y-axes are pixel intensities [65].

For the MATLAB code, please see Appendix F

4   Material and Equipment

4.1   List of Materials

Material	Description	Purpose of use	Fabrication
Fresh water	Regular tap water	Base fluid for preparing WBMs	Tap water
XC-polymer	It is a biopolymer	It provides higher viscosity, gel strength and yield point	
Bentonite	Clay minerals	Provides viscosity to the drilling fluid and reduces fluid-loss	Satisfies API and EOCMA
Lignosulfonate	It is a dispersant made from Byproduct from cellulose production. It is a drilling mud thinner	It was used for control of viscosity, yield point, gel strength and fluid loose. It works best at pH-level > 10.00	M-I SWACO Schlumberger
Anti-foam agent	Silicon anti-foaming agent	It was used to remove/reduce air bubbles in the mud system especially when using Lignosulfonate.	Merck KGaA Germany
Barite ($BaSO_4$)	Weighting agent: A dense sulfate that has a specific density of ca. 4.2 to 4.60 sg	It was used for increasing density of the drilling mud.	M-I SWACO Schlumberger
NaOH	Sodium hydroxide, also known as caustic soda	It was used to increase pH-level of the drilling mud, especially when using lignosulfonate.	
Metal oxides: (Cr_2O_3 and Fe_2O_3)	Chrome oxide and iron oxide pigments	They were used as the color indicator to differentiate between the heavy (red)-and the light (green) drilling fluids and to give a good contrast while taking photos during the rotation procedure on the rig.	Kremer Pigmente GmbH & Co.KG Germany
1,2-propylene glycol	Antifreeze agent, red and blue color	It was used to study the effect of rpm on the development of mixing zone at the HOL-interface.	Biltema Norway

Table 4-1:List of the materials

4.2 List of Equipment:

The list of the actual figures of the equipment is found in Appendix A.

Equipment	Description	Purpose of use	Fabrication
Protective glasses	Special laboratory safety eyewear	Used to protect the eyes from hazardous liquids or objects.	
Laboratory scale	An accurate measuring tool. It can measure from 0.10g up to 1300g	Used to precisely weight quantity of the materials	
Heidoph-Overhead Stirrer RZR 50	Consist of a head and a mixing stand	Used to prepare drilling fluids	Heidolph /Germany
Baroid Mud balance	It is a device that consists of a base and graduated arm with lid, cup, knife-edge, built-in spirit level, rider, and counter-weight. It has the unit pound per gallon (ppg), and it is calibrated to specific density of fresh water (8.33 ppg)	It is a device that provides a simple method for the accurate measurement of mud density.	
Fann-viscometer VG-35	It consists of a rotational cylinder and bob instrument with seven rotations (600, 300, 200, 100, 60, 30, 6 and 3 rpm) available. It is also called direct-indicating because at a given speed (rpm) the dial reading ($^0\theta$) is a true unit for viscosity (cP)	It is used to measure viscosity and gel strength of drilling mud. Using dial reading at different rpm, rheological parameters, such as plastic viscosity (PV), apparent viscosity (η) yield point (YP) and gel strength can be calculated using rheological models	Fann instrument company /USA
Drilling Machine	A regular electric drilling machine	Used to rotate the drill pipe inside the casing	Bosch
Laboratory stand	A metal stand of 230 cm with an arm	Used to hold the drilling machine	UIS Workshop
Trestle (jack) stand	Consists of three legs with adjustable height	Used to hold the casing (acrylic tube) during experiments performed in horizontal direction.	Bought at Biltema Norge
Acrylic cylinder	Acrylic tube with length of 200 cm and ID of 1.0 cm , 2.0 cm and 3.0 cm	Used as casing/well	
Aluminum rod	An aluminum with length of 200 cm and OD of 0.60, 1.2, 2.0and 2.55 cm	Used as drill pipe rotation inside the casing	UIS workshop
Transparent hose connected to funnel	Plastic hose connected to a funnel	Used to fill the lower part of the casing with light fluid to avoid contamination of the upper part	
Mechanical pump	A manual pump with capacity of 500ml connected to a 30cm long plastic hose	Used to pump down the heavy fluid into the casing after running the drill pipe inside the casing	BilXtra Norway
Measuring tape	A flexible ruler made of aluminum	Placed alongside the casing to measure the height/length of the mixing zone	Biltema /Norway
Camera	iPhone 7-plus camera with multiple self-timer shooting application	Used to take pictures each 30-second during the experiments. The images were used to observe and document the development of the mixing zone	iPhone
LED-lamp	1-meter LED lamp	Placed behind the casing to provide a excellent background for the pictures taken during the procedure.	IKEA
Protecting Cabin	(70 cm X 70 cm X 200 cm) cabin covered by blackout curtains	Used for housing of the rig. Protecting the rig (casing) from disturbing lights while taking pictures during the experiments.	Designed by the author and made in UIS workshop

Table 4-2: List of the equipment

5   Working Procedures

5.1   Well Design In The Horizontal Direction

The well in the horizontal direction was represented by a plastic hose with the length of 10.0 m and 1.0cm in the inner diameter. A hard wire with the outer diameter of 0.60 cm, which represented the drill pipe, was mounted to a drilling machine during the experiments. Since no any mixing between the fluids was observed, the length of the well was reduced to 2.0 m. Of this purpose acrylic cylinders with different inner diameters (*2.0 cm and 3.0 cm*) were used. The cylinder was set on jack stands, and a measuring tape was mounted along the cylinder.

Setting the rotation *rpm* of this type of drilling machine on a fixed speed was not possible. It varied between 50 up to 350 *rpm*. The speed was estimated by accounting the number of the rotations per time using a slow-motion video camera.
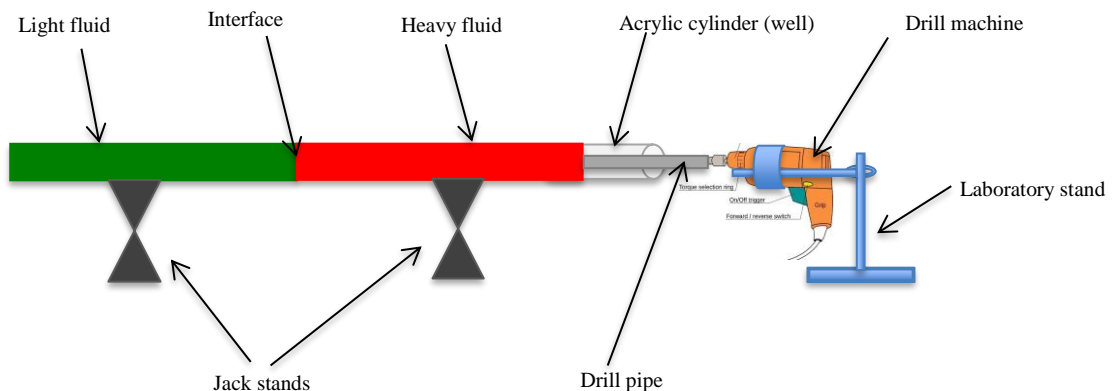
Figure 5-1: A schematic set-up of the well in horizontal direction [60].

5.2   Rig Design In The Vertical Direction

A simple small-scale experimental rig was build, where an aluminum rod, representing the drill string, was rotated in an acrylic cylinder, representing the wellbore/casing. Then, the cylinder was placed in a cabin covered by blackout curtains to protect the experiments from the disturbing lights while taking photos during the procedure. The drilling machine was mounted on a laboratory stand with an adjustable height of up to 2.50 m. A LED-lamp was placed inside the cabin just behind the cylinder to provide light and hence a contrasting background.

The light fluid was placed in the lower part of the acrylic cylinder with the heavy fluid on the top. Two different color indicators, green in the light and red in the heavy fluid, were used.

The actual photos of the rig and the well are shown in Appendix B.
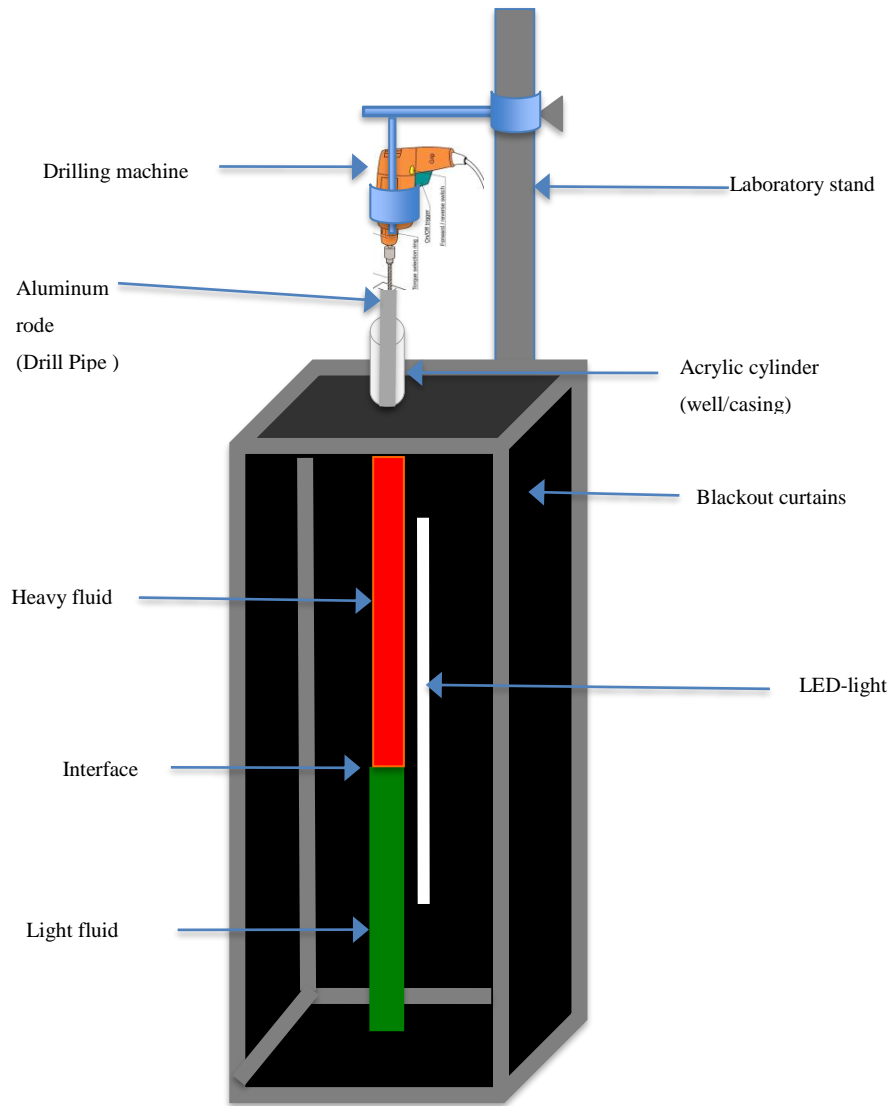
Figure 5-2: A schematic set-up of the rig in vertical direction [60].

5.3 General Experimental Set-Up

The entire work of this master thesis was divided into four main parts to investigate the impact of different parameters on the development of the mixing zone at the interface between the heavy and the light fluid in the HOL-configuration. These parameters include the effect of *rpm* and the rheological parameters of the fluids such as viscosity, gel strength and the yield point. A number of experiments were performed and repeated to get statistically significant data and observations. The fluid specifications and other data are presented in the tables in chapter 6. The visually estimated height of the mixing zone during each experiment is also recorded and shown in the same tables.

The work started with performing a group of experiments in the horizontal direction (*figure 5-1*) in order to study the effect of *rpm* on the mixing zone. The effect of this parameter was also studied in the vertical direction. Furthermore, the rest of the experiments, during this work, were performed only in the vertical direction using the rig shown in figure 5-2. Each experiment was performed in three main steps as follows:

1. Preparing The Drilling Muds

The deploying drilling fluids were simple WBMs that were prepared by mixing water, xanthan-XC polymer and bentonite (**premixed mud**). From this pre-mixture both the light and the heavy fluids, with desired density, were further prepared by adding barite. Lignosulfonate was added for diluting the mud systems or adjusting the gel strength and the yield point. NaOH was added to increase the pH-level of the fluids when using lignosulfonate. Metal oxides with two different the colors were used as color indicator. Furthermore, an anti-foaming agent was added to reduce the air bubbles in the mud systems. The procedure is described in detail in Appendix C.

2. Measuring The Rheological Characteristics

Before transferring the drilling fluids into the cylinder (well), the density and rheological properties were measured as described in Appendix C. The measured data were plotted using the rheological models, the Bingham Plastic and Herschel Bulkley model (*see Appendix E).* The purpose of the analysis of the rheological properties was to find the best suitable rheological model and thereby determine the plastic viscosity and gel properties of the fluids.

The plastic viscosity was determined using the Bingham plastic model. It was found that the measured data of the fluids fitted best to the Herschel Bulkley model, especially at low shear rates. Therefore, the second mentioned model was used to determine the yield stress of the fluids. Equation 3.19 was used to calculate the low shear yield stress (LSYS) directly from dial reading at

θ_3 and θ_6 on the viscometer. The obtained values were reported as the yield point (YP) of the fluids. The calculated yield points should multiply by the factor of 1.067 (*equation 3.20*) in order to be expressed in lb/100ft^2, but this was neglected since the factor is insignificant.

3. Transferring The Fluids into The Well

The lower part, with a depth of about 1 m, of the cylinder was filled with the light fluid (*green colored*) using a funnel connected to a smaller plastic hose. The plastic hose was long enough to reach the bottom of the cylinder. This was done to prevent the upper part of the well from being contaminated by the light fluid. Afterward, the aluminum rode was set inside the cylinder and placed in the cabin. The cylinder was then fastened to the bottom and top of the rig using strong tape. The drilling machine was connected to the pipe and rotation was started. A camera was mounted on the camera stand and placed in the cabin. While rotating the drill pipe, the heavy fluid (*red colored*) was added into the upper part of the well with the help of a mechanical pump.

During the experiments, photos of the mixing zone were taken at regular time intervals of 30 sec. The height of the mixing zone was determined by analyzing the images visually, and the results were reported in the tables in chapter 7. An image analysis tool in MATLAB was also used to verify the results of all experiments in part IV.

Mathematical Calculation of The Height of The Mixing Zone

Since the drilling fluids were not transparent, another practical method was used to verify the results of few experiments in part IV. The purpose of this method was to confirm that the images did not only represent the color of the surface inside the cylinder.

The procedure was performed as follow:

At the end of the selected experiments, and before pulling out the pipe out of the well, the heavy fluid on the top of the mixing zone was collected. It was important to perform this step carefully to make sure that the gathered heavy fluid was pure and non-contaminated with the light fluid. The volume of the fluid was then measured and subtracted from the volume before starting the experiment. Thus, the difference between the volumes assumed to be the amount of the heavy fluid that had mixed with the light fluid in the mixing zone. Since the cross-sectional area of the gap between the well and the pipe was known, the height of the mixing zone was calculated and compared to the one that observed visually. The density of the collected heavy fluid was also measured and compared to the density before starting the experiments. To see the whole procedure in detail, please the see Appendix D.

6 Experimental Data & Result Overview

All experiments were performed according to HSE- standards of the University of Stavanger at room temperature and atmospheric pressure.

6.1 Part I: Effect Of The Pipe Rotation

Impact of *rpm* on the development of the mixing zone was studied in both horizontal and vertical direction.

Experiments In The Horizontal Direction

In this part of the work, it was performed eight experiments employing regular WBMs with same as well as different densities and rheological properties. Additionally, different pipe/well combinations were employed. The fluid specifications and the other data, as well as the observed height of the mixing zone, is presented in table 6-1.

During performing experiments 1, 2, 3 and 4, premixed muds with the same density and relative similar gel properties were tested. The rotation speed of the pipe was varied between 50 up to 350 *rpm,* and the experiments were run for 30 minutes.

However, during experiments 5, 6, 7 and 8, the light fluid was similar to the one used in the previous experiments, while the density of the heavy fluid was set to be 1.35 sg. Each experiment was run for about 45 min. During the process, photos were taken at regular intervals and the visually determined height of the mixing zone is recorded and presented in the table.

Exp. nr.	Density of fluids [sg]		Plastic viscosity of fluids [cP]		Yield point of fluids [100lb/ft^2]		Well and Drill pipe dimension			Rotation data [speed and time]		Result Overview
	Light fluid ρ_l	Heavy fluid ρ_h	Light fluid $(PV)_l$	Heavy fluid $(PV)_h$	Light fluid $(YP)_l$	Heavy fluid $(YP)_h$	Well ID [cm]	Drill pipe OD [cm]	Well length [cm]	Rotation speed [rpm]	Rotation time [min]	Length of Mixing zone [cm]
1	1.02	1.02	6	6	5	5	1.0	0.70	1000	50-350	30	≈ 0
2	1.02	1.02	6	6	5	5	2.0	1.2	200	50-300	30	≈ 0
3	1.03	1.03	7	7	5.5	5.5	3.0	2.0	200	100-230	30	≈ 0
4	1.03	1.03	7	7	5.5	5.5	3.0	1.5	200	100-230	30	≈ 0
5	1.03	1.35	7	12	6	26	1.0	0.70	500	50-300	45	≈ 0
6	1.03	1.35	7	12	6	26	2.0	1.20	200	50-300	45	≈ 5
7	1.02	1.35	6.5	13	5	24	3.0	2.50	200	50-300	45	≈ 3.5
8	1.02	1.35	6.5	13	5	24	3.0	2.0	200	50-350	45	≈ 9

Table 6-1: Experimental data, where the effect of *rpm* in the horizontal direction was studied.

Experiments In the Vertical Direction:

During this part, 1,2-propylene glycol with two different colors but with the same properties was used. The glycol was diluted with water in order to get a plastic viscosity of around 7 to 8 cP. The mixture behaved as a Newtonian fluid without exhibiting any gel properties.

The lower part of the well was filled with blue colored glycol (*up to ca. 1 m*) with the red colored on the top. The rotation speed of the pipe was set on about 50 to 350 *rpm*. Three experiments utilizing three different pipe/well combinations were performed. Each experiment was run for 40 to 50 min, and photos were taken at an interval of 30 sec to monitor the mixing zone. The fluid specifications and other data are presented in table 6-2.

Exp. nr.	Density of fluids [sg]		Plastic viscosity of fluids [cP]		Yield point of fluids [100lb/ft^2]		Well and drill pipe dimension			Rotation data [speed and time]		Result Overview
	Lower fluid ρ_l	Upper fluid ρ_h	Lower fluid $(PV)_l$	Upper fluid $(PV)_h$	Lower fluid $(YP)_l$	Upper fluid $(YP)_h$	Well ID [cm]	Drill pipe OD [cm]	Well depth [cm]	Rotation speed [rpm]	Rotation time [min]	Length of Mixing zone [cm]
1	1.05	1.05	8	8	0	0	3.0	2.5	200	50-350	50	Stable
2	1.05	1.05	8	8	0	0	3.0	2.0	200	50-350	40	Stable
3	1.05	1.05	8	8	0	0	1.0	0.6	200	50-350	40	Stable

Table 6-2: Experimental data, where the effect of *rpm* in the vertical direction was studied.

6.2 Part II: Effect of The Viscosity

The study of the effect of the viscosity on the mixing zone was carried out by performing two groups of experiments, where using different types of light fluids with different densities and gel properties. However, the heavy fluids had relative similar rheological characteristics in both groups.

Group nr. 1

The first group included four experiments using regular WBMs as the heavy fluid (*red colored*) while the light fluid (*blue colored*) was made of mixing 1,2-propylene glycol with water and adding salt (NaCl) as the weighting agent.

For experiments 1 and 2, both the heavy and the light fluids had relative similar plastic viscosity while they were different in densities. However, in experiments 3 and 4, both fluids had the same density and plastic viscosity.

The fluid specifications, wellbore data, as well as the visual observation of the mixing zone are shown in table 6-3.

Group nr. 1		**Heavy Fluid**	Water + Xanthan Polymer + Bentonite + Barite											
		Light Fluid	water + NaCl+ + 1,2-popylenglycol											
	Density of fluids [sg]		Plastic viscosity [cP]		Yield point [100lb/ft^2]		Gel strength (10 sec/10 min) [100lb/ft^2]		Well and drill pipe dimensions			Rotation data [speed and time]		Result Overview
Exp. nr.	Light fluid ρ_l	Heavy fluid ρ_h	Light fluid (PV)$_l$	Heavy fluid (PV)$_h$	Light fluid (YP)$_l$	Heavy fluid (YP)$_h$	Light fluid	Heavy fluid	Well ID [cm]	DP. OD [cm]	Well depth [cm]	Speed [rpm]	Time [min]	Height of Mixing zone [cm]
1	1.1	1.21	7.5	9	1	13	1 / 1	15 / 26	3.0	2.0	200	50-300	0.70	Completely mixed ≈ 190
2	1.1	1.21	7.5	9	1	13	1 / 1	15 / 26	3.0	2.0	200	50-300	0.70	≈ 190
3	1.1	1.10	7	7.5	1	7	1 / 1	11 / 21	3.0	2.0	200	50-300	5 min	≈ 190
4	1.1	1.10	7	7.5	1	7	1 / 1	11 / 21	3.0	2.0	200	50-300	5 min	≈ 190

Table 6-3: Experimental data and the observed results of the 1st group of experiments, where the effect of PV was studied.

Group nr. 2

For the second group, premixed drilling mud with sufficient gel strength and yield point was used as the light fluid. The density and the rheological properties of the heavy fluid were the same as used in the group 1.

The experiments were set up as described in the previous sections and they were run for 30 minutes.

The fluid specifications and the observed height of the mixing zone are presented in table 6-4.

Group nr. 2		Heavy Fluid	Water + Xanthan-polymer + Bentonite + Barite											
		Light Fluid	**Water + Xanthan-polymer + Bentonite**											
	Density of fluids [sg]		Plastic viscosity [cP]		Yield point [100lb/ft^2]		Gel strength (10 sec/10 min) [100lb/ft^2]		Well and drill pipe dimensions			Rotation data [speed and time)		Result Overview
Exp. nr.	Light fluid ρ_l	Heavy fluid ρ_h	Light fluid (PV)$_l$	Heavy fluid (PV)$_h$	Light fluid (YP)$_l$	Heavy fluid (YP)$_h$	Light fluid	Heavy fluid	Well ID [cm]	DP. OD [cm]	Well dep. [cm]	Speed [rpm]	Time [min]	Height of Mixing zone [cm]
1	1.03	1.20	7	14	10	17	13 / 26	23 / 37	3.0	2.0	200	50-300	30	≈ 12
2	1.03	1.20	6	15	8	14	12 / 23	21 / 32	3.0	2.0	200	50-300	30	≈ 22
3	1.03	1.20	7	13	7	12	11 / 20	18 / 29	3.0	2.0	200	50-300	30	≈ 28
4	1.03	1.20	6	13	5	12	9 / 19	18 / 29	3.0	2.0	200	50-300	30	≈ 41

Table 6-4: Experimental data and the observed results of the 2nd group of experiments, where the effect of PV was studied.

6.3 Part III: Effect of The Gel Properties

The impact of the gel properties, the yield point, and gel strengths, of the heavy and the light, was studied separately by performing two groups of experiments on the rig shown in figure 5-2. The first group included the experiments where the gel strength and the yield point were kept relatively constant while reducing these properties of the light fluid. However, in the second group, the mentioned properties were maintained at a regular interval for the light fluid while decreasing them for the heavy fluid.

The fluids were WBMs and prepared by adding barite as weighting material into the premixed drilling mud (Water + xanthan-polymer + bentonite) The density of the light and the heavy fluid were set at 1.10 sg, and 1.30 sg respectively. Thus, the density difference, $\Delta\rho$ (ρ_h -ρ_l), was 0.20 sg during all the experiments in this part of the work.

Effect of The YP and Gel Strengths of The Light Fluid

For this part, it was performed seven experiments, where the yield point of the light fluid was stepwise reduced from 14 lb/100ft^2 (*experiment 1*) down to 4 lb/100ft^2 (*experiment 7*) as seen in table 6-5. The experiments were planned in such way that one could perform 2 or 3 experiments using the same heavy fluid. Thus, it was possible to maintain the yield point of the heavy fluid between 11.5 and 12.5 lb/100ft^2. The tests were run for up to 45 min depending on the stability of the mixing zone.

Based on the visual analysis of the photos, the observed height of the mixing zone of the experiments was recorded and presented in the table below.

Exp. nr.	Density of fluids [sg]		Plastic viscosity [cP]		Yield point [100lb/ft^2]		Gel strength (10 sec/10 min) [100lb/ft^2]		Well and drill pipe dimension			Rotation Data		Result Overview
	Light fluid ρ_l	Heavy fluid ρ_h	Light fluid (PV)$_l$	Heavy fluid (PV)$_h$	Light fluid (YP)$_l$	Heavy fluid (YP)$_h$	Light	Heavy	Well ID [cm]	DP. OD [cm]	Well dep. [cm]	Speed [rpm]	Time [min]	Height of Mixing zone [cm]
1	1.10	1.30	8	17	14	12.5	15 / 28	21 / 37	3.0	2.0	200	50-300	40	≈ 0
2	1.10	1.30	7.5	17	11	12.5	13 / 24	21/37	3.0	2.0	200	50-300	40	≈ 8
3	1.10	1.30	8	17	8.5	12.5	12 / 22	21/ 37	3.0	2.0	200	80-250	40	≈ 23
4	1.10	1.30	6	15	7	11.5	11 / 19	19 / 33	3.0	2.0	200	50-300	40	≈ 28
5	1.10	1.30	6	15	6.5	11.5	9 / 18	19 / 33	3.0	2.0	200	50-300	40	≈ 32
6	1.10	1.30	6	15	5.5	11.5	7 / 14	19 / 33	3.0	2.0	200	50-300	40	≈ 40
7	1.10	1.30	6.5	15	4	12	4 / 9	20 / 34	3.0	2.0	200	50-300	5	Completely mixed ≈ 190

Table 6-5: Experimental data and the observed results, where the effect of the YP of the light fluid was studied.

Effect of The YP and Gel Strengths of The Heavy Fluid

For this group of experiments, the yield point of the heavy fluids was reduced from 15 lb/100ft^2 (*experiment 1*) to 2 lb/100ft^2 (*experiment 6*). The mentioned property of the light fluid was kept between 9.5 and 11 lb/100ft^2. The experiments were run for up to 45 min and the rotation speed of the pipe was assumed to be between 50 and 300 *rpm*. The experimental data, and the visually estimated height of the mixing zone are shown table 6-6.

Exp. nr.	Density of fluids [sg]		Plastic viscosity [cP]		Yield point [100lb/ft^2]		Gel strength (10 sec/10 min) [100lb/ft^2]		Well and drill pipe dimension			Rotation Data		Result Overview
	Light fluid ρ_l	Heavy fluid ρ_h	Light fluid $(PV)_l$	Heavy fluid $(PV)_h$	Light fluid $(YP)_l$	Heavy fluid $(YP)_h$	Light fluid	Heavy fluid	Well ID [cm]	DP. OD [cm]	Well dep. [cm]	Speed [rpm]	Time [min]	Height of Mixing zone [cm]
1	1.10	1.30	7	14	11	15	14 / 27	19 / 32	3.0	2.0	200	≈ 50-300	45	≈ 0
2	1.10	1.30	7	16	11	12	14 / 27	16 / 25	3.0	2.0	200	≈ 50-300	45	≈ 3
3	1.10	1.31	9	8	10	8	15 / 25	9 / 22	3.0	2.0	200	≈ 50-300	45	≈ 21
4	1.10	1.30	8	17	10	6	15 / 25	8 / 19	3.0	2.0	200	≈ 50-300	45	≈ 26
5	1.10	1.30	8	13	9.5	4.5	13 / 23	6 / 11	3.0	2.0	200	≈ 50-300	45	≈ 33
6	1,10	1.30	8	9	9.5	2	13 / 23	2 / 4	3.0	2.0	200	≈ 50-300	5	Completely mixed ≈ 190

Table 6-6: Experimental data and results overview, where the effect of the YP of the heavy fluid was studied.

6.4 Part IV: The Growth of The Mixing Zone

In part III the impact of the yield point and the gel strengths of the heavy and the light fluid was studied by maintenance $\Delta\rho(\rho_h-\rho_l)$ constant. The purpose of performing this part of the work was studying the growth of the mixing zone as the function of both $\Delta\rho(\rho_h-\rho_l)$ as well as the gel properties of the fluids. During this of the work, it was performed four groups of experiments of four different $\Delta\rho$ ($\rho_h-\rho_l$). The density of the light fluid for all groups was set at 1.10 sg while increasing the density of the heavy fluid from 1.40 sg up to 1.80 sg.

Within each group, it was performed four experiments, where the yield point of the fluids was set at four intervals as presented in table 6-7.

Experiment nr.	The yield points of the fluids [lb/100ft²]	Comments
Exp. 1	$28 \leq YP_{(heavy\ f.)} \leq 34$ $10 \leq YP_{(light\ f.)} \leq 12$	
Exp. 2	$12 \leq YP_{(heavy\ f.)} \leq 14$ $10 \leq YP_{(light\ f.)} \leq 12$	The same $(YP)_{light\ f.}$ as for experiment 1 while the $(YP)_{heavy\ f.}$ was reduced.
Exp. 3	$12 \leq YP_{(heavy\ f.)} \leq 14$ $6 \leq YP_{(light\ f.)} \leq 6.5$	The same $(YP)_{heavy\ f.}$ as for experiment 2 while the $(YP)_{light\ f.}$ was reduced
Exp. 4	$6.5 \leq YP_{(Heavy)} \leq 7.5$ $6 \leq YP_{(Light)} \leq 6.5$	The same $(YP)_{light\ f.}$ as for experiment 3 while the $(YP)_{heavy\ f.}$ was reduced

Table 6-7: Experimental set-up of each group of experiments in part IV.

Group nr. 1 ($\Delta\rho = 0.30$ sg)

It was performed four experiments with the density of the heavy fluid of 1.40 sg. Barite was added as weighting material; thereby the rheological properties of the fluids were regulated by adding lignosulfonate into the mud system. The fluid specifications and other data, as well as the height of the mixing zone are presented in table 6-8.

Group number: 1														
	Density of fluids [sg]		Plastic viscosity [cP]		Yield point [100lb/ft²]		Gel strength (10 sec/10 min) [100lb/ft²]		Well and drill pipe dimension			Rotation Data		Result Overview
Exp. nr.	Light fluid ρ_l	Heavy fluid ρ_h	Light fluid $(PV)_l$	Heavy fluid $(PV)_h$	Light fluid $(YP)_l$	Heavy fluid $(YP)_h$	Light fluid	Heavy fluid	Well ID [cm]	DP. OD [cm]	Well dep. [cm]	Speed [rpm]	Time [min]	Height of Mixing zone [cm]
1	1.10	1.41	7	17	10	28	14 / 27	34 / 50	3.0	2.0	200	50-350	45	≈ 3
2	1.10	1.40	7	12	10	14	14 / 27	24 / 37	3.0	2.0	200	50-300	45	≈ 7
3	1.10	1.40	10	12	**6**	14	**8 / 19**	24 / 37	3.0	2.0	200	50-300	43	≈ 12
4	1.10	1.40	10	12	6	6.5	9 / 25	10 / 24	3.0	2.0	200	50-300	45	≈ 21

Table 6-8: Experimental data and result overview of the 1st group of experiments ($\Delta\rho$ of 0.30 sg)

Group nr. 2 (Δρ = 0.50 sg)

For this group of tests, the density of the heavy fluid was set at about 1.60 sg. The measured rheological and the physical properties of the fluids, as well as other specific data of four experiments, are presented in table 6-9. The height of the mixing zone for each test was visually estimated, and shown in the same table.

Group number: 2													
	Density of fluids [sg]		Plastic viscosity [cP]		Yield point [100lb/ft^2]		Gel strength (10 sec/10 min) [100lb/ft^2]		Casing and drill pipe dimension			Rotation Data		Result Overview
Exp. nr.	Light fluid ρ_l	Heavy fluid ρ_h	Light fluid $(PV)_l$	Heavy fluid $(PV)_h$	Light fluid $(YP)_l$	Heavy fluid $(YP)_h$	Light fluid	Heavy fluid	Well ID [cm]	DP. OD [cm]	Well dep. [cm]	Speed [rpm]	Time [min]	Height of Mixing zone [cm]
1	1.10	1.60	8	17.5	12	32	19 / 37	39 / 54	3.0	2.0	200	50-300	45	≈ 6
2	1.10	1.60	7	14	10.5	13.5	15 / 33	17 / 32	3.0	2.0	200	50-300	45	≈ 14
3	1.10	1.60	8.5	14	6	13.5	10 / 19	17 / 32	3.0	2.0	200	50-350	60	≈ 19
4	1.10	1.60	8.5	11	6	7	10 / 19	9 / 16	3.0	2.0	200	50-300	60	≈ 70

Table 6-9: Experimental data and result overview of the 2nd group of experiments (Δρ of 0.50 sg)

Group nr. 3 (Δρ = 0.62 sg)

The heavy fluid was prepared with the density of about 1.72 sg, and its viscosity was kept between 11 and 16 cP with the help of adding lignosulfonate. The fluid specifications were measured, and the height of the mixing zone for each test was visually estimated. All necessary data are shown in table 6-10.

Group number: 3													
	Density of fluids [sg]		Plastic viscosity [cP]		Yield point [100lb/ft^2]		Gel strength (10 sec/10 min) [100lb/ft^2]		Casing and drill pipe dimension			Rotation Data		Result Overview
Exp. nr.	Light fluid ρ_l	Heavy fluid ρ_h	Light fluid $(PV)_l$	Heavy fluid $(PV)_h$	Light fluid $(YP)_l$	Heavy fluid $(YP)_h$	Light fluid	Heavy fluid	Csg. ID [cm]	DP. OD [cm]	Well dep. [cm]	Speed [rpm]	Time [min]	Height of Mixing zone [cm]
1	1.10	1.70	8	16	12	33	16 / 29	35 / 62	3.0	2.0	200	50-350	45	≈ 10
2	1.10	1.72	8	18	12	14	16 / 29	17 / 32	3.0	2.0	200	50-350	60	≈ 16
3	1.10	1.72	8.5	18	6.5	14	8 / 18	17 / 32	3.0	2.0	200	50-350	65	≈ 82
4	1.10	1.72	8.5	11	6.5	7.5	8 / 18	10 / 22	3.0	2.0	200	50-350	5	Completely mixed ≈ 190

Table 6-10: Experimental data and result overview of the 3rd group of experiments (Δρ of 0.60 sg)

Group nr. 4 ($\Delta\rho(\rho_h - \rho_l) = 0.71$sg)

The heavy fluid was prepared with the density of about 1.81 sg, which was the largest density tested during this master thesis. The experimental data and the result overview are shown in table 6-11.

Group number: 4		$\rho_2 - \rho_1 = 1.81 - 1.10 = 0.71$ sg											
	Density of fluids [sg]		Plastic viscosity [cP]		Yield point [100lb/ft²]		Gel strength (10 sec/10 min) [100lb/ft²]		Casing and drill pipe dimension			Rotation Data		Result Overview
Exp. nr.	Light fluid ρ_l	Heavy fluid ρ_h	Light fluid $(PV)_l$	Heavy fluid $(PV)_h$	Light fluid $(YP)_l$	Heavy fluid $(YP)_h$	Light fluid	Heavy fluid	Csg. ID [cm]	DP. OD [cm]	Well dep. [cm]	Speed [rpm]	Time [min]	Height of Mixing zone [cm]
1	1.10	1.81	8.5	16	10	31	14 / 26	36 /57	3.0	2.0	200	50-350	60	≈ 18
2	1.10	1.80	8.5	18	10	12	14 / 26	15 / 32	3.0	2.0	200	50-350	50	≈ 28
3	1.10	1.80	7.5	18	6	12	7 / 13	15 / 32	3.0	2.0	200	50-350	60	≈ 85
4	1.10	1.81	7.5	19	6	7	7 / 13	9 / 17	3.0	2.0	200	50-350	5	Completely mixed ≈ 190

Table 6-11: Experimental data and result overview of the 4th group of experiments ($\Delta\rho$ of 0.70 sg)

6.5 Part V: Impact of The Annular Gap Around The Drill Pipe

The impact of the increasing the gap between the well and the pipe was studied, which was not a part of the main focus during this master thesis. The purpose of performing this part of the work was to obtain a better understanding of the behavior of the fluids in the mixing zone and thereby improve the validity of the investigation.

Thus the new (pipe OD)/(well ID) dimension was 2.5cm/4.0cm. Thus the radius of the annular gap was increased to 1.5 cm, i.e., an increase of 50% compared to the dimension used in the previous parts.

The fluid specifications of three experiments with the density difference of 0.60 sg are presented in table 6-12.

Exp. nr.	Density of fluids [sg]		Plastic viscosity [cP]		Yield point [100lb/ft^2]		Gel strength (10 sec/10 min) [100lb/ft^2]		Casing and drill pipe dimension (New Geometry)			Rotation Data		Result Overview
	Light fluid ρ_l	Heavy fluid ρ_h	Light fluid $(PV)_l$	Heavy fluid $(PV)_h$	Light fluid $(YP)_l$	Heavy fluid $(YP)_h$	Light fluid	Heavy fluid	Csg. ID [cm]	DP. OD [cm]	Well dep. [cm]	Speed [rpm]	Time [min]	Height of Mixing zone [cm]
1	1.10	1.60	9	17	7.5	14	9/ 17	20 / 33	4.0	2.55	200	80-250	6	Completely mixed ≈ 190
2	1.10	1.60	7	20	10	18	11 / 23	22 / 37	4.0	2.55	200	50-300	60	≈ 92
3	1.10	1.60	8.5	20	12	18	14 / 26	22 / 37	4.0	2.55	200	50-300	60	≈ 80

Table 6-12: Experimental data and result overview where the effect of the annular gap was investigated.

7 Analysis of The Results

At the end of each experiment, the images were visually analyzed, and the height of the mixing zone was measured. Furthermore, the results obtained in part IV were analyzed in MATLAB. Additionally, the height of the mixing zone of three experiments, presented in table 6-10 and 6-11, were mathematically calculated. The method was based on the volume of the collected heavy fluid on the top of the mixing zone and at the en of each experiment. This method is described in detail in Appendix D. The purpose of this method was to verify that the image analysis did not only represent the inside surface of the cylinder.

7.1 Part I: Effect Of The Pipe Rotation

Horizontal direction:

The experiments were divided into two groups depending on the density difference between the fluids. Each experiment was run for about 30 -45 min and the speed of the pipe rotation varied between 50 to 350 *rpm*. This speed is much higher than regular rate of penetration of a drill pipe while drilling in an oilfield, which is usually between 50 up to 150 *rpm*.

Group 1:

The results of the first group of experiments (experiment 1, 2, 3, and 4), where the fluids had the same densities and rheological properties, showed that no further development of the mixing zone occurred regardless of the rotation speed. The difference in the diameter of the annular gap around the pipe didn't seem to have any significant effects on the results. The photos of the interface between the fluids at different times taken during experiment 1 and 4 are shown in figure 7-1. The experiment seen in the figure to the left differs from the one on the right regarding the well/pipe dimension. Increasing the cross-sectional area of the gap between the well and the pipe didn't cause any mixing of the fluids at the interface.
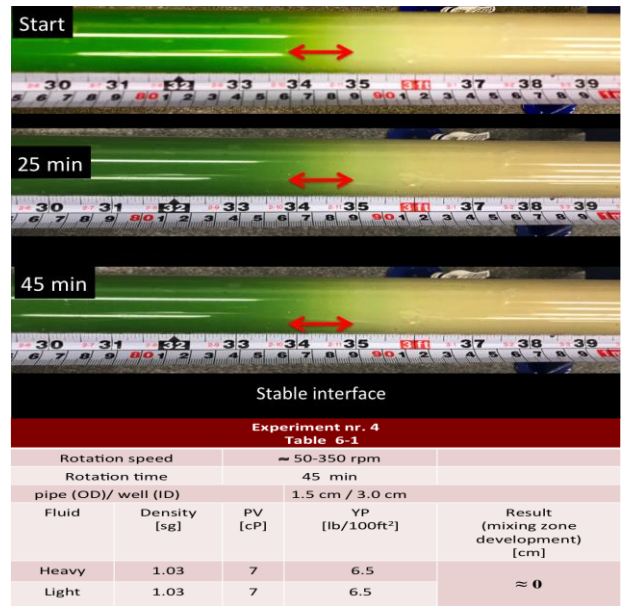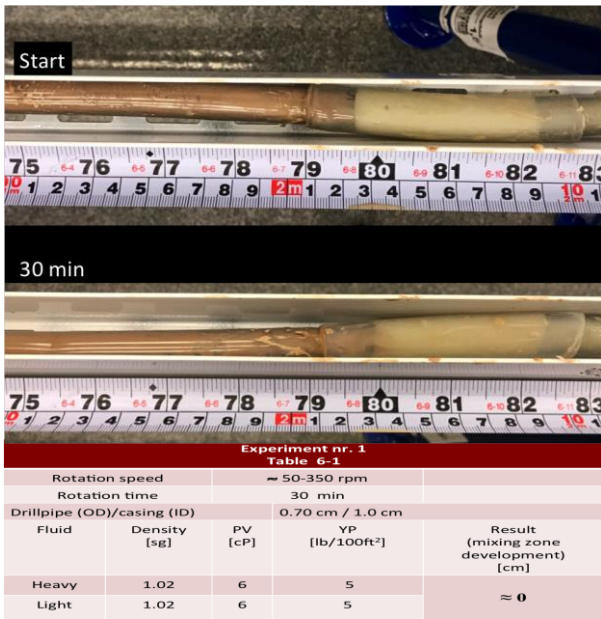
Figure 7-1: Illustrates the results of the experiments 1 and 4, where the impact of *rpm* in horizontal direction was studied.

Group 2:

This group includes experiment 5, 6, 7, and 8, where the density difference between the fluids was of 0.33 sg. The result of the experiment 8 is shown in figure 7-2, where the diameter of the gap between the well and the pipe gap was 1.0 cm, the mixing zone grew up to 9 cm.
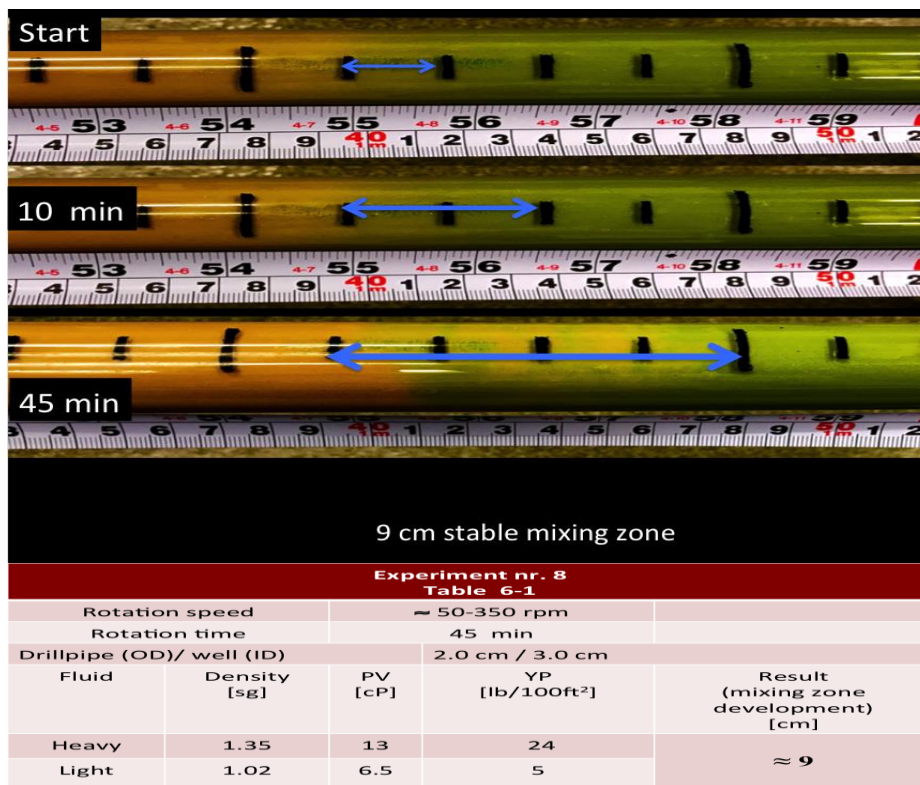

Figure 7-2: Shows the results of the exp. 8, where the impact of *rpm* in horizontal direction was studied

The graph in figure 7-3, presents the width of the mixing zone during the experiments shown in table 6-1. The red line represents the results of experiment 1, 2, 3 and 4, where $\Delta\rho$ is 0.00 sg. The blue line represents the results of experiment 5, 6, 7 and 8, where $\Delta\rho$ was 0.33 sg.

Based on this observation, the mixing zone was developed between fluids with larger $\Delta\rho$. The mixing zone was also affected by the annular gap around the pipe. The larger the gap, the greater the mixing zone. Thus, the results of these two groups of experiments indicate that the mixing zone was developed under the impact of the $\Delta\rho$ and the annular gap. On the other, the rotation speed didn't show any significant effect on the results.
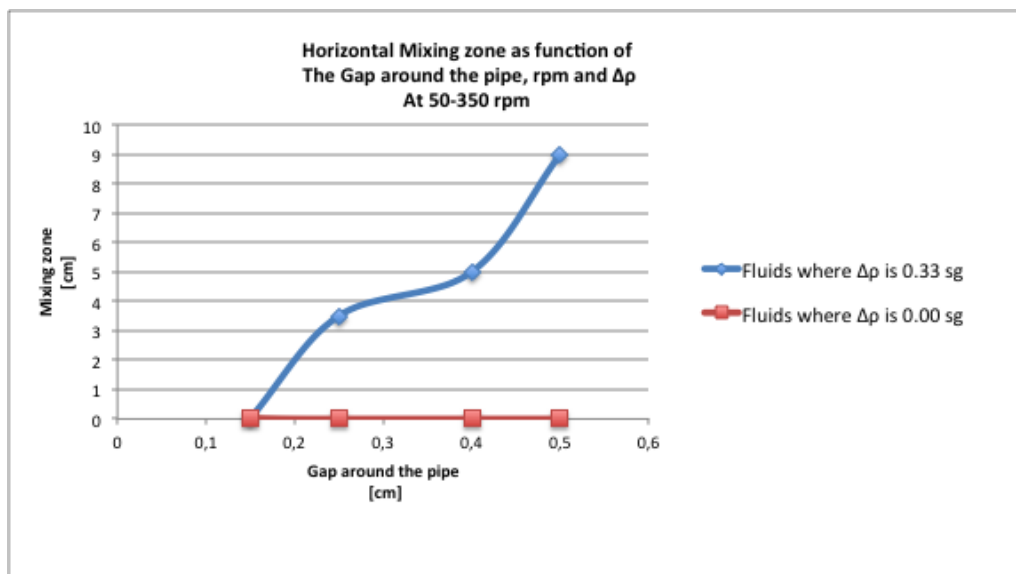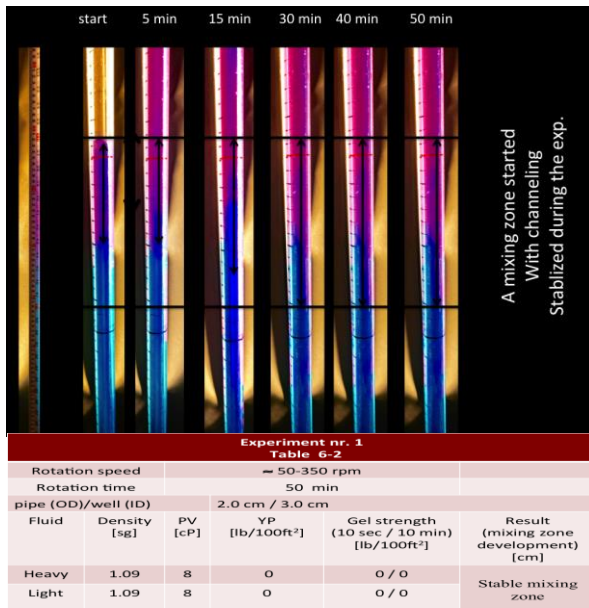

Figure 7-3: The graph shows the impact of $\Delta\rho$ and annular gap on the mixing zone in the horizontal direction
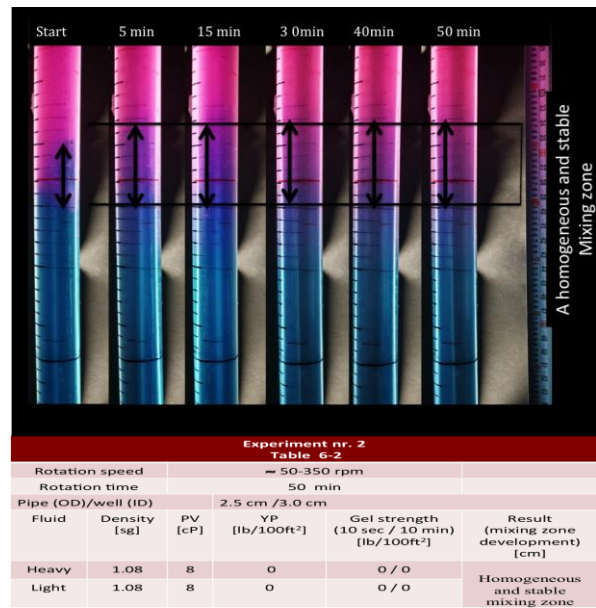
.

Vertical Direction:

The results of the experiments performed in the vertical direction (*table 6-2*) were visually analyzed. Based on the photos, it was seen that a mixing zone was developed at the start, but stayed stable throughout the experiments regardless of *rpm*. This indicated that neither in the vertical direction the high rpm had a significant effect on the further development of the mixing zone. Additionally, it was observed that the mixing zone was more stable, where the annular gap around the pipe was smallest.

The images of the mixing zone for two experiments are shown in figure 7-4. The fluids that were examined during these experiments were made by mixing 1,2-propylene glycol, and water. The only difference between the experiments was the gap between the wellbore wall and the pipe, which was smaller in 7-4.b than in 7-4.a. Comparing the results of these two experiments, one can see that the mixing zone in the figure on the right is shorter and more homogenous. Since the fluids were transparent, the pipe inside the well could easily be seen in the photos.

			Experiment nr. 1 Table 6-2		
Rotation speed			≈ 50-350 rpm		
Rotation time			50 min		
pipe (OD)/well (ID)			2.0 cm / 3.0 cm		
Fluid	Density [sg]	PV [cP]	YP [lb/100ft²]	Gel strength (10 sec / 10 min) [lb/100ft²]	Result (mixing zone development) [cm]
Heavy	1.09	8	0	0 / 0	Stable mixing zone
Light	1.09	8	0	0 / 0	

a) Illustrates a mixing zone that stayed stable during the experiment regardless *rpm*. The rotation started after transferring the upper fluid.

			Experiment nr. 2 Table 6-2		
Rotation speed			≈ 50-350 rpm		
Rotation time			50 min		
Pipe (OD)/well (ID)			2.5 cm /3.0 cm		
Fluid	Density [sg]	PV [cP]	YP [lb/100ft²]	Gel strength (10 sec / 10 min) [lb/100ft²]	Result (mixing zone development) [cm]
Heavy	1.08	8	0	0 / 0	Homogeneous and stable mixing zone
Light	1.08	8	0	0 / 0	

b) Shows a more homogeneous and shorter mixing zone than one in a).

Figure 7-4: Studying the impact of *rpm* on the mixing zone in vertical direction.

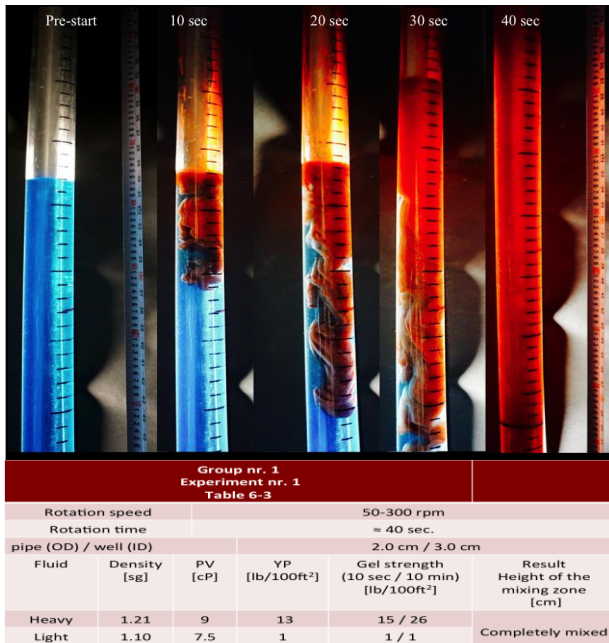## 7.2   Part II: Effect of The Viscosity

The photos were visually analyzed, and the heights of the mixing zones for both groups of the experiments are presented in table 6-3.
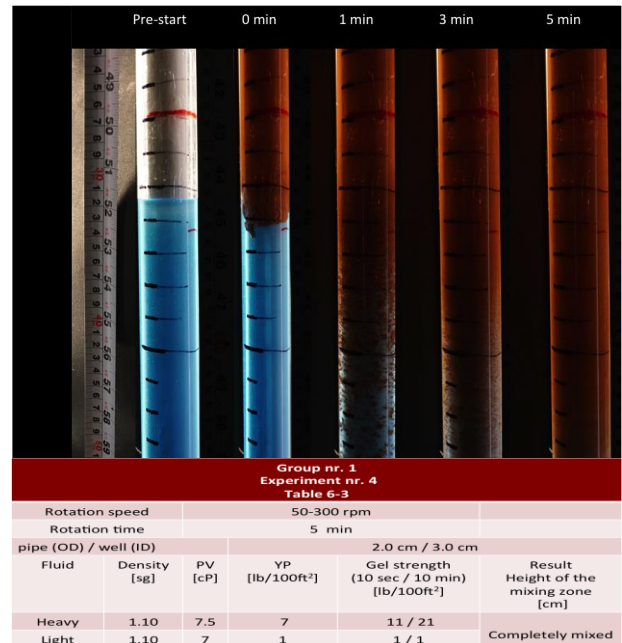
Group nr. 1

This group includes four experiments where the heavy fluid was regular WBM while the light fluid was made of mixing water, glycol and salt.

In experiment 1 and 2, the heavy fluid with the density of 1.20 sg exhibited both viscosity and gel property, while the light fluid, with the density of 1.10 sg and viscosity of 7.5 cP, didn't show any gel properties.

In experiments presented in figure 7.5.a, the fluids were immediately mixed as soon as the heavy fluid pumped down into the well. The heavy fluid penetrated through the interface in the form of a lump and then formed a homogeneous mixture as seen in the figure. However, in experiment 3 and 4, the effect of the density difference on the system was excluded since both fluids had the same density (1.10 sg). The result seen in figure 7-5.b illustrates another behavior of the barite particles. The mixing between the fluids was gradually started, and the barite particles settled down to the bottom in smaller lumps. Even though it was not any different in densities between the fluids, the mixing still occurred and completed within 4-5 minutes.

Group nr. 1 Experiment nr. 1 Table 6-3					
Rotation speed		50-300 rpm			
Rotation time		≈ 40 sec.			
pipe (OD) / well (ID)		2.0 cm / 3.0 cm			
Fluid	Density [sg]	PV [cP]	YP [lb/100ft²]	Gel strength (10 sec / 10 min) [lb/100ft²]	Result Height of the mixing zone [cm]
Heavy	1.21	9	13	15 / 26	Completely mixed
Light	1.10	7.5	1	1 / 1	

a) The density difference between the fluids was 0.10 sg while they exhibit relative similar viscosity. The fluids were mixed within 40 sec.

Group nr. 1 Experiment nr. 4 Table 6-3					
Rotation speed		50-300 rpm			
Rotation time		5 min			
pipe (OD) / well (ID)		2.0 cm / 3.0 cm			
Fluid	Density [sg]	PV [cP]	YP [lb/100ft²]	Gel strength (10 sec / 10 min) [lb/100ft²]	Result Height of the mixing zone [cm]
Heavy	1.10	7.5	7	11 / 21	Completely mixed
Light	1.10	7	1	1 / 1	

b) The same fluids as in a) but with the same density. The fluids were completely mixed within 5 min.

Figure 7-5: Illustrates the result of 1st of the experiments, where the effect of PV was studied.

Group nr. 2

The results of the tests presented in table 6-4 were analyzed in this part. The heavy fluid was similar to the one used in the previous group with the density of 1.20 sg and PV between 13-15 cP. The light fluid was regular premixed slam with the density of 1.03 sg and plastic viscosity 6-7 cP. Both fluids exhibited gel properties.

Figure 7-6 shows the photos that were taken while performing experiment 1 and 3. In figure 7-6.a, a homogeneous mixing zone with the height of 12 cm was observed. The mixing zone stayed stable throughout the experiment. However, reducing the gel properties of the same type of fluids while keeping the PV constant, demonstrated a higher mixing zone with downward channelings.

A stable mixing zone of 12 cm

			Group nr. 2 Experiment nr. 1 Table 6-4		
Rotation speed			50-300 rpm		
Rotation time			30 min		
pipe (OD) / well (ID)			2.0 cm / 3.0 cm		
Fluid	Density [sg]	PV [cP]	YP [lb/100ft^2]	Gel strength (10 sec / 10 min) [lb/100ft^2]	Result Height of the mixing zone [cm]
Heavy	1.20	14	17	23 / 37	
Light	1.026	7	10	13 / 26	≈ 12 cm
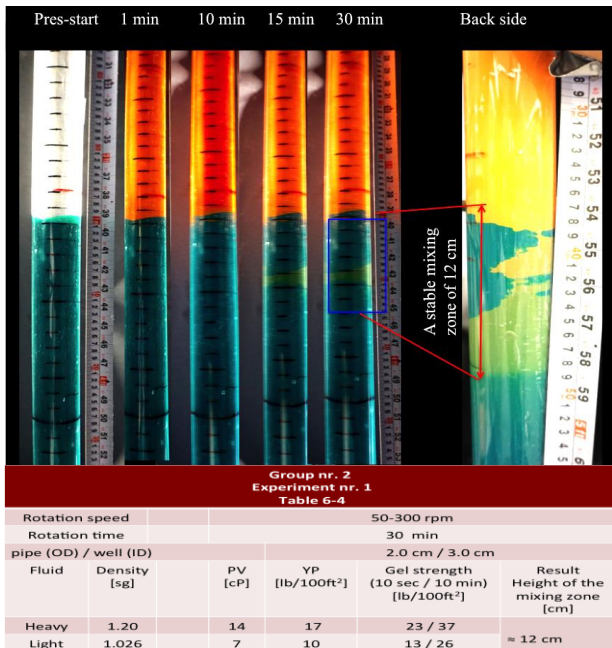
a) Despite the larger density difference (Δρ= 0.17), compared to fluids in Group 1, the mixing zone was controllable and stabilized within 10 -15 min.

A mixing zone of 28 cm with channeling

			Group nr. 2 Experiment nr. 3 Table 6-4		
Rotation speed			50-300 rpm		
Rotation time			30 min		
pipe (OD) / well(ID)			2.0 cm / 3.0 cm		
Fluid	Density [sg]	PV [cP]	YP [lb/100ft^2]	Gel strength (10 sec / 10 min) [lb/100ft^2]	Result Height of the mixing zone [cm]
Heavy	1.20	13	12	18 / 29	
Light	1.03	7	7	11 / 20	≈ 28 cm
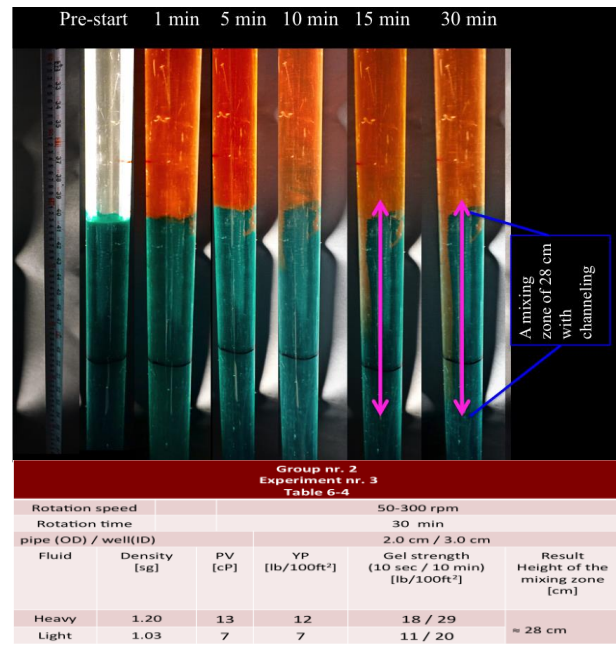
b) The same fluids as in a) but with less YP and gel strength, which resulted in a higher mixing zone than in a).

Figure 7-6: Represents the results of the 2nd group of experiments where the effect of the viscosity was studied.

7.3 Part III: Effect of Yield Point and Gel Strengths

The effect of the yield point and the gel strengths of the heavy and the light fluid on the growth of the mixing zone were separately investigated. The density difference between the fluids was 0.20 sg for all the experiments in this part. The visual analyses of the photos taken during the procedure are presented in the following sections.

Effect of The Yield Point of The Light Fluid

The impact of the gel properties of the light fluid was studied by performing seven experiments presented in table 6-5, where the yield point of the heavy fluid was set at 11.5 to 12.5 lb/100ft^2.

In figure 7-7, there are demonstrated the photos of four experiments, whose data are presented in table 6-5. Based on the analysis of these photos, it was seen that when the yield point of the light fluid was about 14$lb/100ft^2$, the interface was stable without any growth of the mixing zone (*figure 7-7.a*). Furthermore, it was observed that the height of the mixing zone increased by decreasing the mentioned parameter for the light fluid. As the yield point was reduced to below 6 lb/100ft^2, the mixing zone became unstable, and at 4 lb/100ft^2 the fluids were mixed utterly within few minutes (*figure 7-7.d*).
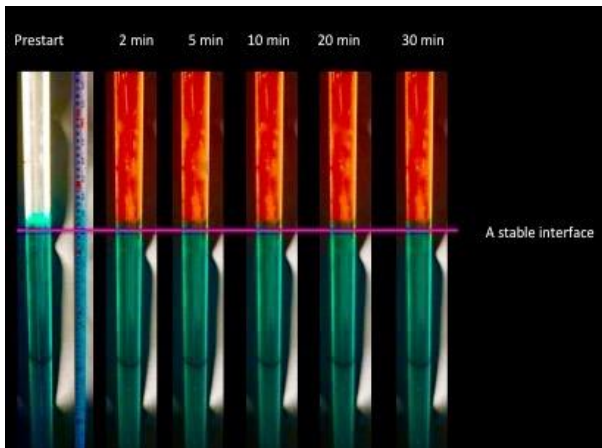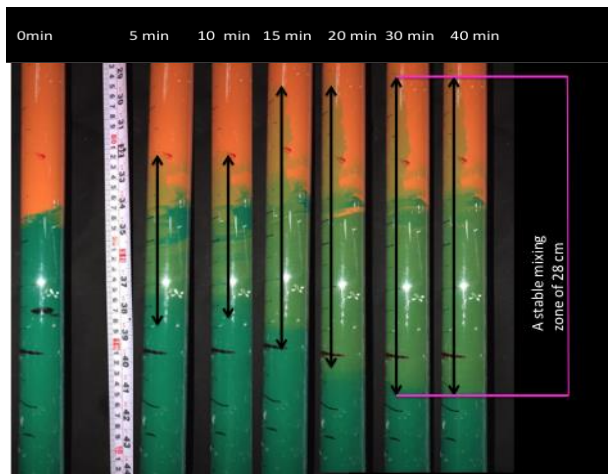
Experiment nr. 1
Table 6-5

Rotation speed	≈ 50-300 rpm				
Rotation time	40 min				
pipe (OD)/well(ID)	2.0 cm / 3.0 cm				
Fluid	Density [sg]	PV [cP]	YP [lb/100ft²]	Gel strength (10 sec / 10 min) [lb/100ft²]	Result Height of the mixing zone [cm]
Heavy	1.30	17	12.5	21 / 37	≈ 0
Light	1.10	8	14	16 / 31	

a) A light fluid with a yield point above 10 lb/100ft² provides a stable interface.
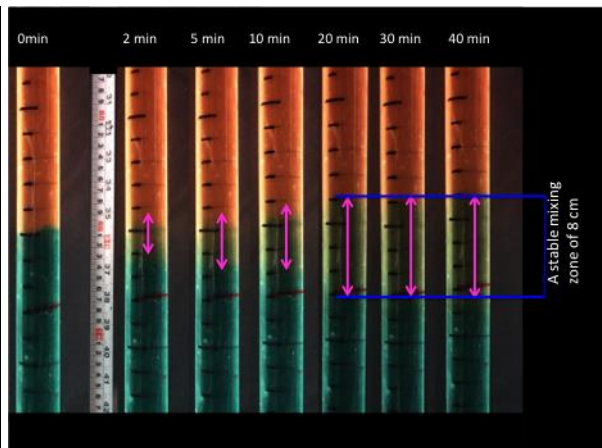
Experiment nr. 2
Table 6-5

Rotation speed	≈ 50-300 rpm				
Rotation time	40 min				
pipe (OD)/well(ID)	2.0 cm / 3.0 cm				
Fluid	Density [sg]	PV [cP]	YP [lb/100ft²]	Gel strength (10 sec / 10 min) [lb/100ft²]	Result Height of the mixing zone [cm]
Heavy	1.30	17	12.5	21 / 37	≈ 8
Light	1.10	7.5	11	13 / 24	

b) Decreasing the gel properties of the light fluid resulted in the development of the mixing zone. This mixing zone reached stability at t= 20 min.

Experiment nr. 4
Table 6-5

Rotation speed	≈ 50-300 rpm				
Rotation time	40 min				
pipe (OD)/well (ID)	2.0 cm / 3.0 cm				
Fluid	Density [sg]	PV [cP]	YP [lb/100ft²]	Gel strength (10 sec / 10 min) [lb/100ft²]	Result Height of the mixing zone [cm]
Heavy	1.30	15	11.5	19 / 33	≈ 28
Light	1.10	6	7.5	11 / 19	

c) Illustrates a faster development of the mixing zone due to decreasing gel properties. The mixing zone reached stability at t=30 min.
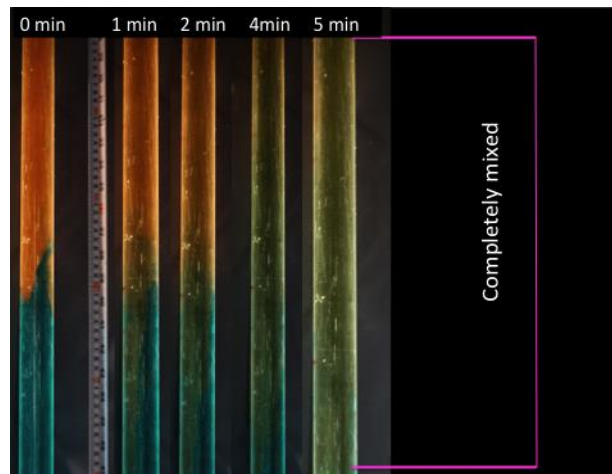
Experiment nr. 7
Table 6-5

Rotation speed	50-300 rpm				
Rotation time	5 min				
pipee (OD)/well(ID)	2.0 cm / 3.0 cm				
Fluid	Density [sg]	PV [cP]	YP [lb/100ft²]	Gel strength (10 sec / 10 min) [lb/100ft²]	Result Height of the mixing zone [cm]
Heavy	1.30	15	12	20 / 34	Completely mixed
Light	1.10	6.5	4	4 / 9	

d) Very low gel properties resulted in the complete mixing of the fluids

Figures 7-7: Shows the results of four experiments where the effect of the YP of the light fluid was studied.

69

The measured heights of the mixing zone during the experiments presented in the table 6-5 are plotted as the function the yield point of the light fluids and shown in figure 7-8. The mixing zone with the height of 190 cm, which is the sum of the height of both fluids in the well, represents the complete mixing of the fluids. On the x-axes, the YP of the light fluids are presented, and y-axes represent the height of the mixing zone.
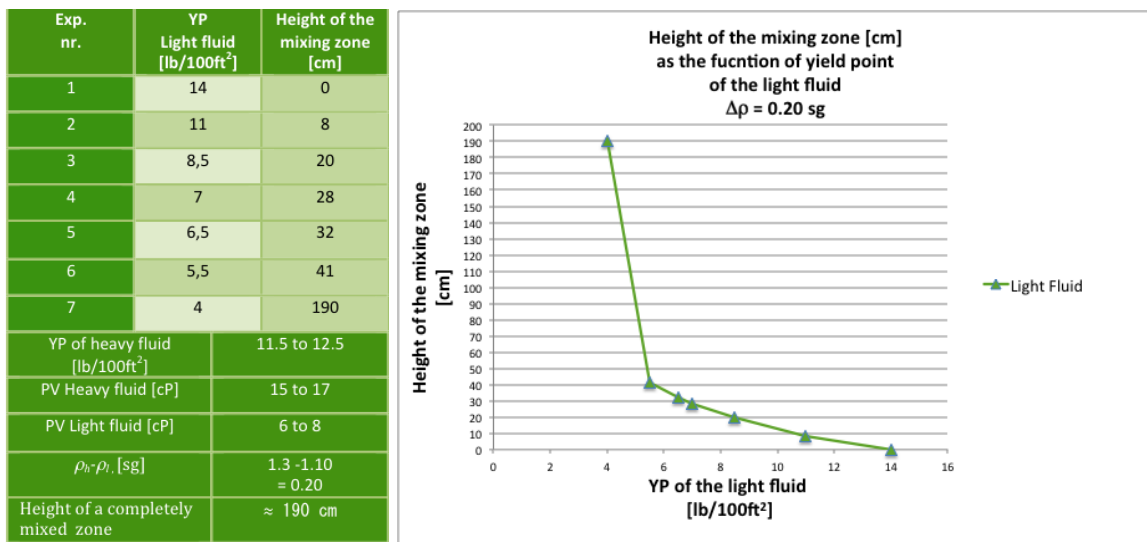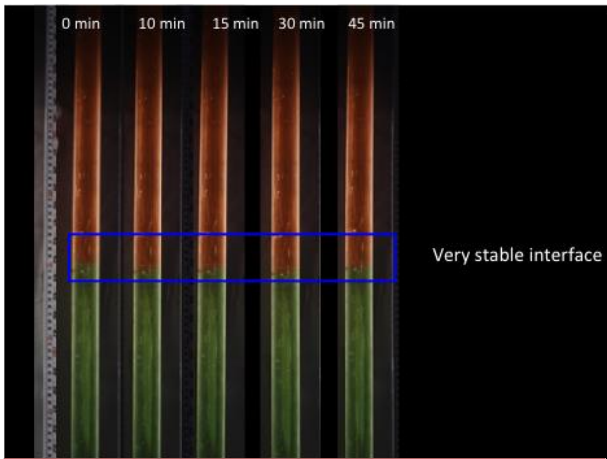
Exp. nr.	YP Light fluid [lb/100ft²]	Height of the mixing zone [cm]
1	14	0
2	11	8
3	8,5	20
4	7	28
5	6,5	32
6	5,5	41
7	4	190
YP of heavy fluid [lb/100ft²]	11.5 to 12.5	
PV Heavy fluid [cP]	15 to 17	
PV Light fluid [cP]	6 to 8	
ρ_h-ρ_l [sg]	1.3 -1.10 = 0.20	
Height of a completely mixed zone	≈ 190 cm	

Figure 7-8: A graph illustrates the effect YP of the light fluid on the development of the mixing zone.

Effect of the yield point of the heavy fluid

During this part of the work, the results of the four experiments presented in table 6-6 were analyzed, and the photos are shown in figure 7-9. The yield point of light fluid was kept relatively constant and set between 9.5 and 11 lb/100ft² while reducing the mentioned parameter of the heavy fluid down to 2 lb/100ft² (figure 7-9.d).

Based on the visual analysis of the pictures, the interface between the fluids stayed stable when the yield point of both fluids was above 10 lb/100ft² (figure 7-9.a). However, reducing the gel properties of the heavy fluid resulted in the growth of the mixing zone (figure 7-9.b and c). When the mentioned properties of the heavy fluid reached below 4 lb/100ft², the fluids were completely mixed within few minutes as it is seen in the figure 7-9.d.

Experiment nr. 1
Table 6-6

Rotation speed				≈ 50-300 rpm	
Rotation time				45 min	
pipe (OD)/well (ID)				2.0 cm / 3.0 cm	
Fluid	Density [sg]	PV [cP]	YP [lb/100ft²]	Gel strength (10 sec / 10 min) [lb/100ft²]	Result Height of the mixing zone [cm]
Heavy	1.30	14	15	19 / 32	≈ 0
Light	1.10	7	11	14 / 27	

a) High yield point and gel strength provides a stable interface in the HOL-configuration
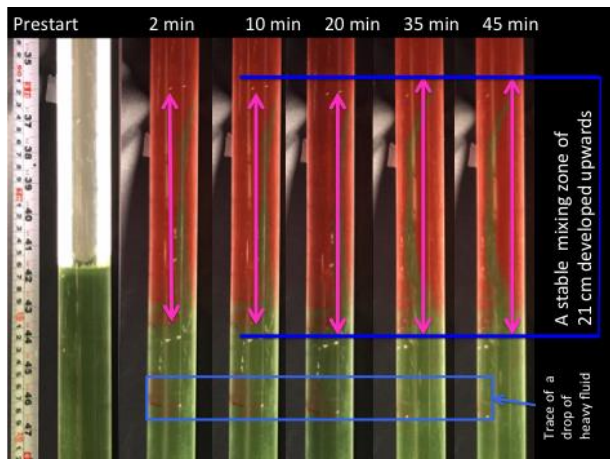
Experiment nr. 3
Table 6-6

Rotation speed				≈ 50-300 rpm	
Rotation time				45 min	
pipe (OD)/well (ID)				2.0 cm / 3.0 cm	
Fluid	Density [sg]	PV [cP]	YP [lb/100ft²]	Gel strength (10 sec / 10 min) [lb/100ft²]	Result Height of the mixing zone [cm]
Heavy	1.30	8	8	9 / 22	≈ 21
Light	1.10	9	10	15/ 25	

b) Decreasing the yield point of the heavy fluid resulted in the growth of the mixing zone that reached stability at t=10 min.
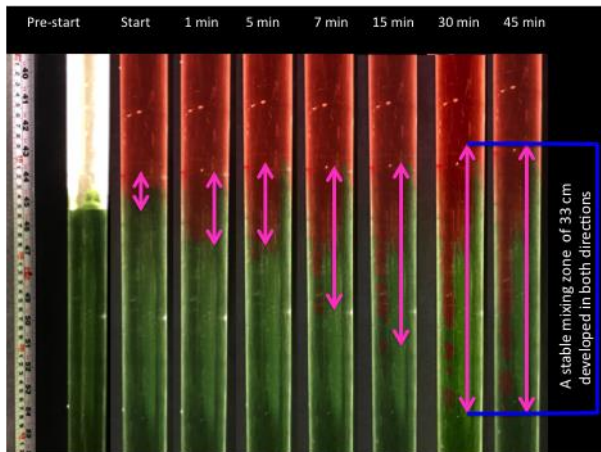
Experiment nr. 5
Table 6-6

Rotation speed				≈ 50-300 rpm	
Rotation time				45 min	
pipe (OD)/well (ID)				2.0 cm / 3.0 cm	
Fluid	Density [sg]	PV [cP]	YP [lb/100ft²]	Gel strength (10 sec / 10 min) [lb/100ft²]	Result Height of the mixing zone [cm]
Heavy	1.30	8	4.5	6 / 11	≈ 33
Light	1.10	9	8	12 / 21	

c). The mixing zone is still controllable at the yield point of 4.5lb/100ft², while keeping this parameter for the light fluid around 10 lb/100ft².
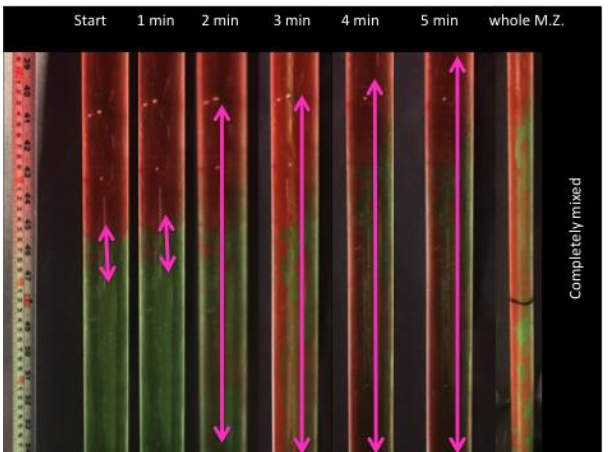
Experiment nr. 6
Table 6-6

Rotation speed				≈ 50-300 rpm	
Rotation time				5 min	
pipe (OD)/well (ID)				2.0 cm / 3.0 cm	
Fluid	Density [sg]	PV [cP]	YP [lb/100ft²]	Gel strength (10 sec / 10 min) [lb/100ft²]	Result Height of the mixing zone [cm]
Heavy	1.30	9	2	2 / 4	Completely mixed
Light	1.10	8	8	12 / 21	

d). The fluids were completely mixed at the yield point below 4 lb/100ft².

Figure 7-9: Illustrates the photos of four experiments where the effect of the gel properties of the heavy fluid was studied.

As shown in the figure 7-10, decreasing YP of the heavy fluid (on x-axes) resulted in increasing the instability of the mixing zone. The height of the mixing zone (y-axes) increased due to diluting the heavy fluid.
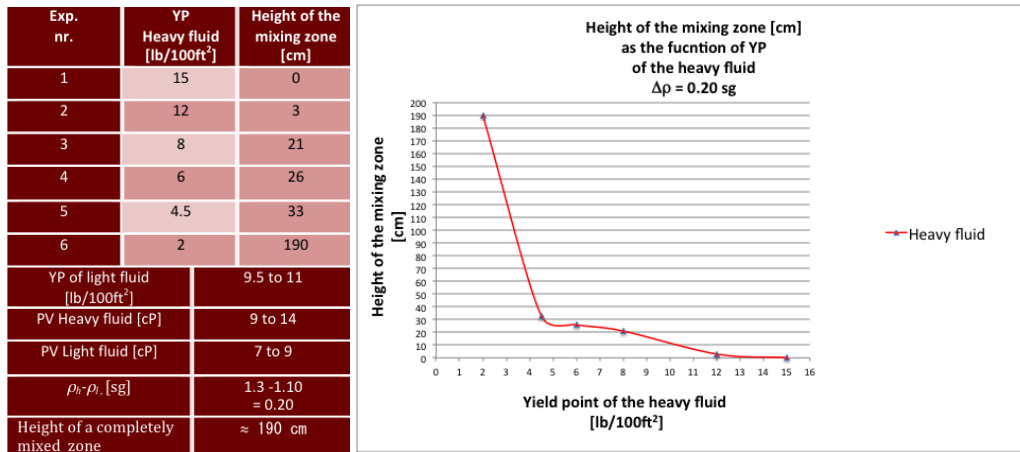

Figure 7-10: A graph shows the effect of the YP of the heavy fluid on the mixing zone.

Based on the results presented in this part, the mixing zone between the fluids was controllable as long as the YP of the fluids was larger than 6 lb/100ft^2. The contribution of YP of both fluids in a HOL-system was compared and demonstrated in the following figure.
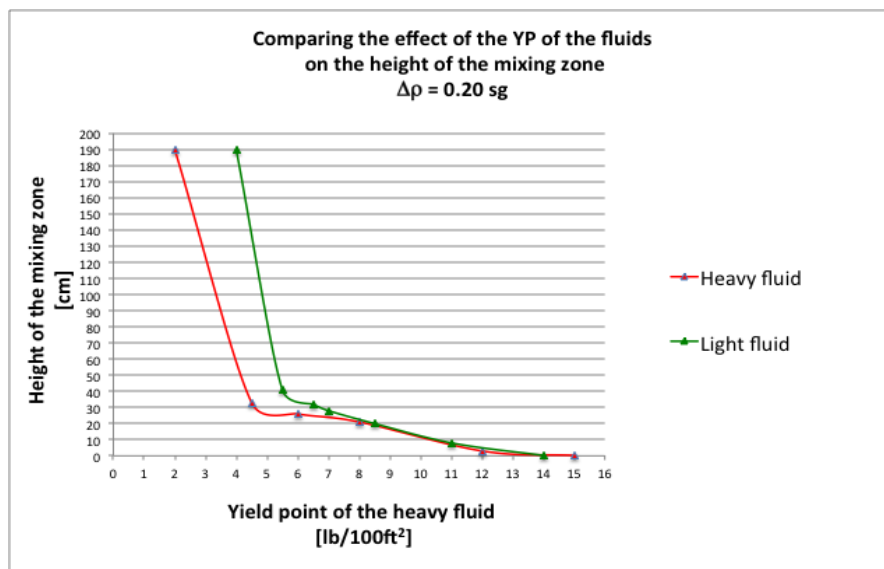
Figure 7-11: Comparing the impact of YP of the fluids on the growth of the mixing zone.

7.4   Part IV: Development of The Mixing Zone as Function Of Δρ

The focus in this part of the work was to study the growth of the mixing zone as the function of the density difference between the fluids exhibiting different gel properties.

The height of the mixing zone was determined by analyzing the photos visually, and by an image analysis tools in MATLAB. Additionally, another method as described earlier was used to confirm the analysis of the first-mentioned methods.

Group nr. 1: Δρ = 0.30 sg

The heights of the mixing zone that developed during the experiments presented in table 6-8 indicated that the mixing zone was controllable as long as the yield point of the heavy and the light fluids were above 6 lb/100ft^2. The result and the photo analysis of experiment 1 and 4 are presented in the following section:

Experiment 1

For larger YP, as in experiment 1, the interface was stable, and the height of the mixing zone was insignificant (*figure 7-12*).

Gropu nr. 1 Experiment nr. 1 Table 6-8					
Rotation speed	≈ 50-350 rpm				
Rotation time	45 min				
pipe (OD)/well (ID)	2.0 cm / 3.0 cm				
Fluid	Density [sg]	PV [cP]	YP [lb/100ft²]	Gel strength (10 sec / 10 min) [lb/100ft²]	Result Height of the mixing zone [cm]
Heavy	1.41	17	28	34 / 50	≈ 3
Light	1.10	7	10	14 / 27	
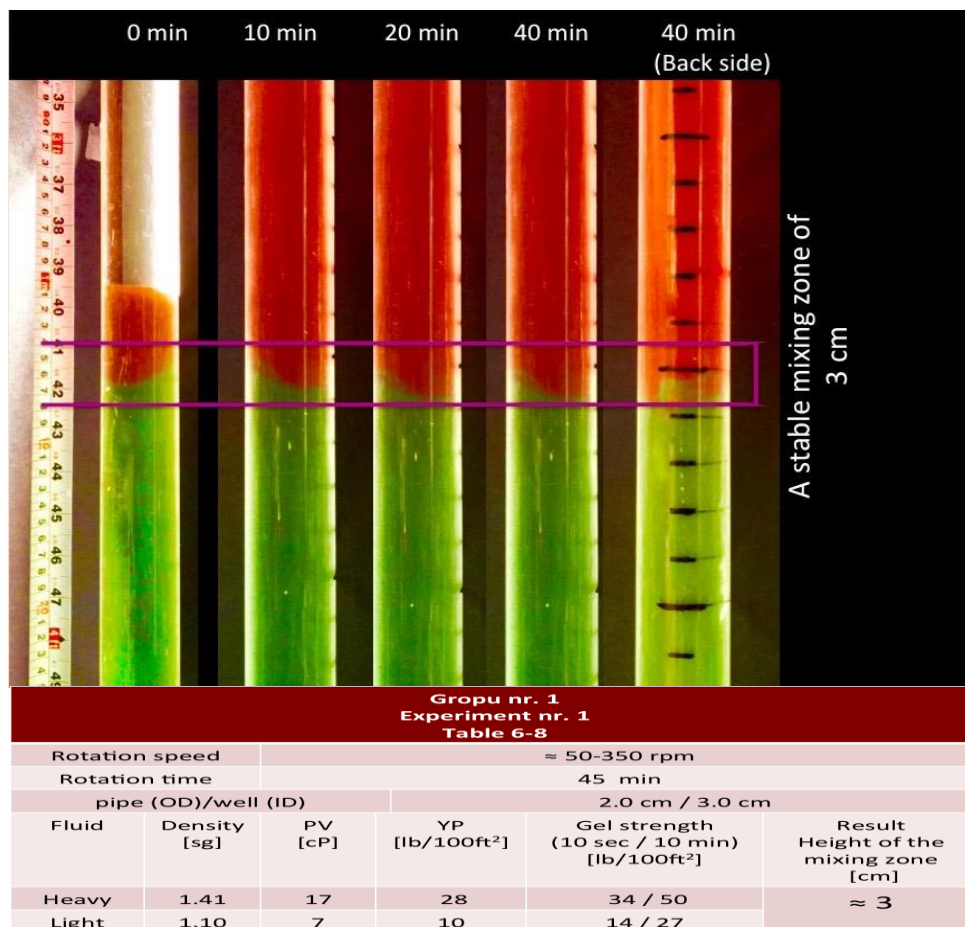
Figure 7-12: Shows the result of experiment 1 from group 1.

Experiment 4

In figure 7-13, the result of experiment 4 is presented. The mixing zone was developed at the highest speed during the first 10 minutes, but the system reached stability within about15-25 min. The final mixing zone of 21 cm was seen at t = 30. The experiment was run for 60 min, but no further development of the mixing zone was noticed. The yellow color on the sides in the figure is just reflection of the light from the LED-lamp placed behind the cylinder. The well was carefully checked and no any traces of the fluids were seen above or below the mixing zone.

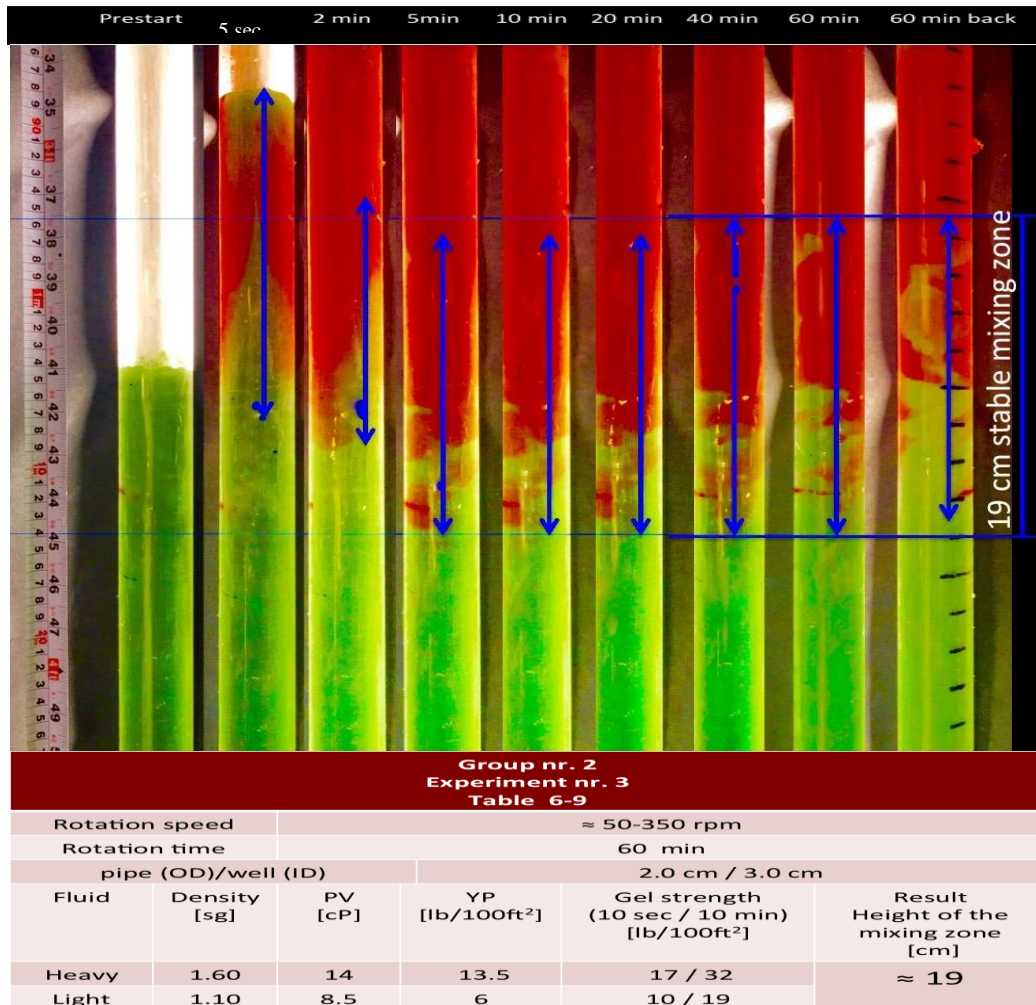| Gropu nr. 1 Experiment nr. 4 Table 6-8					
Rotation speed	≈ 50-350rpm				
Rotation time	60 min				
pipe (OD)/well (ID)	2.0 cm / 3.0 cm				
Fluid	Density [sg]	PV [cP]	YP [lb/100ft²]	Gel strength (10 sec / 10 min) [lb/100ft²]	Result Height of the mixing zone [cm]
Heavy	1.40	12	6.5	10 / 24	≈ 21
Light	1.10	10	6	9 / 25	
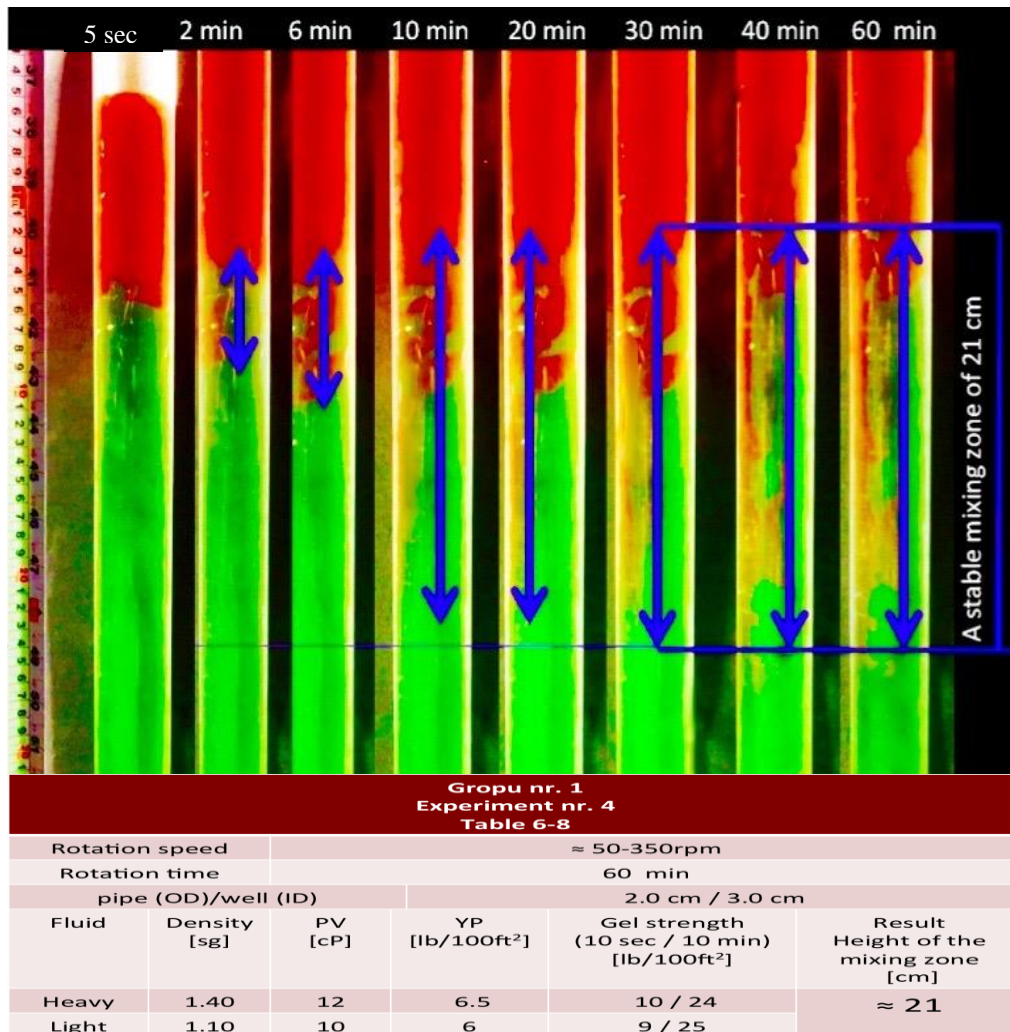
Figure 7-13: Illustrates the growth of the mixing zone in experiment 4 from group 1.

MATLAB Analysis

The photos in figure 7-13 were analyzed using MATLAB analysis tool and shown in figure 7-14. The green curve represents the light fluid while the red one represents the heavy fluid. The pixel intensities (y-axes) are plotted at different depth of the well (x-axes).

The interface between the fluids was located at the well depth of 107 cm. During the first minute, the mixing zone started to grow upward; thereby the downward development was dominating. As seen in the figure, the height of the mixing zone at t = 60 min was almost the same as at t =40 min. Therefore, the experiment was ended, and the final height of the mixing zone was determined to be 18 cm.
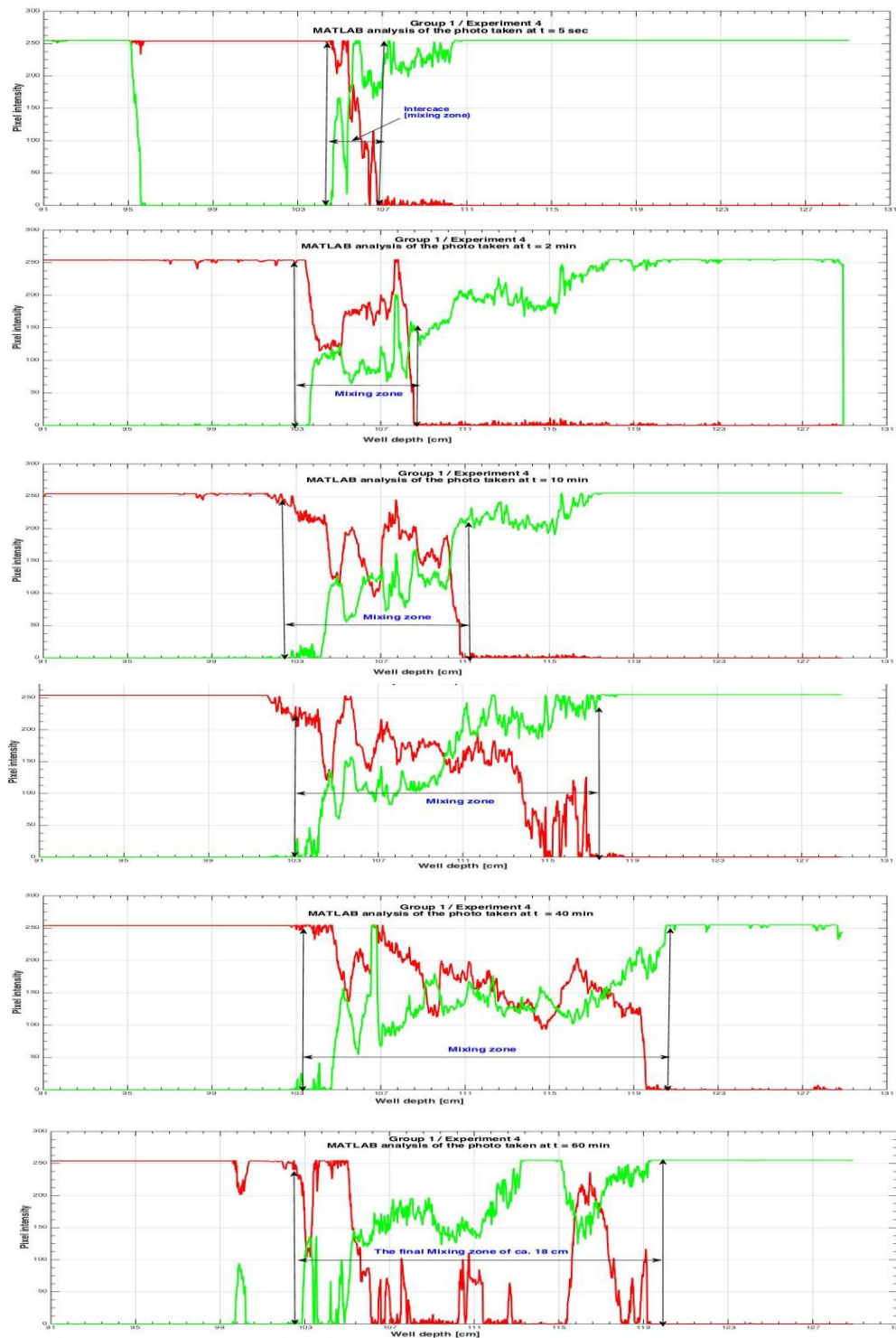
Figure 7-14: MATLAB analysis of the photos taken during experiment 4 from group 1.

Group nr. 2: Δρ = 0.50 sg

After running the experiments, presented in table 6-9, for about 45-60 min, the photos were visually analyzed, and the height of the mixing zone was recorded and presented in the same table.

Experiment 1

The photos taken at different times during experiment 1 are shown in figure 7-15. The yield point of the heavy and the light fluids were about 32 and 12 lb/100ft^2 respectively.

At the moment the heavy fluid came into contact with the light fluid an insignificant mixing occurred. However, it wasn't observed any further development of the mixing zone regardless of the speed of the pipe rotation.

Group nr. 2 Experiment nr. 1 Table 6-9					
Rotation speed	≈ 50-300 rpm				
Rotation time	45 min				
pipe (OD)/well (ID)	2.0 cm / 3.0 cm				
Fluid	Density [sg]	PV [cP]	YP [lb/100ft²]	Gel strength (10 sec / 10 min) [lb/100ft²]	Result Height of the mixing zone [cm]
Heavy	1.60	17.5	32	39 / 54	≈ 6
Light	1.10	8	12	19 / 37	
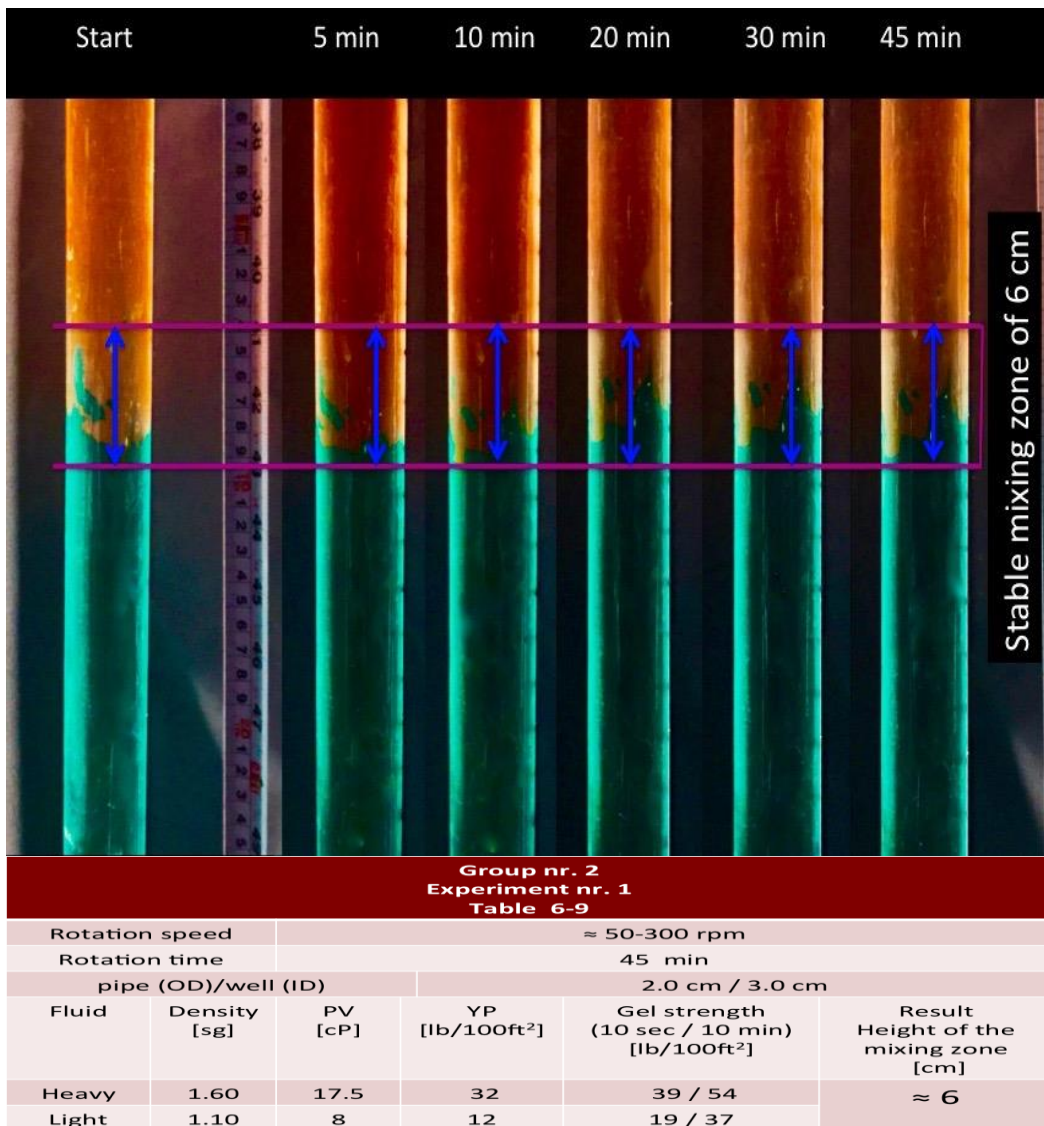
Figure 7-15 : Shows the result of the experiment 1 from group 2.

Experiment 3

Considering experiment 3, illustrated in figure 7-16, where the yield point of the light fluid was reduced to 6 lb/100ft^2, a quick mixing at the interface was seen during the first 5 seconds. Thereby, the speed of the mixing process slowed down and a final mixing zone with the height of about 19 cm was built within 10-15 minutes. The experiment was run for 60 min, but no further development of the mixing zone was noticed regardless of the rotation speed of the pipe. The rheological properties of the fluids are shown in the figure as well.

Group nr. 2 Experiment nr. 3 Table 6-9					
Rotation speed		≈ 50-350 rpm			
Rotation time		60 min			
pipe (OD)/well (ID)		2.0 cm / 3.0 cm			
Fluid	Density [sg]	PV [cP]	YP [lb/100ft²]	Gel strength (10 sec / 10 min) [lb/100ft²]	Result Height of the mixing zone [cm]
Heavy	1.60	14	13.5	17 / 32	≈ 19
Light	1.10	8.5	6	10 / 19	

Figure 7-16: Illustrates the growth of the mixing zone in exp. 3 from group 2.

MATLAB Analysis

The photos from this experiment (*figure 7-16)* were analyzed using MATLAB, and the graphs are presented in figure 7-17. The mixing zone started to build upward and then moved downward. At time t = 20 min the system became stable. Based on the MATLAB analysis, the final height of the mixing zone was determined to be 17 cm.
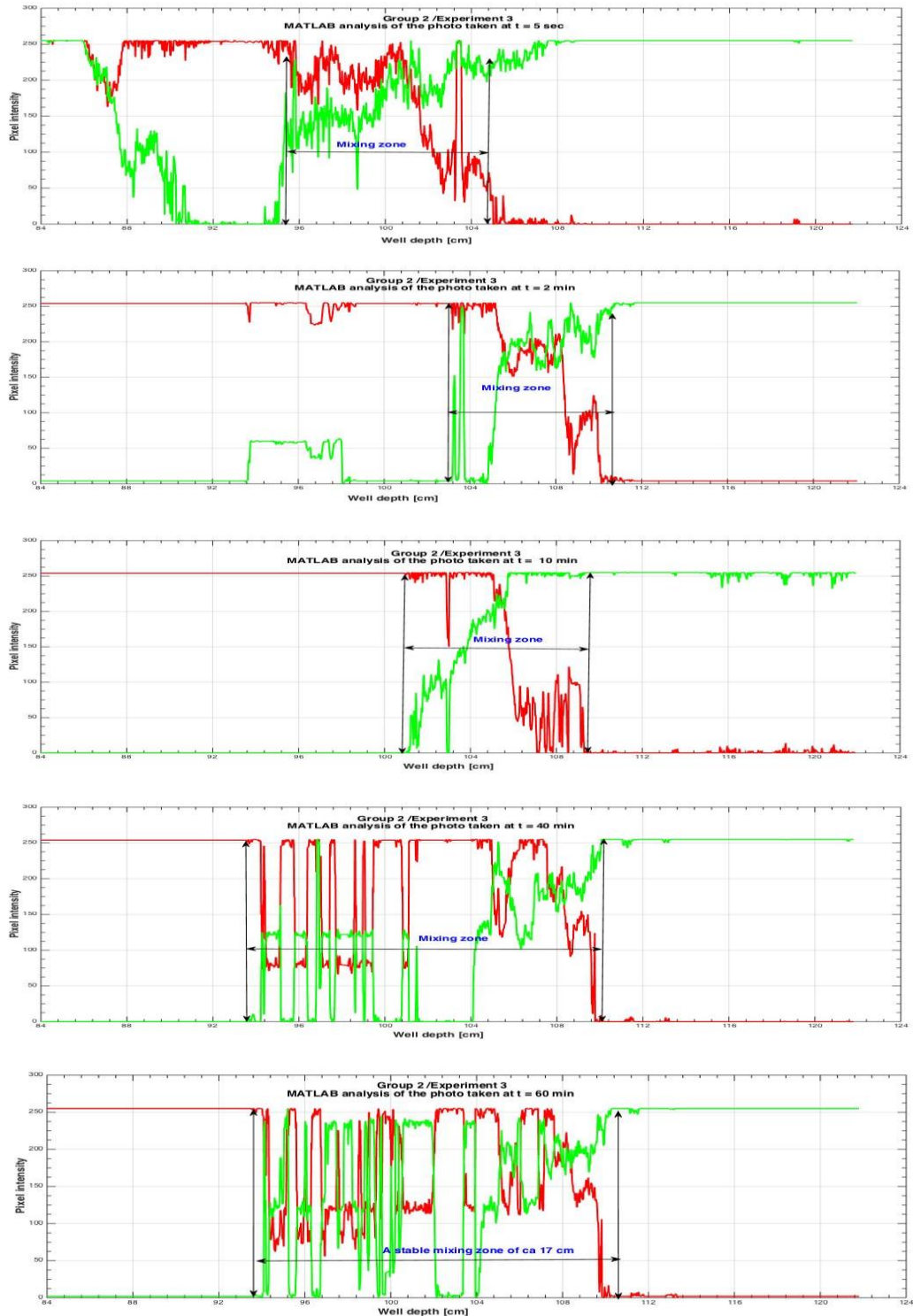
Figure 7-17: MATLAB analysis of the photos of experiment 3 from group 2.

78

Experiment 4

The result of experiment 4 in figure 7-18 shows a larger mixing zone of about 70 cm that started at the well depth of 103 cm. In this experiment, both fluids were diluted, and the yield points were reduced to about 6-7 lb/100ft^2. Due to the fast growth of the mixing zone, the photos were taken at two different heights and shown in two separate figures. The mixing zone developed both upward and downward with a long fingering of the heavy fluid down to the well depth of 152 cm.

Group nr. 2 Experiment nr. 4 Table 6-9					
Rotation speed	≈ 50-350 rpm				
Rotation time	60 min				
pipe (OD)/well (ID)	2.0 cm / 3.0 cm				
Fluid	Density [sg]	PV [cP]	YP [lb/100ft²]	Gel strength (10 sec / 10 min) [lb/100ft²]	Result Height of the mixing zone [cm]
Heavy	1.60	11	7	9 / 16	≈ 70
Light	1.10	8.5	6	10 / 19	
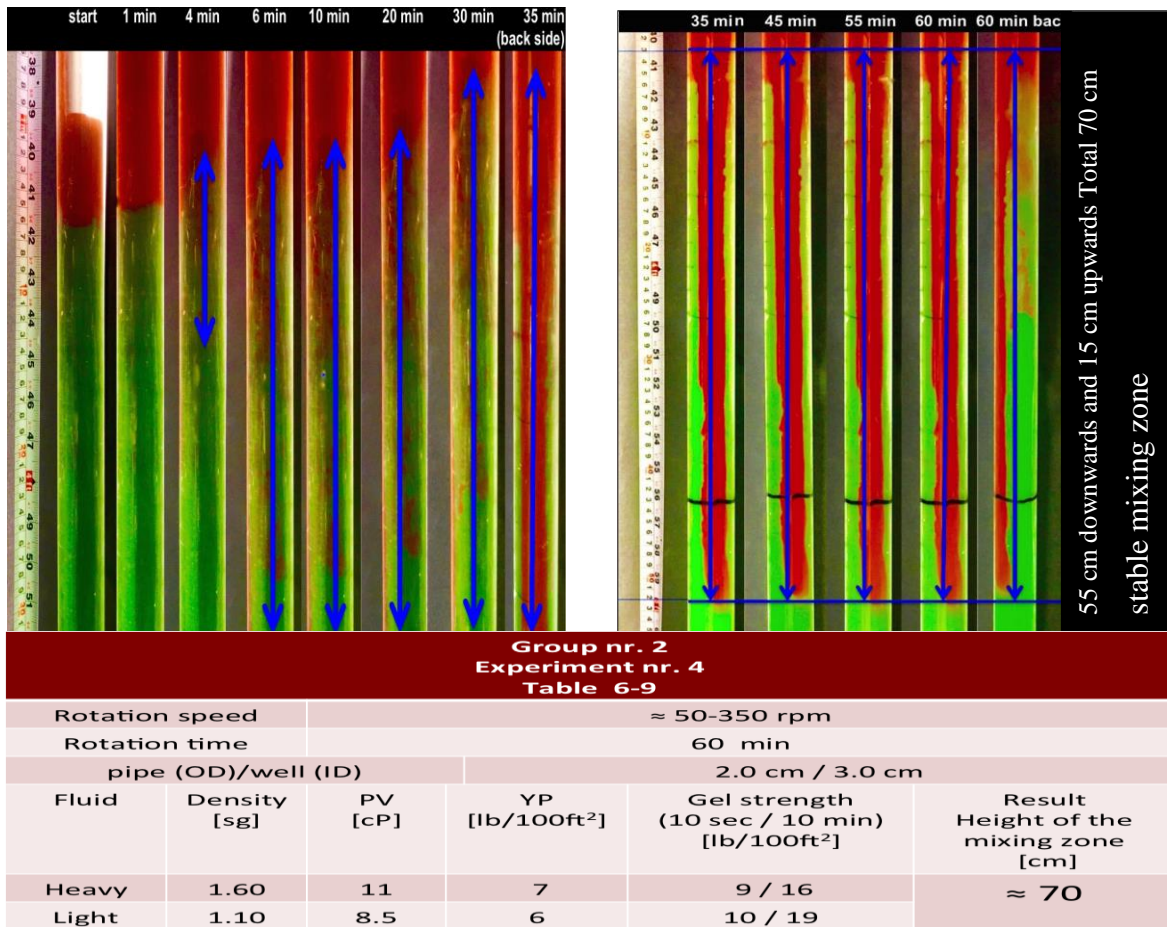
Figure 7-18: Illustrates the result of experiment 4 from group 2.

Group nr. 3 Δρ = 0.60 sg

The photos of experiment 1 and 2 in this group (*table 6-10*) were analyzed visually as well as in MATLAB. Furthermore, the result of experiment 2 was mathematically checked based on the gathered heavy fluid from the top of the mixing zone. Thereby, the density of the collected heavy fluid was measured, and compared to its density before start of the experiment.

Experiment 1

The photos from experiment 1 are presented in figure 7-19. After running the experiment for about 45 min, no further development of the mixing zone was noticed. The mixing zone was stable and looked homogeneous without exhibiting of any channeling outside the mixing zone.

		Group nr. 3 **Experiment nr. 1** **Table 6-10**			
Rotation speed		≈ 50-350 rpm			
Rotation time		45 min			
pipe (OD)/well (ID)		2.0 cm / 3.0 cm			
Fluid	Density [sg]	PV [cP]	YP [lb/100ft²]	Gel strength (10 sec / 10 min) [lb/100ft²]	Result Height of the mixing zone [cm]
Heavy	1.70	16	33	35 / 62	≈ 10
Light	1.10	8	12	16 / 29	
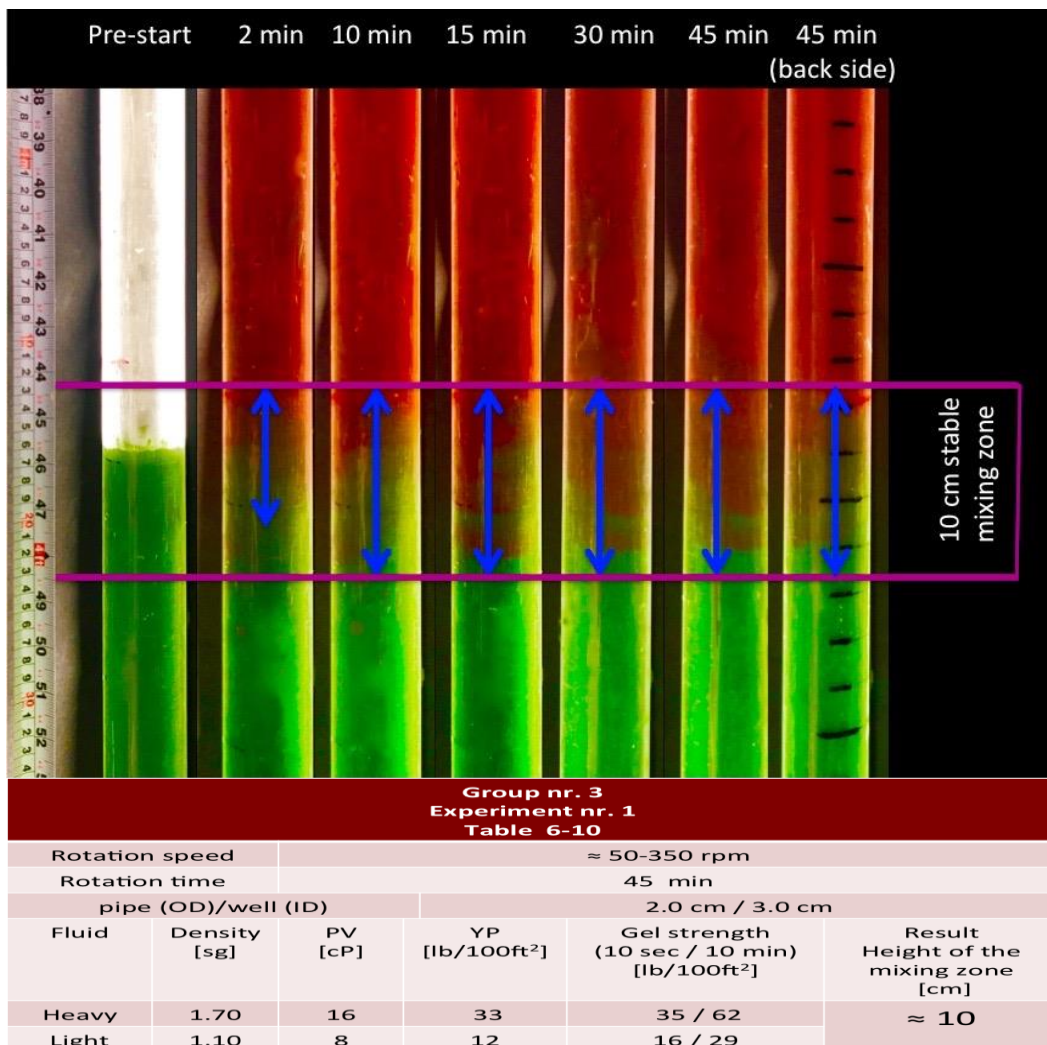
Figure 7-19: Illustrates the photos of the mixing zone in experiment 1 from group 3.

MATLAB Analysis

The MATLAB analysis of the images of this experiment is presented in figure 7-20. Based on this analysis, it was confirmed that the mixing zone was stable throughout the test. The interface between the fluids was at the well depth of 116 cm. The mixing zone with a height of about 9 cm expanded upward and downward as seen on the x-axes.
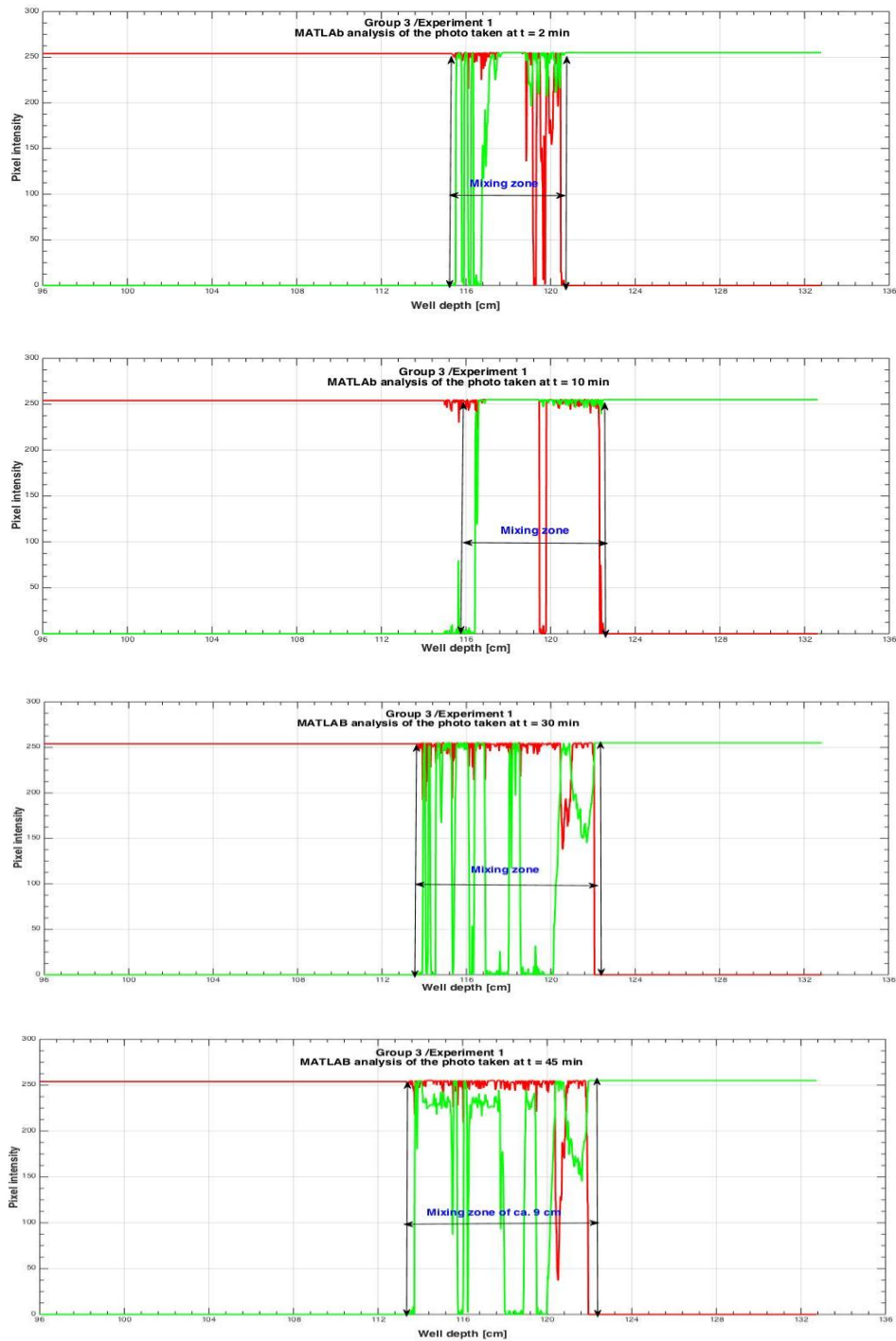
Figure 7-20: MATLAB analysis of experiment 1 from group 3

Experiment 2

The result of experiment 2, where the yield point of the heavy and the light fluids were 13 and 10 lb/100ft^2 respectively, is presented in figure 7-21. A homogeneous and well-mixed zone with the final height of about 16 cm reached stability within 30-40. The experiment was run for 60 min, but no further development of the mixing zone was observed.

Group nr. 3 Experiment nr. 2 Table 6-10					
Rotation speed	≈ 50-350 rpm				
Rotation time	60 min				
pipe (OD)/well (ID)	2.0 cm / 3.0 cm				
Fluid	Density [sg]	PV [cP]	YP [lb/100ft²]	Gel strength (10 sec / 10 min) [lb/100ft²]	Result Height of the mixing zone [cm]
Heavy	1.72	18	14	17 / 32	≈ 16
Light	1.10	8	12	16 / 29	
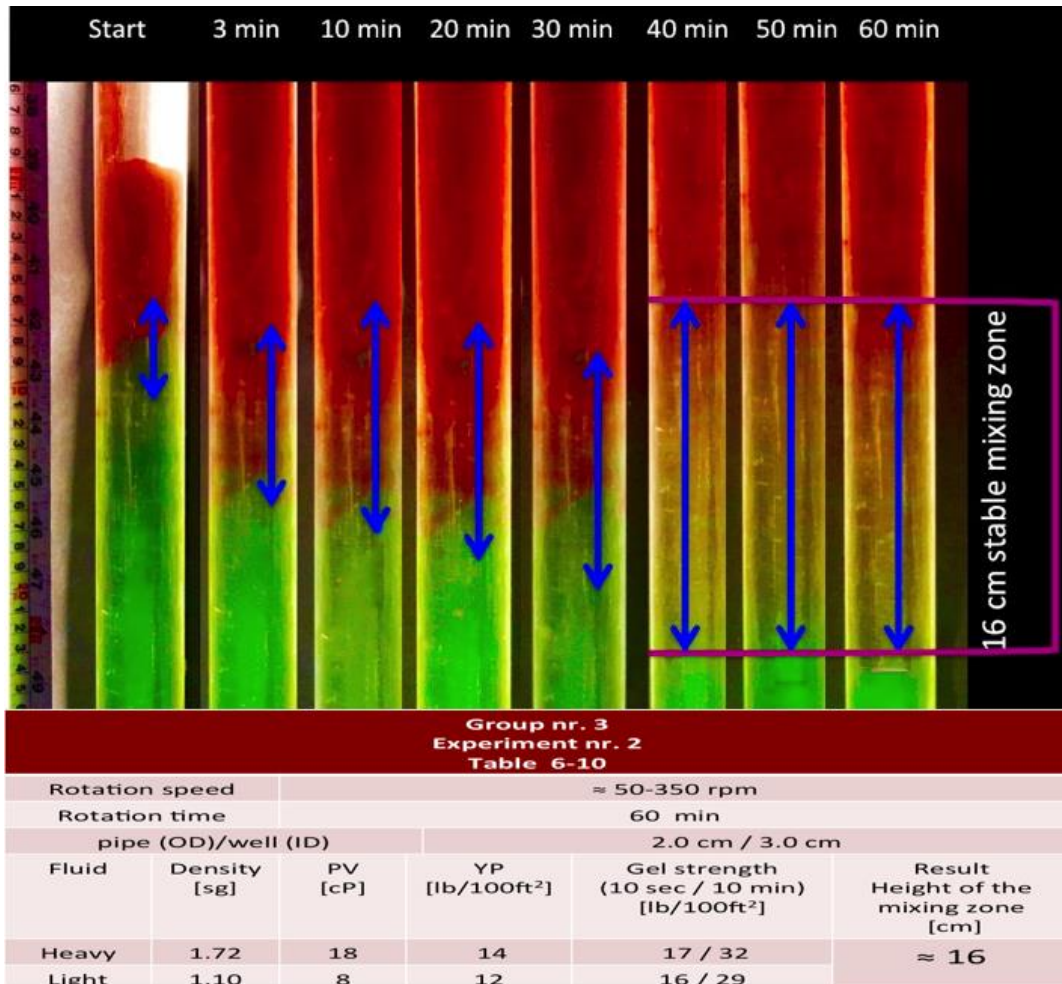
Figure 7-21: Shows the images of experiment 2 from group 3.

Mathematical Check of the Result

At the end of the experiment and before pulling out the pipe of the well, the heavy fluid on the top of the mixing zone was gathered for further analysis. The volume and density of the collected fluid were measured. The result indicated that the collected fluid had the same density as before starting the experiment. By subtracting the collected volume from the amount heavy fluid that been pumped down in the well (*pre-start volume*), the volume of the fluid that been mixed with light fluid was determined. By dividing this volume with the cross-sectional area of the gap around the pipe, the height of the mixing zone was estimated.

82

<u>Calculation</u>:

It was collected 372 ml non-contaminated heavy fluid. The measured density was the same before and after the experiment (1.70 sg). Thus, the height of the mixing zone was calculated as follow:

$$h_{mixing\ zone} = \frac{V_{mixed\ volume\ of\ heavy\ fluid}}{A_{cross-sectional}}$$

$$A_{cross-sectional} = \frac{\pi}{4}(OD^2 - ID^2)$$

Pre-start volume was 460 ml = 460 cm^3

The volume of the collected non-contaminated heavy fluid was 373 ml = 373 cm^3

The volume of the heavy fluid that been mixed with the light fluid in the mixing zone:

= (460 - 373) cm^3 = **87 cm^3**

$$h_{mixing\ zone} = \frac{87\ cm^3}{\frac{\pi}{4}(3^2-2^2)} = 22\ cm$$

MATLAB Analysis

The MATLAB analysis of this experiment is illustrated in figure 7-22. The mixing zone started at the well depth of 109 cm and developed both up-and downward. The analysis verified the visual interpretation of the photos presented in the figure 7-21 and the height of the mixing zone was estimated to be 16 cm.
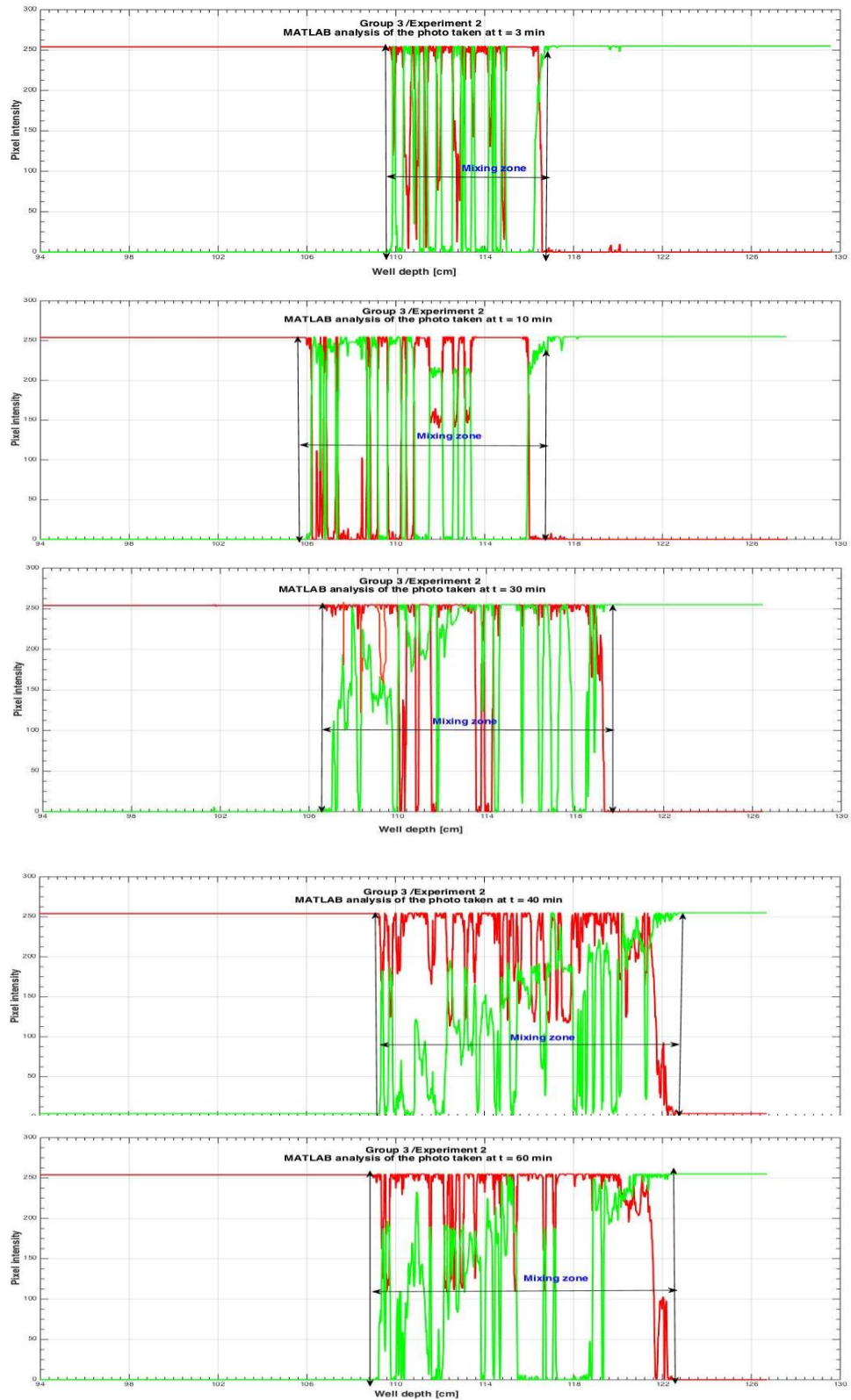
Figure 7-22: MATLAB analysis of the photos taken during experiment 2 of group 3.

Considering experiment 3 from this group (*table 6-10*), where the yield point of the light fluid reduced to 6 lb/100ft^2, the growth of mixing zone was continued until it reached a height of 82 cm and then stabilized. Furthermore, a complete mixing between fluids was seen in experiment 4, where the yield points of both fluids were reduced to 6-7 lb/100ft^2.

Group nr. 4 Δρ = 0.71 sg

For this group, it was performed four experiments where the density of the heavy fluid was 1.81sg. Following are the analysis of three experiments both visually as well as using MATLAB.

The height of the mixing zone developed in experiment 2 was also checked mathematically based on the collected heavy fluid at the end of the experiments.

Experiment 1

Based on the visual analysis of the photos taken in experiment 1 (*figure 7-23*), a mixing zone of about 18 cm was detected on the back side of the cylinder at t ~ 20 min, and it stayed stable during the experiment. The mixing had probably occurred at the start of the experiment. At the end of the experiment, the well was checked and no any traces or channelings were detected above or below the mixing zone.

Group nr. 4 Experiment nr. 1 Table 6-11					
Rotation speed	≈ 50-350 rpm				
Rotation time	60 min				
pipe (OD)/well (ID)	2.0 cm / 3.0 cm				
Fluid	Density [sg]	PV [cP]	YP [lb/100ft²]	Gel strength (10 sec / 10 min) [lb/100ft²]	Result Height of the mixing zone [cm]
Heavy	1.81	16	31	36 / 57	≈ 18
Light	1.10	8.5	10	14 / 26	
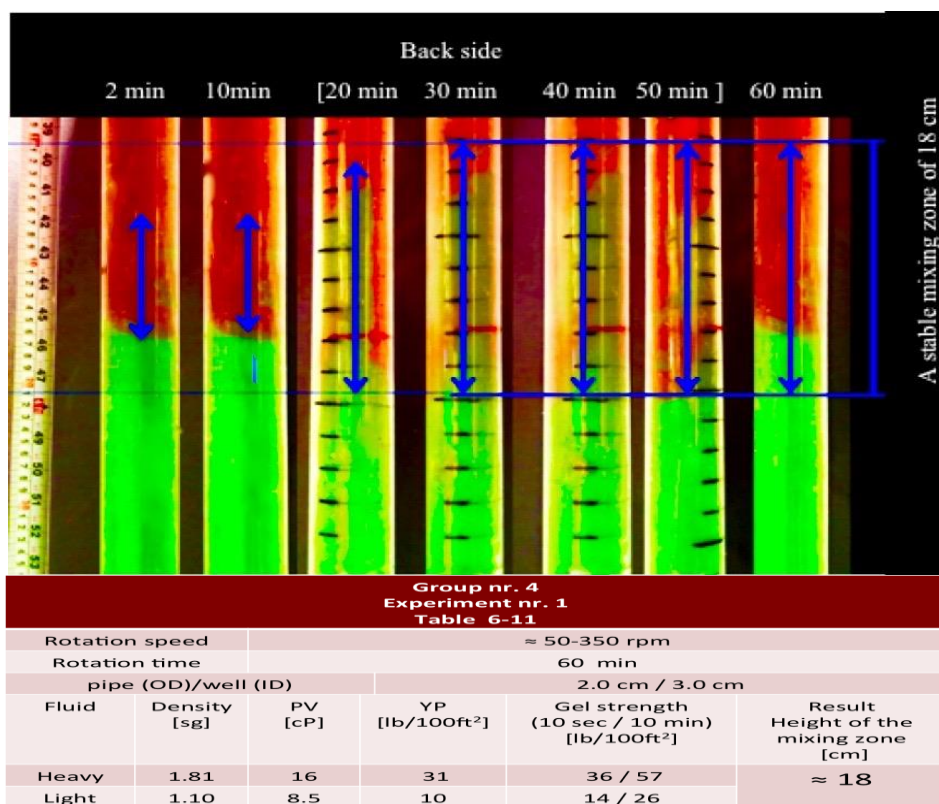
Figure 7-23: Illustrates the development of the mixing zone in experiment 1 from group 4.

Experiment 2

Figure 7-24 illustrates the photos taking while running experiment 2 of this group. The first and the second picture were taken using a slow-motion video camera. As seen in the figure, the rate of the growth of the mixing zone was highest during the first 3 minutes. Thereby, it slowed down, and the system reached stability at t ~ 20 min. There are some channelings and traces inside the mixing zone. However, nothing like that was noticed outside the zone.

	Group nr. 4 Experiment nr. 2 Table 6-11				
Rotation speed	≈ 50-350 rpm				
Rotation time	50 min				
pipe (OD)/well (ID)	2.0 cm / 3.0 cm				
Fluid	Density [sg]	PV [cP]	YP [lb/100ft²]	Gel strength (10 sec / 10 min) [lb/100ft²]	Result Height of the mixing zone [cm]
Heavy	1.80	18	12	15 / 32	≈ 28
Light	1.10	8.5	10	14 / 26	
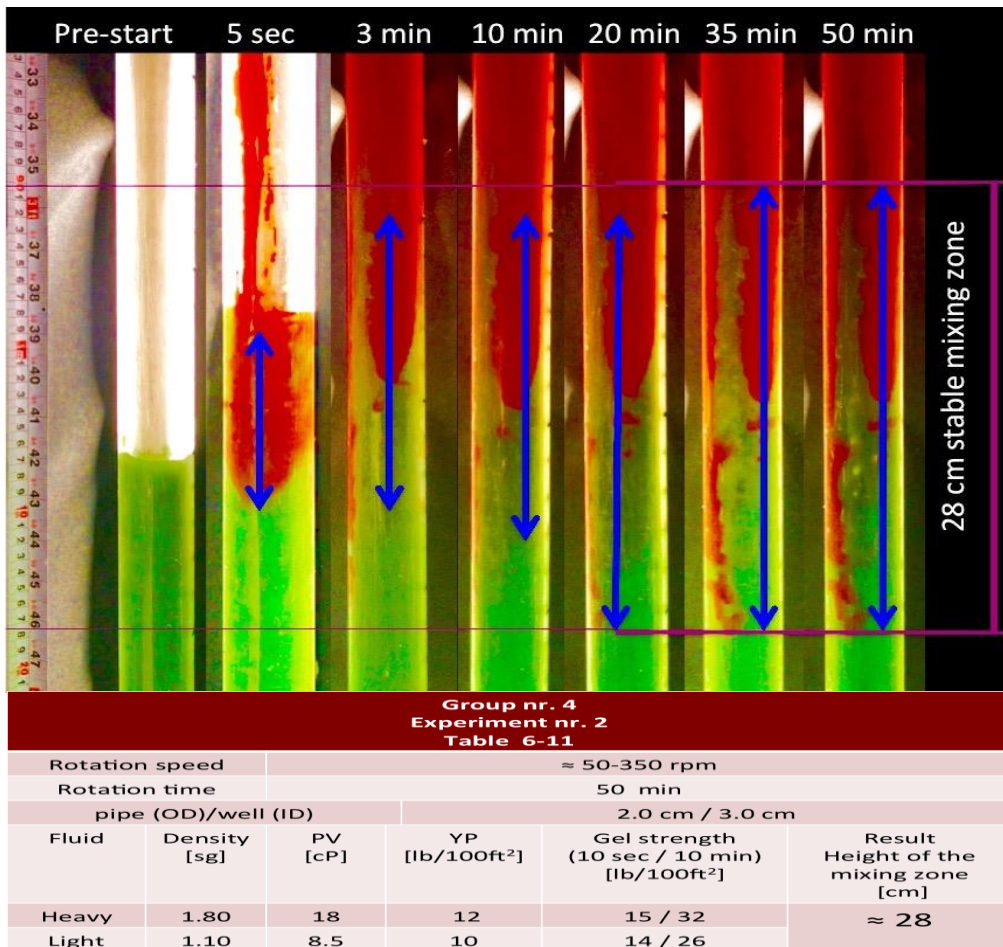
Figure 7-24: Shows the photos of experiment 2 from group 4.

MATLAB Analysis:

In addition, the photos in figure 7-24 were analyzed by MATLAB, and the results are presented in figure 7-25. The interface was located at a depth of 106 cm. The mixing zone started by fingering of the light fluid upward with a height of about 14 cm. Thereby, at t ~ 10 min, the mixing zone growth downward and the system reached stability at the time between 20 to 30 min.
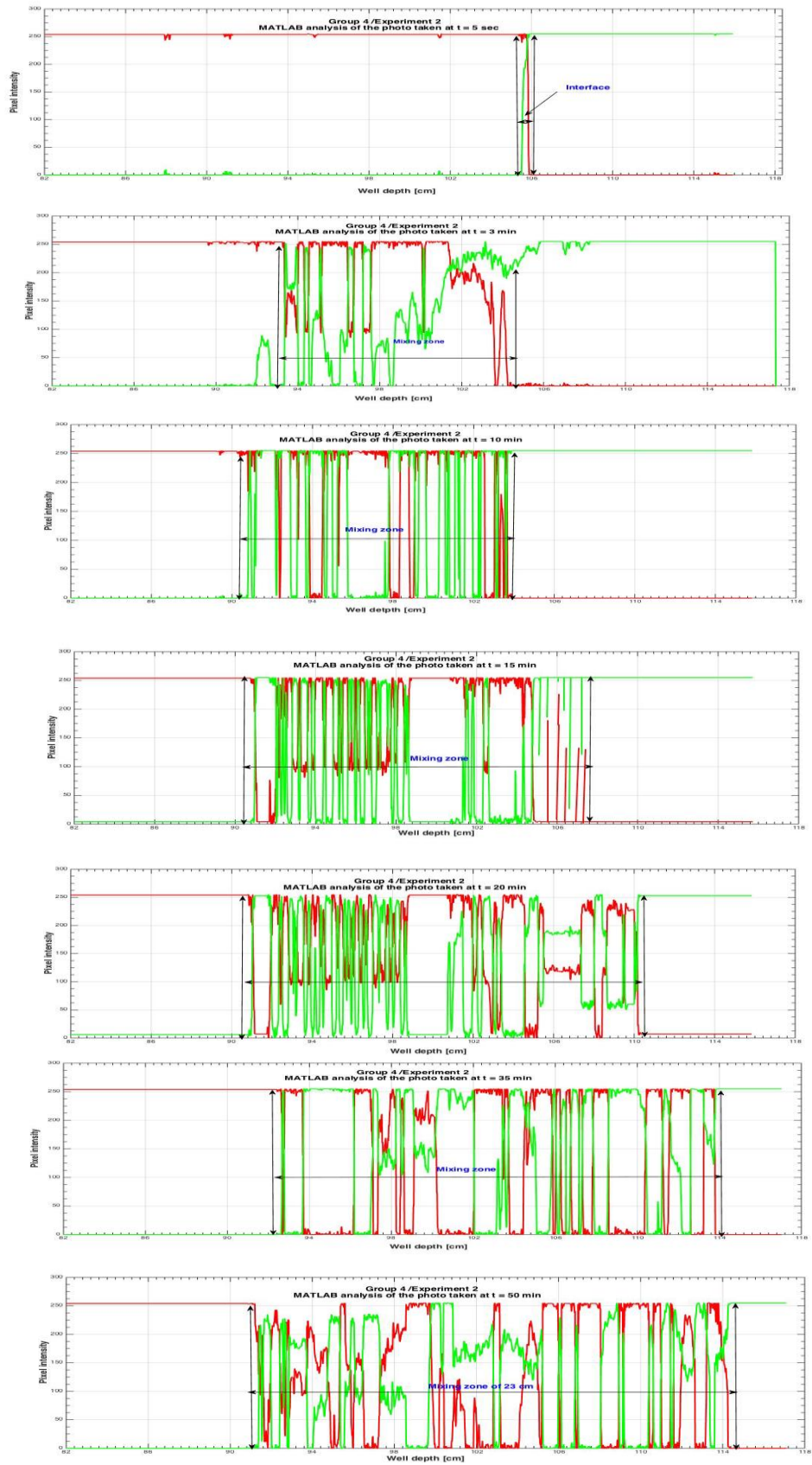
Figure 7-25: MATLAB analysis of experiment 2 from group 4

Mathematical Check of the Result

The same procedure as described before was performed in order to check whether there were existed any hiding channeling outside the mixing zone. The heavy fluid on the top of the zone was gathered, and its density was checked and compared to the density before starting the experiments. It wasn't any difference between the densities before and after the experiment, which indicated that no any channeling outside the mixing zone has occurred. Furthermore, the volume of the collected heavy fluid was used to estimate the height of the mixing zone as follows:

Calculation:

Pre-start volume the heavy fluid was 470 ml = 470 cm^3

The volume of the collected non-contaminated heavy fluid = 340ml = 340 cm^3

The volume of the heavy fluid mixed with the light fluid = (470-340) cm^3 = **130 cm^3**

$$h_{mixing\ zone} = \frac{130\ cm^3}{\frac{\pi}{4}(3^2 - 2^2)} = 33\ cm$$

Experiment 4

Consider the experiment 4, where the yield point of both fluids was reduced to 6 lb/100ft^2, which result in complete mixing of the fluids completely within 5 minutes. The photos from this experiment are shown in figure 7-26.

Group 4 Experiment nr. 4 Table 6-11					
Rotation speed			50-350 rpm		
Rotation time			5 min		
pipe (OD)/well (ID)				2.0 cm / 3.0 cm	
Fluid	Density [sg]	PV [cP]	YP [lb/100ft²]	Gel strength (10 sec / 10 min) [lb/100ft²]	Result Height of the mixing zone [cm]
Heavy	1.81	19	7	9 / 17	Completely mixed 190 cm
Light	1.11	7.5	6	7 / 13	
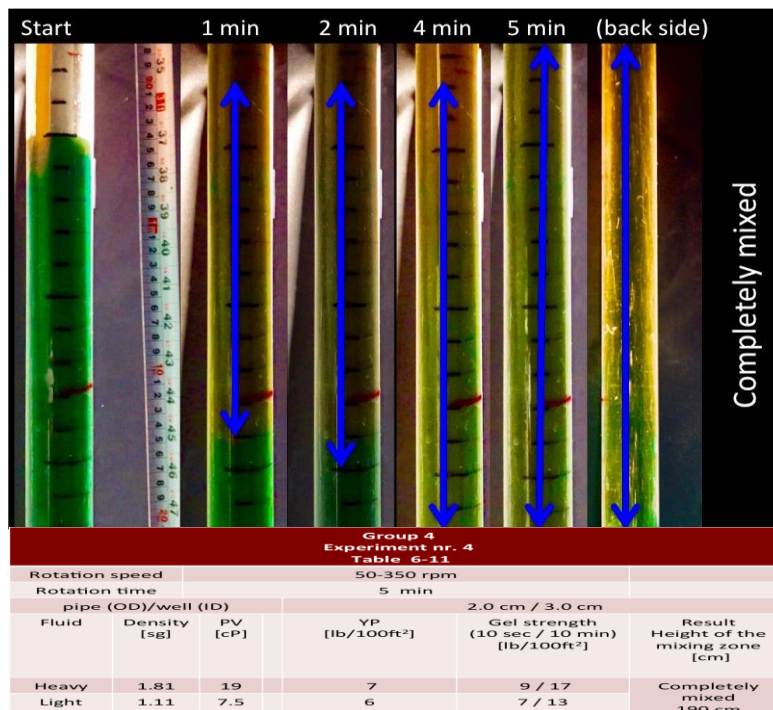
Figure 7-26: Illustrates the photos taken of the mixing zone in experiment 3 from group 4

<u>**Summary of The Results Analysis of Part IV**</u>

The result analysis of the experiments from this part of the work were compared and presented in a chart that is illustrated in figure 7-27. The graph was made of plotting the height of the mixing zone of 16 experiments (y-axes) as the function of $\Delta\rho$ (x-axes), at four different yield point intervals. Each column represents the height of the mixing zone developed during a specific experiment. The gel properties are presented in table 6-7.

The pink colored columns represent the height of the mixing zone in mud systems, where the yield point of the heavy fluid was between 28 to 33 lb/100ft^2 while this parameter of the light fluid was between 10 to 12 lb/100ft^2. For fluids that exhibited such gel properties, the minimum mixing zone was about 3 cm that developed when $\Delta\rho$ was 0.30 sg. For the same HOL-system, the maximum height of the mixing zone was about 18 cm, which occurred when $\Delta\rho$ was about 0.70 sg.

The blue column is the height of the mixing zone where the yield point of both fluids was between 10-14 lb/100ft^2. The mixing zone between the fluids that exhibited such rheological properties was stable and controllable for all groups of experiments, i.e., for $\Delta\rho$ up to 0.71 sg. The maximum height of the mixing zone was 28 cm (*for $\Delta\rho$ of 0.71 sg*) while the minimum mixing zone was 7 cm ($\Delta\rho$ of 0.30 sg).

The red columns represent the height of the mixing zone of the experiments where the yield point of the heavy fluid was between 12-14 lb/100ft^2 while this property of the light fluid was about 6 lb/100ft^2. The growth of the mixing zone for all experiments was controllable, but it increased significantly for $\Delta\rho > 0.50$ sg (*group 3 and 4*). Thus, the maximum height of the mixing zone was 89 cm (for $\Delta\rho$ of 0.71 sg) while the minimum height was 12 cm (*for $\Delta\rho$ of 0.30 sg*).

The columns in green colored represent the height of the mixing zone developed when the mud systems exhibited the lowest possible gel properties, i.e., when the YP of both heavy and the lights fluids was between 6 to 7.5 lb/100ft^2. During the experiments in this group, the mixing zone was controllable only when $\Delta\rho \leq 0.5$.

The height of the mixing zone of 190 cm represents an entire mixing, which is equivalent to the sum of the height of both fluids inside the acrylic cylinder (well).

Height of the mixing zone as function of Δρ at four different YP-intervals

Legend:
- 28 ≤ YP(heavy f.) ≤ 33, 10 ≤ YP(light f.) ≤ 12
- 12 ≤ YP(heavy f.) ≤ 14, 10 ≤ YP(light f.) ≤ 12
- 12 ≤ YP(heavy f.) ≤ 14, 6 ≤ YP(light f.) ≤ 6.5
- 6.5 ≤ YP(Heavy) ≤ 7.5, 6 ≤ YP (Light) ≤ 6.5

Fluids with controllable mixing zone

Fluids with non-controllable mixing zone
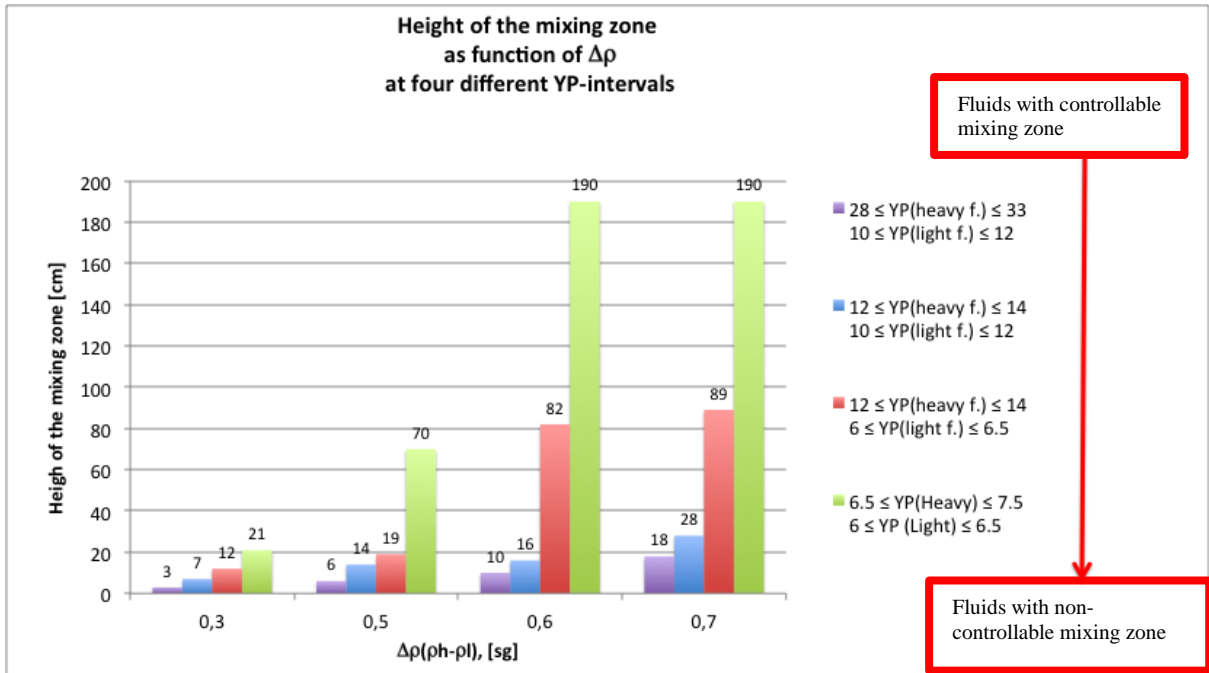
YP [lb/100ft²]	Height of the mixing Four different groups of experiments			
	Height of the mixing zone at Δρ (1.40-1.10)= 0.30 sg	Height of the mixing zone at Δρ (1.60-1.10)= 0.50 sg	Height of the mixing zone at Δρ (1.70-1.10)= 0.60 sg	Height of the mixing zone at Δρ (1.80-1.10)= 0.70 sg
28 ≤ YP(heavy f.) ≤ 33 10 ≤ YP(light f.) ≤ 12	3 cm	6 cm	10 cm	18 cm
12 ≤ YP(heavy f.) ≤ 14 10 ≤ YP(light f.) ≤ 12	7 cm	14 cm	16 cm	28 cm
12 ≤ YP(heavy f.) ≤ 14 6 ≤ YP(light f.) ≤ 6.5	12 cm	19 cm	82 cm	89 cm
6.5 ≤ YP(Heavy) ≤ 7.5 6 ≤ YP(Light) ≤ 6.5	21 cm	70 cm	190 cm (Complete mixing)	190 cm (Complete mixing)

Figure 7-27: Height of the mixing zone as function of Δρ at different intervals of YP.

7.5   Part V: Effect of The Annular Gap Around The Pipe

In this part, a new pipe/well combination (2.50 cm / 4.0 cm) was implemented and three experiments, where the density difference of 0.5 sg, were performed.

Based on the visual analysis of the experiments, whose data specifications are presented in table 6-12, the mixing zone was unstable where the yield point of one of the fluids was below 10 $lb/100ft^2$. The challenge with this part of the work was to follow the mixing zone correctly, due to it´s fast growing. Since the distance between the camera and the cylinder inside the cabin was too short, the height of the camera had to be adjusted regularly. Therefore, the photos were taken at six different levels as presented in figures 7-28 and 7-29.

Experiment 1

In experiment 1, the yield point of the light was 7 $lb/100ft^2$, and for the heavy one14 $lb/100ft^2$. The fluids were mixed entirely during the first few minutes after starting the process.

Experiment 2

In this experiment, the yield point of the heavy and the light fluids was increased to 18 $lb/100ft^2$ and 10 $lb/100ft^2$ respectively. The mixing process was at the highest speed during the first 75 sec. Afterward, the growth of the mixing zone decreased, and the system reached stability. The final height of the mixing zone was estimated to be about 92 cm and at t ~ 40 min. It was developed about 23 cm upward and 69 cm downwards from the interface as it is seen in figure 7-28. The process was run for 60 min, but no further growth of the mixing was observed during the last 20 minutes.

Experiment 3

Then in experiment 3, the yield point of the light fluid was further increased to 12 $lb/100ft^2$. This, in trun, resulted in decreasing the height of the mixing zone down to 80 cm, i.e., by ca10% compared to the result in experiment 2. In the photos shown in the figure 7-29, the rate of the growth of the mixing zone was the highest during the first 2 minutes, and it was about 20cm/1.25 min (*figure 7-29.a*). The rate of the mixing process gradually decreased, and the system reached stability at t ~ 35 min (*figure 7-29.e*). During the last 15 minutes no any further development of the mixing zone was observed (*figure 7-29.f*).

Figure 7-28: Show the result of the experiment 2, where the effect of the annular gap was studied.
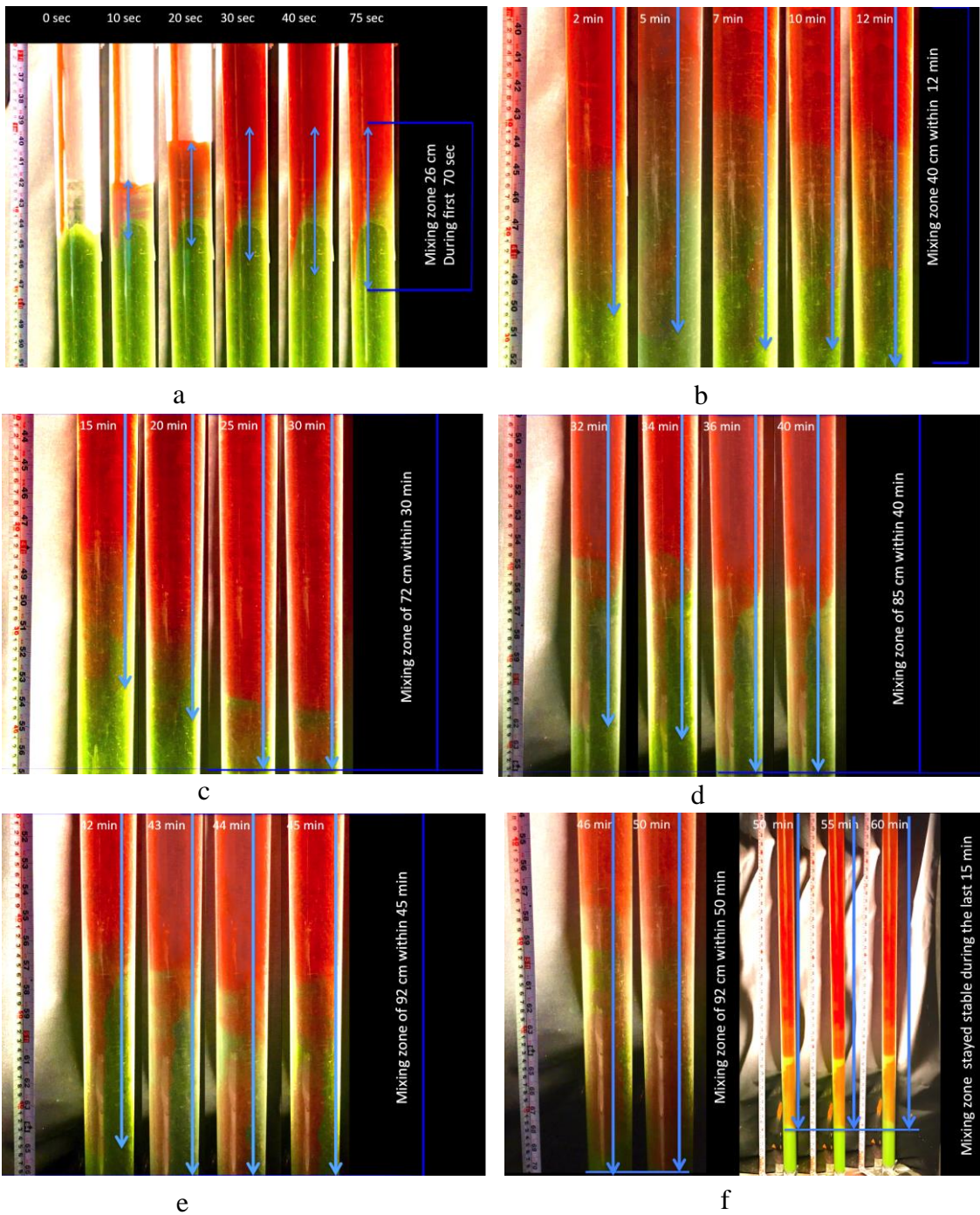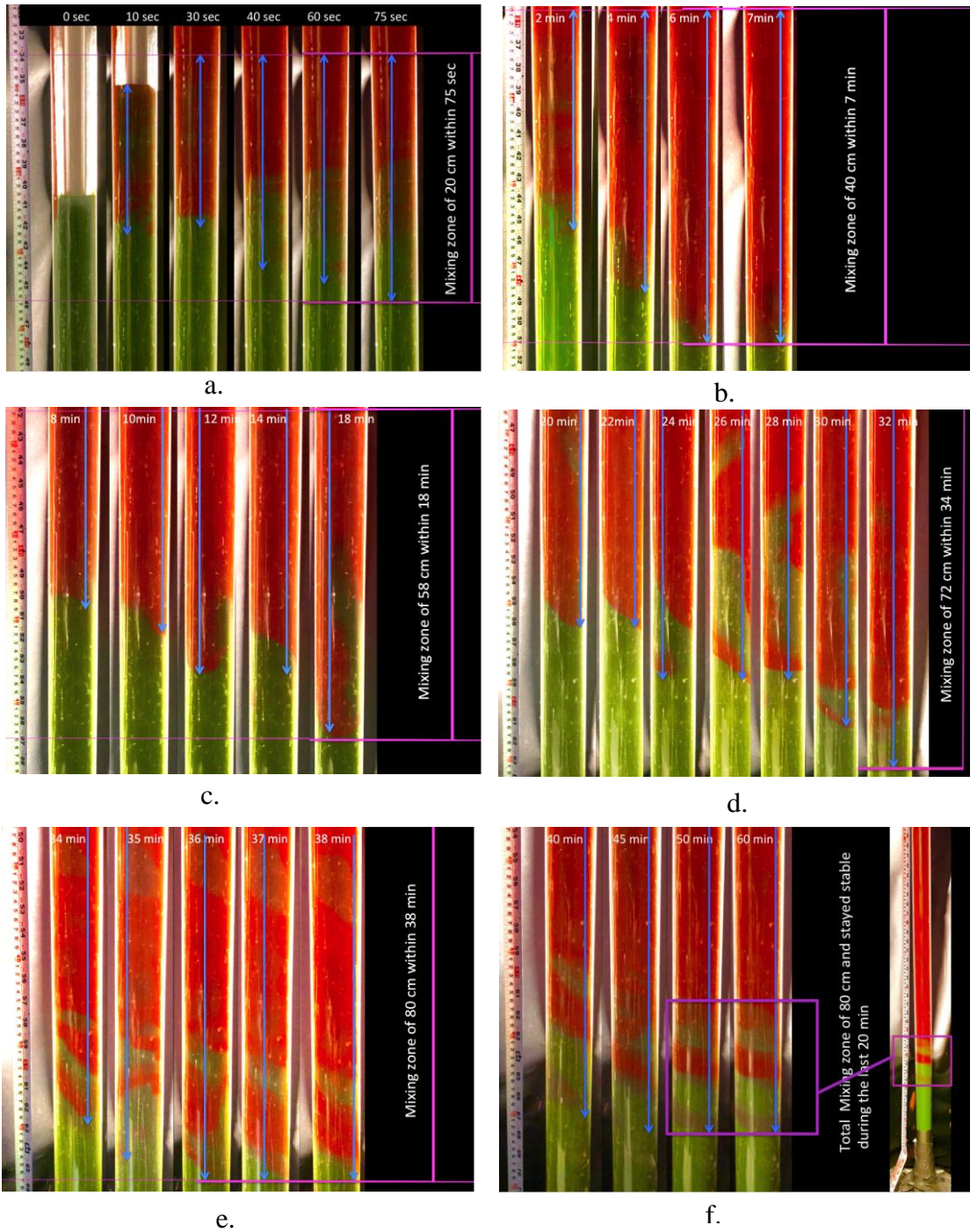
Experiment nr. 3 Table 6-12 New (pipe/well) combination					
Rotation speed		≈ 50-350 rpm			
Rotation time		60 min			
pipe (OD)/well (ID)		2.5 cm / 4.0 cm			
Fluid	Density [sg]	PV [cP]	YP [lb/100ft²]	Gel strength (10 sec / 10 min) [lb/100ft²]	Result Height of the mixing zone [cm]
Heavy	1.60	20	18	22 / 37	≈ 80
Light	1.10	8.5	12	14 / 26	

Figure 7-29: Illustrates the result of the experiment 2, where the effect of the annular gap was studied.

8 Discussion

During this master thesis there were some challenges related to the instruments, materials and preparing the drilling fluids. One of the difficulties during was difficulty with setting the rotation of the pipe on a fixed speed when using such type of drill machine. The speed was therefore estimated by accounting the number of the rotations per minute using a slow-motion video camera, and it was set between 50 to 350 *rpm*. The second issue was the reaction between the first tested color indicators and other additives in the mud, which caused gas bubbles in the system. However, metal oxides were found to be the most proper color indicators, because they didn't react with the other components in the mud. Therefore, tens of experiments were repeated using the new color indicators. Another challenge was preparing the drilling muds with the desired rheological properties. It was time-consuming and quite difficult to reproduce the drilling fluids with similar rheological characteristics.

Based on the analysis of the rheological characteristics (*Appendix E*), the measured data suited best to the Herschel Bulkley model. Of this reason, the low shear yield stress (LSYS) was directly calculated using the mentioned model and reported as the yield point (YP) of the fluids. The 10 sec gel strength of the most of the fluids used in this work was quite similar to LSYS of the fluids. Since these two rheological parameters have a directly proportional relationship to each other, therefore the only focus was on regulating the LSYS to the desired limit.

During this work, determining the gel strength at 30 min was neglected. The reason was the measured gel strengths at 10 min for the majority of the fluids were less than 2 times the gel strength at 10 sec.

The entire work of was divided into four main categories in order to separately study the impact of the rotation speed as well as the effect of the rheological and physical parameter of the fluids on the development of the mixing zone in the HOL-configuration. The results of the experiments presented in chapter 7 will be discussed in this chapter. Also, the effect of the annular gap between the well and the pipe was studied to obtain a better understanding and to make a more reliable conclusion.

8.1 Part I: Effect of The *rpm*

In purpose of understanding the impact of the rotation speed of the pipe (rpm) on the development of the mixing zone, a number of experiments were performed in both horizontal and vertical direction.

<u>Horizontal direction</u>

The purpose of performing the experiments in the horizontal direction was to reduce the effect of gravity on the interface between the fluids and thereby focus on *rpm*. The tests were categorized into two groups depending on the density difference between the fluids.

<u>Group 1</u>

The first group included experiment 1, 2, 3, and 4 (*table 6-1*), where two fluids with identical properties but with two different color indicators were deployed.

According to the theory of the mixture, the mixing processes between two incompressible and miscible fluids are generally divided into physically different categories; diffusion, turbulence and chaotic. Since both fluids in our case were in static condition, therefore the first category (*diffusion*) is applied. Such mixing usually takes a long time to be complete in the absence of other internal or external factors. Since the fluids were identical, the effect of the all other parameters, such as rheological and physical properties, on the interface was excluded. Hence the rotational force, due to *rpm*, was the only factor that could impact the mixing zone. The rotating pipe causes rotational circulations of the processed material (*solid particles and other elements*) around its own center, which, in turn, creates a radial mixing.

<u>Group 2</u>

This group included experiment 5, 6, 7, and 8, where the density of the left side fluid (*beige colored seen in figure 7-2*) was higher than for the fluid on the right side (*green colored*). Thus, the impact of the density was included. Based on the result presented in table 6-2, the fluids were mixed at the interface; and the width of the mixing zone increased by increasing the annular gap around the pipe (*figure 7-2*). After the system had reached stability, no any further growth of the mixing zone was noticed regardless of *rpm*.

Based on the comparing the results from these two groups presented in figure 7-3, no any mixing zone between the fluids was observed regardless of *rpm (red colored curve)*. However, the instability at the interface and the further development of the mixing zone occurred under the impact of the density difference as well as increasing the gap around the pipe. It seems like the second mentioned factor had a significant impact on the growth of the mixing zone between the fluids. This might be occurred due to increasing the contact area at the interface between the fluids and hence enhancement of the mixing process.

Vertical section

During this part of the work, glycol with same density and viscosity was used as both upper (*red colored glycol*) and lower fluid (*blue colored glycol*). The used glycol was diluted by adding water in order to prepare a mixture with the plastic viscosity of 7 cP and without any gel properties. The reason of using glycol with such characteristics was excluding the effect of the other parameters, such as yield point and gel strength as well as the Earth´s gravitational force on the interface between the fluids. This means that the rotation speed of the drill pipe (*rpm*) was the only mechanism that could impact on the interface between the fluids. The system was transparent, and one could see the behavior of the fluids through whole the system and not just at the inside surface of the well. As seen from photos of experiment 1 and 2 shown in figure 7-4, the interface between the fluids was stable throughout the experiments regardless of the rotation speed of the pipe.

Another observation that made was the contribution of the rotational force of the pipe while transferring the upper fluid. If the upper fluid was transferred while rotating the pipe, the growth of the mixing zone was slower, and a more homogeneous mixing with less channeling was observed (*figure 7-4.b*). Additional parameter that might cause the difference between the results of these experiments was the gap between the well and pipe, which was 0.50 cm larger in figure 7-4.a compared to 7-4.b. The larger the gap, the higher the mixing zone.

8.2   Part II: Effect of the plastic viscosity on the mixing zone

In this part, the results of two groups of experiments presented in table 6-3 and 6-4 are discussed. The main difference between the groups was the type and properties of the light fluid that was made of mixing of water, glycol, and salt. The reason for using these components was to prepare a light fluid exhibiting both viscosity and transparency. Thus, the behavior of the settling barite particles from the heavy fluid at the interface could be seen with the naked eye.

Group nr. 1

Studying experiment 1 and 2 (figure 7-5.a), the heavy fluid fingered into the light fluid in the form of lumps and then the fluids were completely mixed immediately, and before starting the rotation of the pipe. The mixing probably occurred under the impact of the gravitational force, but also due to the absence of the gel properties within the light fluid.

In experiment 3 and 4, the impact of the Earth´s gravity was excluded since the fluids had the same densities. Based on the visual analysis of the result of experiment 4, presented in figure 7-5.b, the barite particles gradually settled to the bottom, and the fluids were mixed within 4 to 5 minutes.

Thus, the fall of the barite particle was occurred due to the barite sag since the light fluid didn't exhibit any gel properties to keep the particles suspended.

<u>**Group nr. 2**</u>

Based on the results of the tests presented in figure 7-6, besides the density difference between the fluids, the mixing zone was controllable and the system reached stability within 10-15 minutes from the start of the process. Therefore, it can be concluded that the stability of the interface was provided by the rheological characteristics such as yield point, and gel strength.

Comparing the results obtained from these two groups of tests, it was seen that the viscous drag force was not sufficient to hold the solids in equilibrium or to reduce the settling velocity of the particles. Therefore, the absence of the gel properties in one of the fluids will cause the instability at the interface in the HOL-arrangement. Of this reason, the investigation of the impact of the yield point and the gel strength of the fluids became the central element of the focus during this master thesis.

8.3   Part III: Effect of The Yield Point and Gel Strength

The fluids that were tested during this part and the rest of the work were conventional drilling muds made of fluid water, xanthan-polymer, and bentonite. Barite was added as the weighting material. Preparing the drilling muds with identical components provided compatibility between the heavy and the light fluids, hence excluding the impact of unknown factors on the growth of the mixing zone.

As discussed in the previous part, it was seen that the yield point and gel strength were more critical parameters than viscosity regarding the stability at the interface between the fluids in a HOL-configuration. The effect of these parameters was therefore studied separately by maintenance the YP and gel strength for one of the fluids relative constant while decreasing these parameters for the other one.

<u>**Effect of YP of The Light Fluid**</u>

The gel strength and the yield point of the light fluid were the only variables during the experiments presented in table 6-5. Thus, these properties were the only factors that could impact the outcome of the experiments.

<u>**Effect of YP of The Heavy Fluid**</u>

During the experiments performed in this part (*table 6-6*), the gel strength and the yield point of the heavy fluid were the variables while keeping these parameters at 8-11 lb/100ft^2 for the light fluid.

Therefore, any deviation of the results could be related to the change of the mentioned properties of the heavy fluid.

Based on the visual analysis of the results from this part of the work, the yield point and gel strength of both light and heavy fluids are two critical factors to stabilized the mixing zone. The impact of the rheological characteristics of the light fluid found to be of greater importance than that of the heavy fluid (*figure 7-11*). The similar observation was also seen when studying the effect of the viscosity in Part II (*figure 7-5*), where the system completely mixed due to the absence of gel properties in the light fluid. Therefore, due to its position and function, it is important that it has sufficient carrying capacity to hold the falling particles from the heavy fluid at the interface but also to provide a good hole cleaning. However, these rheological properties should be at the lowest possible limits since the light fluid is the active drilling mud and it continuously circulates. On the other hand, the heavy fluid is the passive drilling mud, and it will be at static condition throughout the drilling operation. Therefore its rheological characteristics can be higher compared to the light fluid.

8.4   Part IV: Development of The Mixing Zone as Function of $\Delta\rho$

This part was performed by dividing the experiments into four groups, as presented in tables (6-8. 6-9, 6-10, and 6-11), depending on the density difference between the fluids. The purpose of setting-up the experiments in such approach was to find the relationship between $\Delta\rho$ (ρ_h-ρ_l) and the height of the mixing zone, but also to estimate the minimum gel properties that the fluids should have at the largest possible $\Delta\rho$.

The results of the experiments, where using fluids with $\Delta\rho$ larger than 0.50 sg, were also checked by an additional method as described in Appendix D. Of this purpose, two experiments in groups 3 and 4 were selected for checking. The calculated height of the mixing zone, using this mathematical calculation, differed from both MATLAB analysis and the visual observation shown in chapter 7.4 only with a small margin; 6 cm for the results from experiment 2 group 3 and 5 cm for experiment 2 group 4. The difference between the results might have caused by losing an amount of the heavy fluid during the transferring to the cylinder or gathering the fluid at the end of the experiment. The analysis from this method confirmed that any hidden channelings inside the fluid system might not exist. This means that the estimated heights of the mixing zone obtained visually as well as by MATLAB were reliable.

In several cases, the MATLAB analyses have shown that the mixing zone first developed upward and then downwards. Such a characteristic can be explained by the RT-instability theory when the

light fluid raised into the heavy fluid in the form in the form of bubbles and then the heavy fluid starts fingering into the light fluid in the form of mushroom-shaped spikes.

According to the results, it was shown that the mixing zone increased by increasing $\Delta\rho$ even though using the drilling fluids with the same rheological properties. This was expected, as the density difference between the fluids is the main factor causes the establishing of the mixing zone in a HOL-arrangement. The growth of the mixing zone, almost during all the experiments, occurred with the highest speed at the first moment when the fluids came into contact with each other. Afterward, the mixing process slowed down significantly. Decreasing the rate of the mixing zone with time may be explained by the theory of the mixture. According to this theory, the density of the new liquid mixture (*the mixing zone in our case*) will be larger than the density of the light fluid and smaller than the density of the heavy fluid. Thus, under the condition of a well-mixing process, two new interfaces will be created; one interface between the mixing zone and the heavy fluid on the top of the zone and one between the mixing zone and the light fluid at the bottom of the zone. A uniform mixing provides the system with a smaller density difference at the new interfaces, and hence reducing the impact of the gravitational force. Consequently, a homogeneous mixing zone may contribute the HOL-arrangement to reach stability much faster compared to the one with channeling effects and didn't exhibit homogeneity.

8.5 Part V: Impact of The Annular Gap Around the Pipe

By deploying the new pipe/well combination (*2.50cm/4.0cm),* the gap around the pipe increased to 1.50 cm, i.e., 0.50 cm larger than the one used during the previous experiments, which means an increase by 50%. Besides increasing in scale, but the ratio of both combinations was still similar; (*2.0cm/3.0cm = **0.66***) compared to (*2.5cm/4.0cm = **0.63***).

The result presented in figure 7-28 indicates that established mixing zone ($h_{m.z.} \approx 92\ cm$) was much higher than the one shown in figure 7-21 ($h_{m.z.} \approx 18\ cm$), even though the fluids had quite the same density and rheological properties. Based on this observation, the gap between the well and the pipe found to be another determining factor on the stability of the mixing zone. Therefore, increasing the cross-sectional area of the annulus between the pipe and the well requires increasing the yield point of the fluids in order to keep the particles suspended. This result has a quite good agreement with the theory part (*chapter 3.6.2).* The reason for requiring higher gel properties when increasing the annular gap of is probably because of increasing the total surface area of the particles where the

shear force is acting (*compared to equation 3.42*). Therefore, a larger shear force is needed to keep the whole system stable when the cross-sectional area of the annulus is increased.

In summary, the results from the experiments had shown that the HOL-arrangement with a density difference of about 0.70 sg between the fluids was controllable when both fluids had YP larger than 10 lb/100ft^2. However, increasing the gap between the well and the pipe lead to a significant increase in the height of the mixing zone. Since the equipment, time, and resources were limited during this master thesis, it was not possible to investigate the establishment of the mixing zone in larger scales.

According to the simulation study done by Reelwell (*chapter 2.2.1*), the full buoyancy of the aluminum dual drillstring (DDS) in a HOL-operation was approached when the density difference between the outer and inner fluid was about 0.60 sg. This, in turn, results in significant decreasing of torque and drag profile of the drillstring. Reducing torque and drag in such extend results into doubling of the length of the world´s record ERD, which at the moment is about 12 km. Applying Reel well drilling method, the need of the number of rigs and wells will drastically be reduced, which in turn leads to reduction of drilling costs and drilling-related hazards in future.

9 Conclusion

The investigations of the development of the mixing zone between the drilling fluids of various densities with the HOL experimental arrangements used here have revealed the following:

- The possibility to have a vertical fluid column, where a higher density fluid is in a stable position above a lower density fluid is confirmed. Consequently, a mixing zone with a height that gradually increases with time will be established and separate the two fluids.
- The rate of the development of the mixing zone was at the highest speed at the start of the experiments, but it decreased with time.
- The yield point and gel strength for the two fluids were found to be determining factors to control the stability and height of the mixing zone.
- The high plastic viscosity of the fluids was not sufficient to provide a stable mixing zone. The fluids were completely mixed within a short period of time, in cases when one of the fluids did not exhibit the gel properties.
- High *rpm* did not have a significant effect on the further development of the established mixing zone. However, the rotation of the rod was important to avoid channeling effects, especially when pumping down the heavy fluid at the start of the experiments.
- With a density difference of about 0.70 sg between the fluids, the mixing zone was stable when both fluids had YP larger than 10 lb/100ft^2.
- The experiments indicated that the relationship between the developed height of the mixing zone and $\Delta\rho$ is non-linear. Further investigations are required to clarify.
- The experiments indicated that the gap between the pipe and the wellbore had a significant effect on the height of the mixing zone. Increasing the gap by 50%, the height of the mixing zone was increased fivefold, even though using fluids with the same physical and rheological properties.

The agreement between our experimental results and the theory is excellent regarding the effect of the investigated parameters on the growth of the mixing zone. However, further investigations with larger well diameters are needed to obtain results representative for field use.

References

1. Vestavik, O., et al. *Extended Reach Drilling-new solution with a unique potential*. in *SPE/IADC Drilling Conference*. 2013. Society of Petroleum Engineers.

2. Demirdal, B., *Managed Pressure Drilling*. Getting Up to Speed. 2010: Society of Petroleum Enginners.

3. Udegbunam, J.E., *Improved well design with risk and uncertainty analysis*. 2014, University of Stavanger: University of Stavanger.

4. Reid, P., et al., *Differential-Sticking Mechanisms and a Simple Wellsite Test for Monitoring and Optimizing Drilling Mud Properties*. SPE Drilling & Completion, 2000. **15**(2): p. 97-104.

5. Aadnøy, B.S., *Modern well design*. 2nd ed. ed. 2010, Boca Raton: CRC Press/Balkema.

6. Nandan, A., S. Imtiaz, and S. Butt, *Robust gain switching control of constant bottomhole pressure drilling*. Journal of Process Control, 2017. **57**: p. 38-49.

7. *A pore pressure graph where UBD, MPD and UBD (conventional drilling) are shown.* . 2015 [cited 2015; Available from: http://www.drillingcontractor.org/wp-content/uploads/2010/02/KenSara-graph.jpg

.
8. Rehm, B. and B. Rehm, *Managed pressure drilling*, in *Gulf Drilling Guides*. 2008, Gulf Pub.

9. Lake, L.W. and L.W.M.R.F. Lake, *Petroleum Engineering Handbook, Volume 2 : Drilling Engineering*. 2006, Richardson: Richardson, US: Society of Petroleum Engineers.

10. Chilingarian, G.V. and P. Vorabutr, *Drilling and drilling fluids*. Updated textbook ed. ed. Developments in petroleum science. Vol. 11. 1983, Amsterdam: Elsevier.

11. Hughes, B., *Drilling Fluids Reference Manual*. Houston, Texas, 2006.

12. Allen, F., et al., *Extended-reach drilling; breaking the 10-km barrier*. Oilfield Review, 1997(4): p. 32-47.

13. W.Walker, M., *Sakhalin extended-reach well pushes ERD envelope to a world record.(Extended reach drilling)*. World Oil, 2012.

14. Mark C. Tynan, G.P.R., Frank V. Perry, Richard E. Kelley, Sean T. Champenios, *A map of the Worldwide Extended reach drilling wells*. June 2017, Department of Energy National Laboratory / U.S.

15. Francis, D., *Extended-reach drilling systems address downhole challenges*. Offshore, 2014. **74**(9).

16. Gao, et al., *Limit analysis of extended reach drilling in South China Sea - Limit analysis of extended reach drilling in South China Sea.* 石油科学: 英文版, 2009(2): p. 166-171.

17. Vestavik, M.A.B.a.O.M., *Deploymnet of Reelwell drilling Method in Shale gas field in Canada.* 2011: p. 9.

18. Jpt, S., *Reelwell Drilling Method Makes Use of Dual-Conduit Drillstring.* Journal of Petroleum Technology, 2012. **64**(08): p. 38-39.

19. Ola M. Vestavik, J.T., Bernd Schmalhorst and Jan Petter Roed *New heavy-over-light drilling fluid solution was also incorporated to solve torque, drag , hole cleaning and ECD control problems.* 2017.

20. AS, R. *The company´s internal figures.*

21. Mirhaj, S.A., E. Kaarstad, and B.S. Aadnoy, *Improvement of torque-and-drag modeling in long-reach wells.* Modern Applied Science, 2011. **5**(5): p. 10.

22. AS, R., *Reelwell AS, A drilling prospect.* 2009, Energy, Oil & Gas

23. Join, S., *Drilling fluid types.*

24. Bloys, B., et al., *Designing and managing drilling fluid.* Oilfield Review, 1994. **6**(2): p. 33-43.

25. Skjeggestad, O., *Boreslamteknologi : teori og praksis.* 1989, Bergen: Alma Mater.

26. Kolle, G. and R. Mesel, *Brønnvæsker : for VK1 brønnteknikk.* Fellesspråklig utg. ed. Brønnvæsker. 1998, Nesbru: Vett & viten.

27. L.L.C., M.-I., *Drilling Fluids Engineering Manual.* 1998: M-I L.L.C.

28. Fink, J.K., *Oil Field Chemicals, Fluid Loss Additives.* 2003: Elsevier Inc. 1-33.

29. Nguyen, T., et al., *Experimental study of dynamic barite sag in oil-based drilling fluids using a modified rotational viscometer and a flow loop.* Journal of Petroleum Science and Engineering, 2011. **78**(1): p. 160-165.

30. Bern, P.A., et al., *Barite sag: Measurement, modeling, and management.* 2000. p. 25-30.

31. Omland, T.H., *Particle settling in non-newtonian drilling fluids.* 2009.

32. Hanson, P., et al. *Investigation of barite" sag" in weighted drilling fluids in highly deviated wells.* in *SPE Annual Technical Conference and Exhibition.* 1990. Society of Petroleum Engineers.

33. Caenn, R., H.C.H. Darley, and G.R. Gray, *Composition and properties of drilling and completion fluids.* 2017, Gulf Professional Publishing.

34. Tanner, R.I., *Engineering rheology.* 2nd ed. ed. Oxford engineering science series. Vol. 52. 2000, Oxford: Oxford University Press.

35. Panton, R.L., *Incompressible flow*. 2013, Wiley: Hoboken, N.J.

36. Growcock, F. and T. Harvey, *Drilling Fluids-Chapter 2*. 2005: Elsevier Inc. 15-68.

37. Power, D. and M. Zamora. *Drilling fluid yield stress: measurement techniques for improved understanding of critical drilling fluid parameters*. in *National Technology Conference "Practical Solutions for Drilling Challenges": American Association of Drilling Engineers, Technical Conference papers, AADE-03-NTCE-35*. 2003.

38. Scott, P.D., M. Zamora, and C. Aldea. *Barite-sag management: challenges, strategies, opportunities*. in *IADC/SPE Drilling Conference*. 2004. Society of Petroleum Engineers.

39. Hodne, H., *Drilling Fluid Technology , PET 210, The Laboratory compendium*, E.a. Petroleumtechnology, Editor. 2014. p. 122.

40. Alan H. Cook, J.E.F.a.K.L.N., *gravity*. 2018: Encyclopædia Britannica, Inc.

41. Gamow, G. and J. Randers, *Gravitasjon*. Gravity. Vol. 28. 1966, Oslo: Cappelen.

42. Newton, I., *The Principia: mathematical principles of natural philosophy*. 1999: Univ of California Press.

43. *density*. 2018: Encyclopædia Britannica, Inc.

44. Ahmadi, M.A., et al., *An accurate model to predict drilling fluid density at wellbore conditions.* Egyptian Journal of Petroleum, 2016.

45. McMordie Jr, W., R. Bland, and J. Hauser. *Effect of temperature and pressure on the density of drilling fluids*. in *SPE Annual Technical Conference and Exhibition*. 1982. Society of Petroleum Engineers.

46. Wu, A., G. Hareland, and M. Fazaelizadeh, *Torque & drag analysis using finite element method.* Modern Applied Science, 2011. **5**(6): p. 13.

47. Skalle, P., et al. *Microbeads as lubricant in drilling muds using a modified lubricity tester*. in *SPE Annual Technical Conference and Exhibition*. 1999. Society of Petroleum Engineers.

48. Amani, M., M. Al-Jubouri, and A. Shadravan, *Comparative study of using oil-based mud versus water-based mud in HPHT fields.* Advances in Petroleum Exploration and Development, 2012. **4**(2): p. 18-27.

49. Mamat, N., et al., *The performance of polymer beads in water-based mud and its application in high-temperature well.* Journal of Petroleum Exploration and Production Technology, 2013. **3**(3): p. 151-158.

50. Lubinski, D. and B. Mallinckrodt, *Neglected Aspects and Truncated Appraisals in Vocational Counseling: Interpreting the Interest–Efficacy Association From a Broader Perspective: Comment on Armstrong and Vogel (2009)*. 2010. p. 226-238.

51. Evje, S. and K.K. Fjelde, *Hybrid Flux-Splitting Schemes for a Two-Phase Flow Model.* Journal of Computational Physics, 2002. **175**(2): p. 674-701.

52. Kuchibhatla, S.C., *Experimental investigation of the effect of initial condition on Rayleight-Taylor instability*, in *Texas A&M University*. 2010, Texas. p. 139.

53. Foroushan, H.K., et al., *On the Instability of the Cement/Fluid Interface and Fluid Mixing.* SPE Drilling & Completion, 2018. **33**(01): p. 063-076.

54. Cook, A.W. and P.E. Dimotakis, *Transition stages of Rayleigh–Taylor instability between miscible fluids.* Journal of Fluid Mechanics, 2001. **443**: p. 69-99.

55. Doludenko, A.N., S.V. Fortova, and E.E. Son, *The rayleigh–taylor instability of newtonian and non-newtonian fluids.* Physica Scripta, 2016. **91**(10): p. 104006.

56. S, R.M. *Experiments and simulations on the incompressible, Rayleigh-Taylor instability with small wavelength initial perturbations*. 2012.

57. Roberts, M.S. and J.W. Jacobs, *The effects of forced small-wavelength, finite-bandwidth initial perturbations and miscibility on the turbulent Rayleigh–Taylor instability.* 2016. **787**: p. 50-83.

58. Kuchugov, P., et al., *The evolution model of the rayleigh-taylor instability development.* Journal of Russian Laser Research, 2012. **33**(6): p. 517-530.

59. Aadnøy, B.S. and E. Society of Petroleum, *Advanced drilling and well technology*. 2009, Richardson, Tex: Society of Petroleum Engineers.

60. Jafr, G., *Drawn Figures* 2018.

61. Piroozian, A., et al., *Impact of drilling fluid viscosity, velocity and hole inclination on cuttings transport in horizontal and highly deviated wells.* Journal of Petroleum Exploration and Production Technology, 2012. **2**(3): p. 149-156.

62. Britannica, T.E.o.E., *Stokes's law*. 2018: Encyclopædia Britannica, Inc.

63. Wikipedia, t.f.e., *Fluid Dynamics*. 2018.

64. Join, S., *Cuttings transport.* PetroWiki.

65. Moler, C. *MATLAB*. 2004 2004; Available from: https://se.mathworks.com/company/newsletters/articles/the-origins-of-matlab.html.

66. Jafr, G., *Camera photos* in *Camera photos* 2018.

67. Oil, N.G., *Mud Density Test*. 2018, https://www.netwasgroup.us/engineering-3/mud-weight-marsh-funnel-viscosity-and-ph.html.

List of Figures

List of Tables

Appendix A: Equipment and Instruments

The following is the list of figures of the equipment and instrument used during this master thesis. For the description of the tools in detail, please see table 4-2.

Equipment	Photo
Protective glasses	
Laboratory scale	
Heidoph-Overhead Stirrer RZR 50	
Baroid Mud balance	
Fann-viscometer **VG-35**	

Table A-1: List of the equipment and instruments [66].

Equipment	Photo
pH-level meter	
Drilling Machine	
Trestle (Jack) stand	
Acrylic cylinder	
Aluminum rod	
Transparent hose connected to funnel	

Table A-2: List of the equipment and instruments, continue..
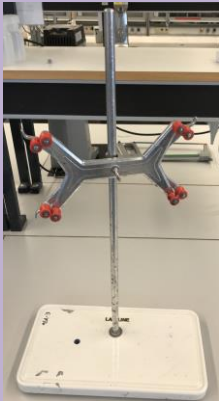
Equipment	Photo
Mechanical pump	
A strong tape	
Camera stand	
LED-lamp	

Table A-3: List of the equipment and instruments, continue..

Appendix B: Rig Design

Horizontal direction

The horizontal well was set-up as in figure 1. The length of the wellbore was from 2.0 m (*acrylic cylinder*) up to 10.0 m (*transparent hose*)
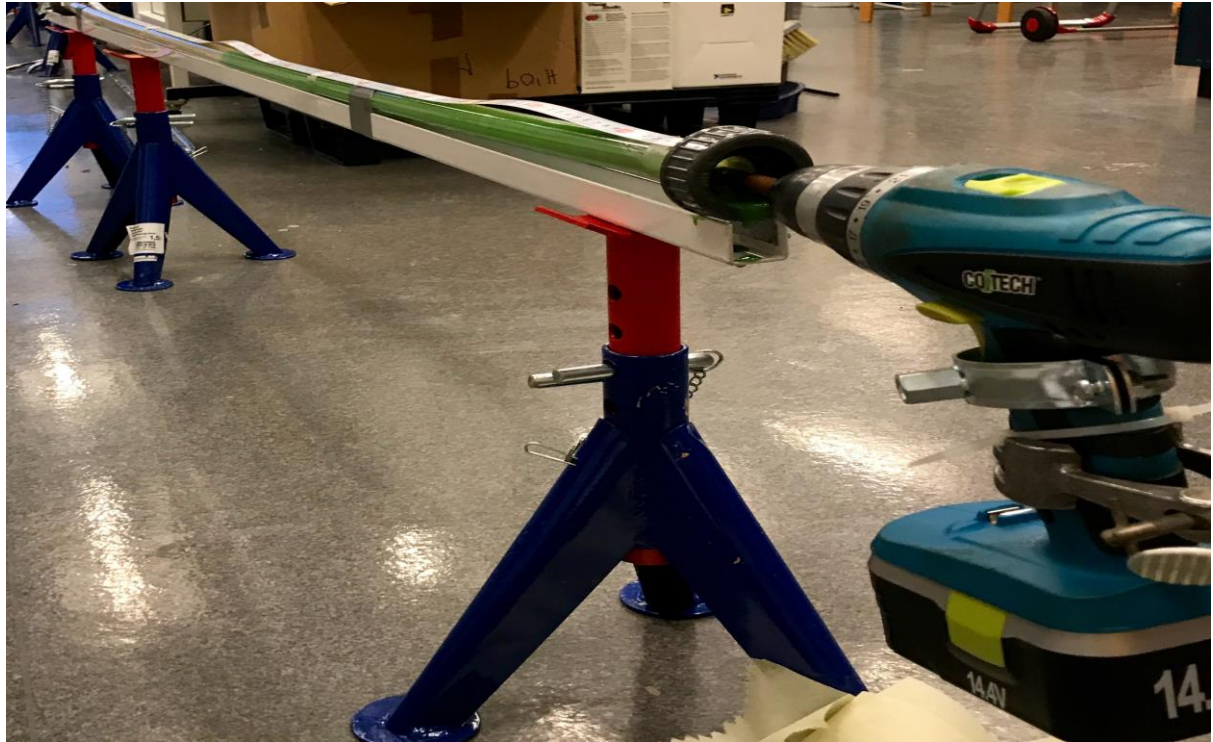
Figure B-1: Shows the actual photo of the horizontal wellbore [66].

Rig in Vertical Direction

The rig in the vertical direction was designed as seen in figure 2. The LED-lamp is mounted inside the cabin to provide light while the camera is taking photos during the experiment.

Drill machine

Blackout curtains

LED-lamp

Measuring Tape

Wellbore/cylinder
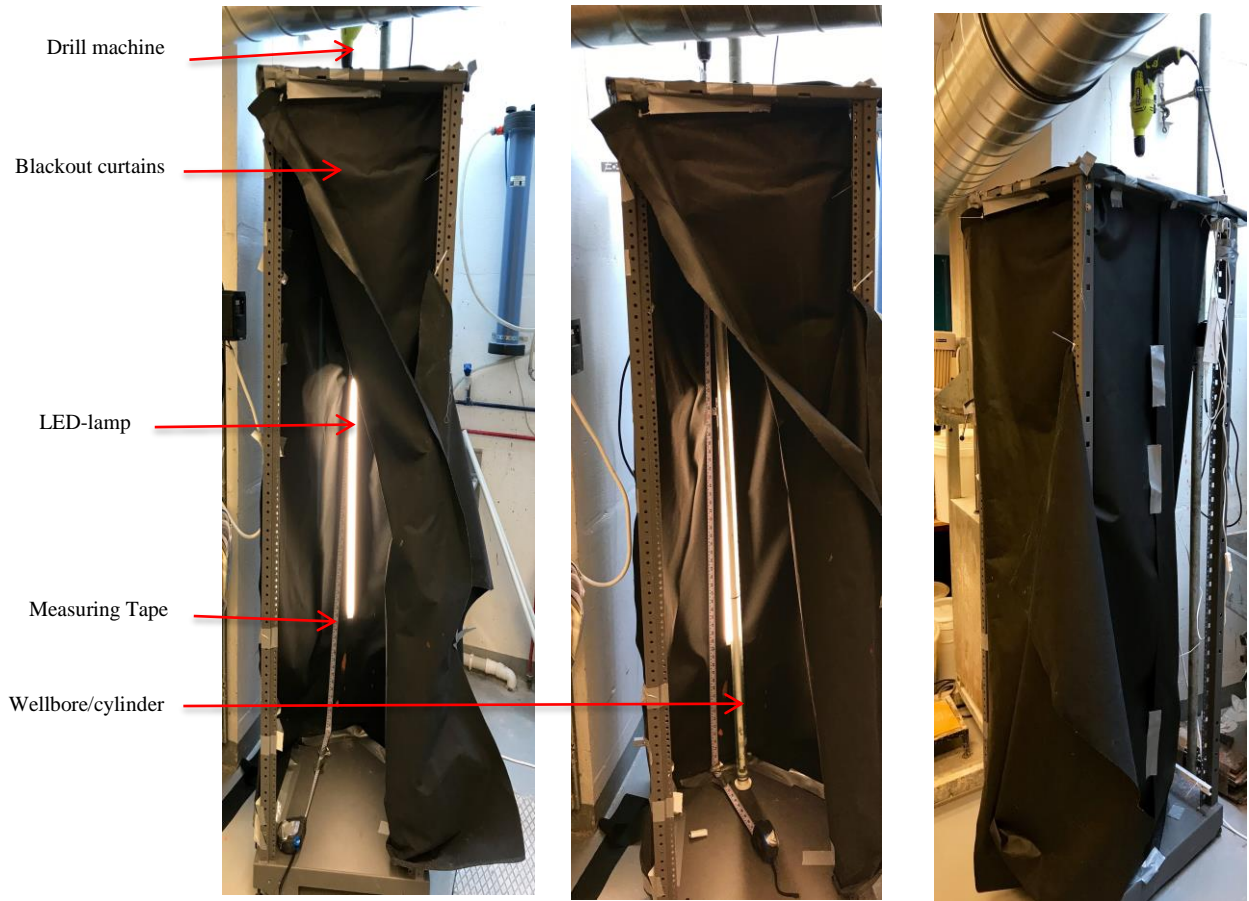
Figure B-2: Illustrates the actual photos of the rig in vertical direction [66].

Appendix C: Work Methods

The procedures of performing the experiments are described as follows:

Preparing The Premixed Mud

A volume of 500 ml premixed mud (water, XC-polymer, and bentonite) was prepared as the following steps:

- 500 g fresh water was weighted in a laboratory beaker.
- 0.50 g xanthan-polymer was gradually (*to avoid lumps in the fluid*) added to the water under mixing (1500-2000 *rpm*), using the Heidoph-Overhead Stirrer RZR 50 (*figure C-1*) and mixed for 5 min.
- 25 g bentonite was gradually added to the mixture under mixing, and the mud was mixed for additionally 5 min.
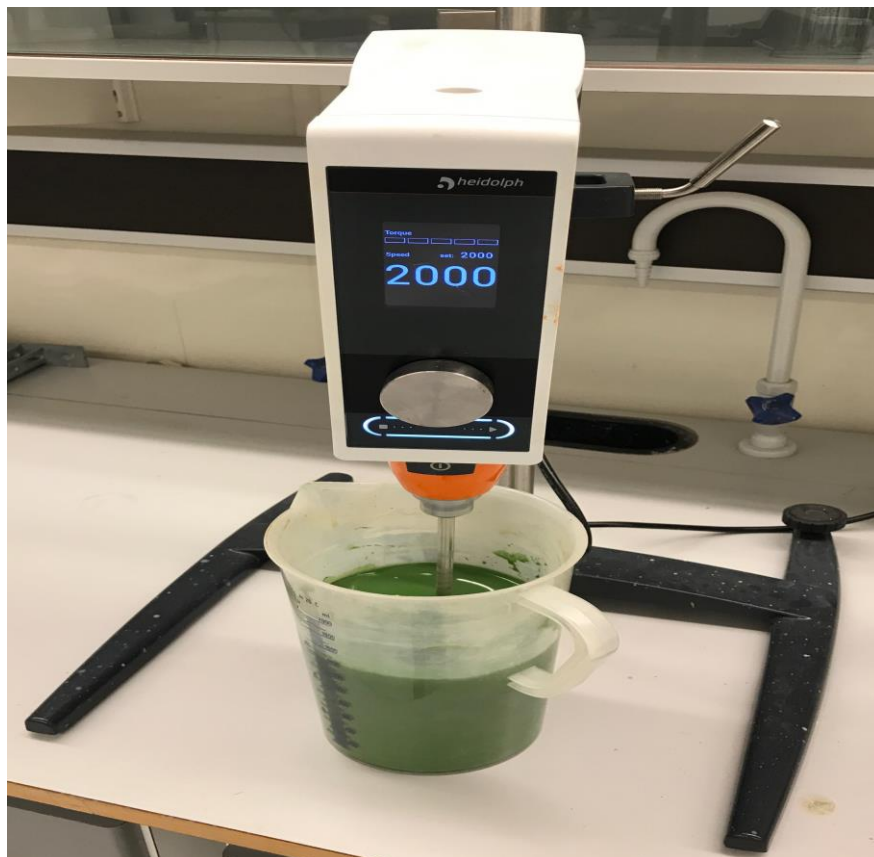
Figure C-1: Illustrates preparing the base mud using Heidoph-Overhead Stirrer RZR 50 [66]

Density Measurement

A Baroid Mud balance (*figure C-2*) was used for measuring the density of the fluids, and the following general was deployed:

- Make sure that the instrument is calibrated.
- The prepared fluid shall be remixed using a laboratory spoon to re-suspend the particles in the fluid before filling the cup of the Mud balance.
- The cup shall be fully filled with the drilling mud to be tested.
- Put the lid on the cup and make sure some mud is expelled through the hole in the cup.
- Outside the cup has to be cleaned with a wet paper and then dry it.
- Place the balance is on the base, with the knife-edge resting on the fulcrum.
- Move the rider until the graduated arm is leveled, as indicated by the built-in-spirit level on the beam.
- Now read the density and record it. The unit that is shown on the graduated arm is pound per gallon (*ppg*).
- The recorded density can be converted to the specific gravity "sg," by dividing with 8.33 *ppg*, which is the density of water that was used for calibrating the instrument.
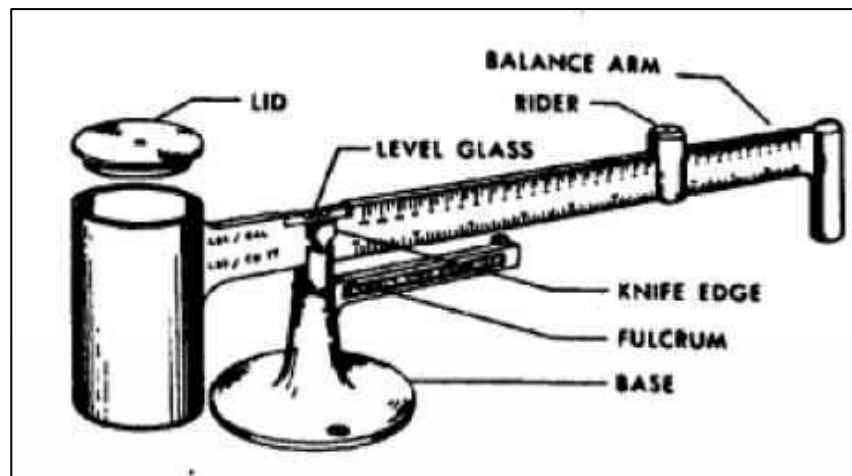
Figure C-2: Illustrates a Baroid Mud Balance [67]

Rheology Property Measurement of The Fluids

Using a calibrated Fann-viscometer VG 35 (figure-4), the rheology of the fluids was measured according to the following procedure:

Procedure:

- Make sure that the instrument is clean.

- Fill the sample cup with the drilling mud up to the scribed line and place it on the instrument stage.

- Raise the stage up to a level, so that the rotor is immersed to the proper immersion depth (*up to line marked in figure C-3*).

- Start the instrument to operate at the highest speed until the dial reader is stabilized.

- Then read the dial at the speeds of 600, 300, 200, 100, 60, 30, 6, and 3 RPM. Record the obtained readings for later calculation.

- From the dial readings, one can calculate Bingham plastic viscosity (PV), effective viscosity and yield point (YP) using the Bingham model. From Herschel Bulkley one can estimate LSYS. (*Please see the theory part chapter 3.7*).

rpm range knob

Dial reading

Scribed line
(inside the cup),
where the mud level
has to be

Main Shaft

Line
(where the fluid
Level shall be)

Sample cup

Rotor

Adjustable Stage
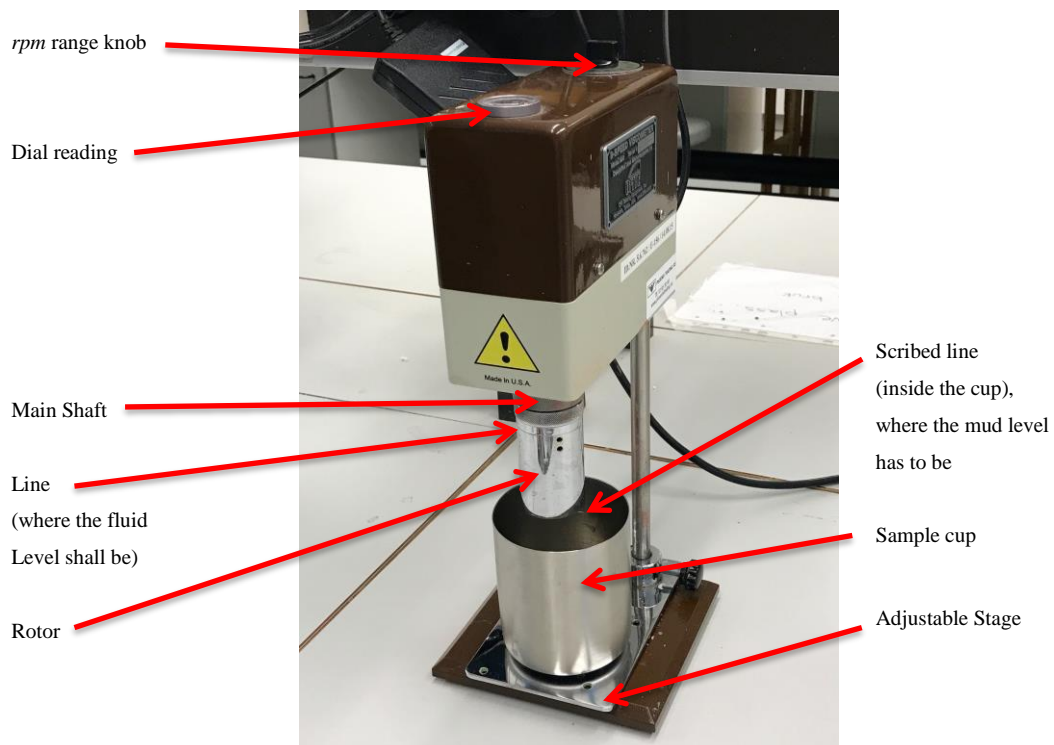
Figure C-3: A Fann-viscometer VG 35 [66].

Gel Strength Measurement

Before removing the sample cup, the gel strength of the fluids was determined according to the following procedures:

10 sec gel strength

Procedure

- Set the rotation speed to 600 *rpm* and let the rotor inside the sample cup to run for 10 seconds.
- Turn off the viscometer, using the power button, and let the fluid to be at rest for 10 seconds (*use timer*).
- During these 10 seconds set the speed to 3 *rpm* (*to be ready*)
- When 10 sec has passed, start the viscometer and record the maximum dial reading you can observe. This value is the 10 sec gel strength and has the unit ($lb/100ft^2$)

10 min gel strength

Procedure

- Set the rotation speed to 600 rpm and let the rotor inside the sample cup to run for 10 seconds i
- Turn off the viscometer and allow the fluids to be at rest for 10 minutes (use timer)
- Start the viscometer at 3 *rpm* after the 10 minutes has passed.
- Record the maximum dial reading you can observe. This value is the 10 min. gel strength and has the unit ($lb/100ft^2$)

30 min gel strength

Procedure

- The same procedure as for 10 sec and 10 min but let the fluid to be at rest for 30 minutes.

Since the 10 min gel strength of the majority of the fluids tested during this master thesis was less than 2 times 10 sec gel strength (*i.e., 10 min gel ≤ 2 * 10 sec gel*), thus the 30 min gel strength was not measured.

Heavy Over Light (HOL) Mud Preparation

The drilling fluids that used in the HOL-configuration were prepared from the premixed mud by adding barite as the weighting material.

Procedure:

- The amount of barite required for preparing the fluids of the desired densities was calculated using equation (5) derived from mass balance equation:

$$m_1 + m_w = m_2 \tag{1}$$

$$\rightarrow \rho_1 * V_1 + \rho_w * V_w = \rho_2 * V_2$$

Where:

$m = \rho * V$

$V_2 = V_1 * V_w$

$$V_w = \left[\frac{\rho_2 - \rho_1}{\rho_w - \rho_2}\right] * V_1 \tag{2}$$

$$m_w = \rho_w * V_w \tag{3}$$

$$m_w = \left[\frac{\rho_2 - \rho_1}{\rho_w - \rho_2}\right] * V_1 * \rho_w \tag{4}$$

$$\rightarrow \boldsymbol{m_w = \left[\frac{\rho_2 - \rho_1}{\rho_w - \rho_2}\right] * \frac{\rho_w}{\rho_1} * m_1} \tag{5}$$

Where:

m_w = Mass of weighting material (*barite*) that has to be added

ρ_1 = The density of the old mud (*premixed mud*)

ρ_2 = The desired density of the fluid to be prepared

ρ_w = The density of the weighting material (here barite = 4.6 sg)

m_1 = Mass of the old mud

- For preparing the light fluid, 10-15 g of the green color indicator (*Chrome Oxide Green, figure C-4*) was added to the mixture, and the mud was mixed for about 5 min.

- For preparing the heavy fluid, 20-30 g of the red color indicator was added while mixing.

- The calculated mass of barite was added to the drilling muds (heavy/light) while mixing the mixture for another min.

- While preparing the heavy fluid with larger densities, it was necessary to add lignosulfonate to the mixture in order to dilute the drilling mud and going over to a deflocculated system (*see the theory part*).

- Since lignosulfonate perform its function at a pH $>$10, NaOH was therefore added to the drilling mud in order to increase the pH-level.

- After adjusting the pH-level, the amount of the lignosulfonate was gradually added. During this step, it was important to be very careful so that the drilling mud was not diluted too much.

- Another Purpose of the using lignosulfonate was to adjust the rheological characteristics such as yield point and the gel strength.

- Density and the rheological properties of the fluids were measured and recorded for the later calculations.

Figure C-4: Shows metal oxides that used as color indicator for the fluids [66].

119

Experimental Set-up

After preparing the fluids with desired densities and rheological characteristics, each experiment was set-up according to the following procedure:

- The volume of the light and heavy fluid used in a 2.0 m high rig was calculated as follow:

$$A_{cross-sectional} = \frac{\pi}{4}(ID^2 - OD^2) \tag{6}$$

$$V_f = A_{cross-sectional} * h_f \tag{7}$$

Where:

$A_{cross-sectional}$ = Cross-sectional area of the annulus, [cm^2]

ID = Inner diameter of the well (*cylinder*), [cm]

OD = outer diameter of the pipe (*the rod*) [cm]

V_f = Volume of the used drilling fluid (*heavy or light*), [ml^3]

h_f = Height of the drilling muds (heavy or light) inside the casing after running the pipe inside the casing, [cm]. It was normally determined to be 100 cm for the vertical rig of 2.0 m.

- The one-end closed acrylic cylinder (the *well*) was set to a deviated position (*about 45°*).

- The measured volume of the light fluid (*green color*) was first transferred to the well using a funnel connected to a transparent plastic hose with the length of about 2.0 m (*figure C-5*). While performing this step, it was important to make sure that the upper part of the well didn´t contaminate by the light fluid, especially when pooling out the hose out of the well.

- After the light fluid had been transferred, into the well, the aluminum rod (*the pipe*) was carefully run into the well.

- The cylinder (*with the light fluid and pipe inside*), was set in front of the LED-lamp position inside the cabin in the vertical (*figure B-2, Appendix B*).

- The well was fastened to the top and bottom of the cabin using a strong tape (*T-Rex tape*) in order to reduce vibration while rotating the pipe.

- The drilling machine was mounted to the top of the pipe and tested for rotation.

- An iPhone with a "*Camera Self-timer multiple shots*" application was mounted on the camera stand and set inside the cabin and made ready for video recording and taking photos during the process.
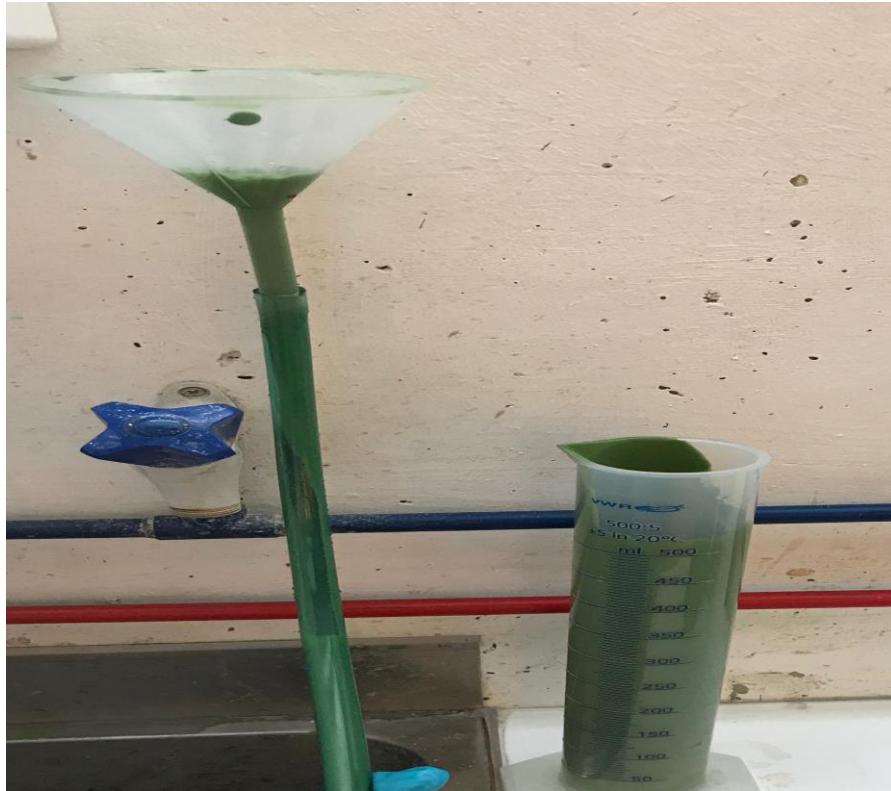
Figure C-5: illustrated the funnel connected to a hose when transferring the light fluid into the cylinder [66].

- The blackout curtain was then pulled down in order to protect the rig from disturbing light while the camera was taking photos during the experiment.
- The pipe was set on rotation. The rotation speed generally varied between 50 and 350 *rpm*.
- While rotating, the heavy fluid was transferred into the casing, using a mechanical pump with the capacity of 500 ml fluid and connected to a plastic hose (*figure C-6*).

Figure C-6: A mechanical pump used for pumping the heavy fluid down into the well

- A video clip of about 2 minutes was recorded, while pumping the heavy fluid down into the well (*placed on top of the light fluid*). This was very important to catch the first moments when the heavy fluid came into contact with the light fluid.

- Each experiment was run for a period of time, depending on the stability/instability of the interface between the fluids.

- If the interface was unstable, the experiments were usually run until a complete mixing occurred.

- However, if the interface was stable or the development of the mixing zone was slow, the experiments were run for about 45 to 60 min. There were usually run for 15-20 min after the mixing zone had been stabilized.

At the end of each experiment, the well was checked carefully for detecting eventual channelings outside the mixing zone. Thereby, the drilling muds were gathered in specific laboratory gallons for disposal. The instruments and equipment were washed with water in order to be ready for the next experiment.

Appendix D: Mathematical Calculation of the Height of The Mixing Zone

In addition to the visual and MATLAB analysis of the photos, the results of some experiments were checked in order to detect any hid channelings that could have extended alongside the pipe and reached outside the mixing zone. Occurring of such channelings was not possible to be detected by naked eye since the fluids were not transparent. Of this reason, four experiments from group 3 (*experiment 1 and 2*) and group 4 (*experiment 1 and 2*) from part IV (chapter 7.4) were selected for checking. Because of large $\Delta\rho$ between the heavy and the light fluid in these two groups *(0.60 and 0.70 sg respectively)*, they were considered as worse case scenario.

The procedure was performed as follows:

- Before pooling out the pipe out of the well, the non-contaminated heavy fluid from the top of the mixing zone was gathered for further analyze. By non-contaminated means the heavy fluid that didn't not content any traces from the light fluid.
- The volume and the density of this post-experimental fluid were measured and compared to the pre-experimental volume and density of the same fluid.

Figure 6 and 7 shows an example of how this procedure was performed. This example is taken from experiment 2/group 4 in Part IV, whose data are presented in table 6-11.

In this example the heavy fluid with the density of 1.80 sg (*14.95 ppg)* was used. As it is shown in figure D-2, the density of the heavy fluid at the end of the experiment is the same as the density of the fluid before starting the experiment. This means that the collected heavy fluid was pure and wasn't contaminated by the light fluid.

The volume of the pre-experimental heavy fluid was 470 ml. At the end of the experiment 340 ml (*figure D-1*) was collected. This means that about 130 ml of the heavy fluids had been mixed with light fluid in the mixing zone. Based on this volume the height of the mixing zone was calculated.

As shown in the figures, no any traces of the light fluid are seen on the surface of the cylinder or around the pipe where the heavy fluid was collected. This is another proof of absent of the hid channeling alongside the pipe.
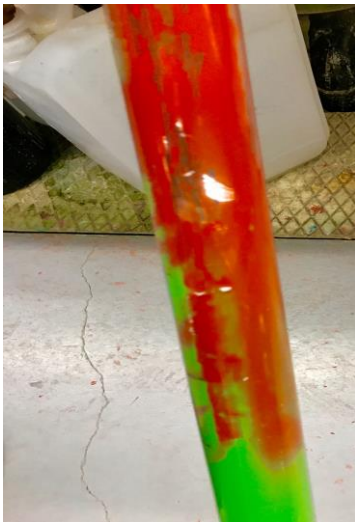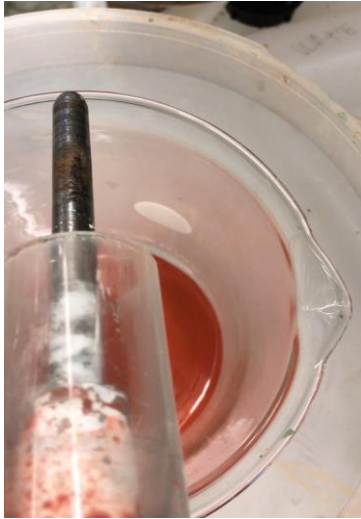
Figure D-1: Illustrates the procedure of collecting the non-contaminated heavy fluid at the end of the experiment [66].

Before

Before

After

After

Figure D-2: Measuring the density of the heavy fluid before and after the experiment [66].

Appendix E: Fluid Specifications and Rheological Analysis

In order to calculate the rheological characteristics such as gel strength and yield point of the muds, the measured data (MD) was analyzed using the rheological models as it is described in theory part.

In this Appendix, the rheological analyses of 12 experiments are shown. These experiments are the same experiments that were analyzed in chapter 7.4.

The measured data (MD) of the fluids are plotted in a graph in order to compare the Bingham plastic to Herschel Bulkley model. The plots indicate that the measured data at all the shear rates are suited best to Herschel Bulkley model, while the Bingham model fits only to the higher shear rate, i.e., at 300 and 600 *rpm*.

The plastic viscosity was calculated using equation 3.8 from the Bingham plastic model:

$$PV = \theta_{600} - \theta_{300}, \qquad [cP, mPa.s]$$

Low shear yield stress (LSYS) was calculated using equation 3.19 from Herschel Bulkley:

$$\theta_0 = (2 * \theta_3 - \theta_6)$$

To express the value of LSYS in [lb/100ft^2], the calculated value from the above equation has to be multiplied by the factor of 1.0678, which was neglected because the factor is insignificant. The low shear yield stress was reported as the yield point of the fluids (YP) in the tables presented chapter 6 and 7.

Rheological Analysis Group 1 (Δρ of 0.30 sg)

➢ Experiment 1:

Experiemnt 1 in Table 6-8		
Components	Light Fluid	Heavy Fluid
Water [g]	500	500
Xanthan [g]	0,5	0,5
Bentonite [g]	25	25
Mixing time [min]	5	5
Baryte [g]	49	273
Color [g]	10	15
Lignosulfonate [g]	0	0
Anti-foam [drops]	10	10
NaOH [ml]	0	0
Mxing time [min]	10	10
PH	8,5	8,4
Measured Data		
Shear rate [rpm]	Dial Readings (Light Fluid)	Dial Readings (Heavy Fluid)
600	42	78
300	35	61
200	32,5	55
100	28,5	47
60	25	44
30	23	40
6	11	30
3	10,5	29
Rheological & Physical properties		
Properties	Light Fluid	Heavy Fluid
Effective Viscsity [cP]	21	39
PV [cP]	7	17
Bingham YP [lb/100ft²]	28	44
LSYS (lb/100ft²)	10	28
Gel Strength at 10 sec [lb/100ft²]	14	34
Gel Strenght at 10 min [lb/100ft²]	27	50
Tetthet [ppg]	9,15	11,75
Tetthet [s.g.]	1,10	1,41
Wellbore geometry		
Well ID [cm]	3	
Pipe OD [cm]	2	
Experimental Results Overview		
Rotation speed [rpm]	50-350	
Rotation time [min]	45	
Height of Mixing Zone [cm]	3	

Measured Data [MD] [lb/100ft²]		
X	Y₁	Y₂
Shear rate [rpm]	Shear stress Light Fluid [lb/100ft²]	Shear stres Heavy Fluid [lb/100ft²]
600	44,85	83,29
300	37,37	65,14
200	34,70	58,73
100	30,43	50,19
60	26,70	46,98
30	24,56	42,71
6	11,75	32,03
3	11,21	30,97
Bigham Model		
X	Y₁	Y₂
Shear rate [rpm]	Shear stress Light Fluid [lb/100ft²]	Shear stress Heavy Fluid [lb/100ft²]
600	44,8476	83,2884
300	37,373	65,1358
0		

Herschel Bulkley Model		
Calculation	Light Fluid	Heavy Fluid
$\Phi_0 = 2 \cdot \Phi_{300} - \Phi_{600}$	10	28
Yield Stress for Φ_0 $(y_0) = 1{,}0678 \cdot \Phi_0$ [lb/100ft²]	10,678	29,8984
n (Φ_{600} and Φ_{300})	0,356	0,599
k (Φ_{600} and Φ_{300}) [lb/100ft².sⁿ]	2,900	0,840

Calculateed data for Herschel Bulkley Curve			
X		Y₁	Y₂
Shear rate [rpm]	Shear rate (Y) [S⁻¹]	Shear stress Light Fluid [lb/100ft²]	Shear stress Heavy Fluid [lb/100ft²]
600	1021,38	44,84	83,26
300	510,69	37,37	65,12
200	340,46	33,78	57,53
100	170,23	28,73	48,14
60	102,138	25,73	43,33
30	51,069	22,44	38,76
6	10,2138	17,31	33,28
3	5,1069	15,86	32,13
0	0	10,68	29,90

Figure E-1: Rheological analysis of experiment 1 presented in Table 6-8

> ## ➢ Experiment 4:

Experiment 4 in Table 6-8		
Components	Light Fluid	Heavy Fluid
Water [g]	500	500
Xanthan [g]	0,5	0,5
Bentonite [g]	25	25
Mixing time [min]	10	10
Baryte [g]	49	273
Color [g]	10	15
Lignosulfonate [g]	0,2	0,5
Anti-foam [drops]	10	10
NaOH [ml]	5	7,5
Mxing time [min]	10	10
PH	10,15	10,54
Measured Data		
Shear rate [rpm]	Dial Readings (Light Fluid)	Dial Readings (Heavy Fluid)
600	34	61
300	24	49
200	20	43
100	14	34
60	11	28
30	8,5	19
6	7	7,5
3	6,5	7
Rheological & Physical properties		
Properties	Light Fluid	Heavy Fluid
Effective Viscsity [cP]	17	30,5
PV [cP]	10	12
Bingham YP(lb/100ft²)	14	37
LSYS (lb/100ft²)	6	6,5
Gel Strength at 10 sec [lb/100ft²]	9	10
Gel Strenght at 10 min [lb/100ft²]	25	24
Tetthet [ppg]	9,2	11,7
Tetthet [s.g.]	1,10	1,40
Wellbore geometry		
Well ID [cm]	3,0	
Pipe OD [cm]	2,0	
Experimental Results Overview		
Rotation speed [rpm]	50-350	
Rotation time [min]	60	
Height of Mixing Zone [cm]	21	

Measured Data [MD] [lb/100ft²]		
X	Y_1	Y_2
Shear rate [rpm]	Shear stress Light Fluid [lb/100f²]	Shear stres Heavy Fluid [lb/100ft²]
600	36,31	65,14
300	25,63	52,32
200	21,36	45,92
100	14,95	36,31
60	11,75	29,90
30	9,08	20,29
6	7,47	8,01
3	6,94	7,47
Bigham Model		
X	Y_1	Y_2
Shear rate [rpm]	Shear stress Light Fluid [lb/100ft²]	Shear stres Heavy Fluid [lb/100ft²]
600	36,31	65,14
300	25,63	52,32
0		
Herschel Bulkley Model		
Calculation	Light Fluid	Heavy Fluid
$\Phi_0 =2*\Phi_{300} -\Phi_{600}$	6	6,5
Yield Stress for Φ_0 $(\gamma_o) =1,0678*\Phi_0,$ [lb/100ft²]	6,4068	6,9407
n (Φ_{600} and Φ_{300})	0,637	0,359
k (Φ_{600} and Φ_{300}) [lb/100ft².sⁿ]	0,362	4,849

Calculate data for Herschel Bulkley Curve			
X		Y_1	Y_2
Shear rate [rpm]	Shear rate (γ) [s^{-1}]	Shear stress Light Fluid [lb/100ft²]	Shear stress Heavy Fluid [lb/100f²]
600	1021,38	36,29	65,11
300	510,69	25,62	52,31
200	340,46	21,25	46,17
100	170,23	15,95	37,54
60	102,138	13,30	32,42
30	51,069	10,84	26,81
6	10,2138	8,00	18,10
3	5,1069	7,43	15,64
0	0	6,41	6,94

Figure E-2: Rheological analysis of experiment 4 presented in Table 6-8

Rheological Analysis Group 2 (Δρ of 0.50 sg)

➢ Experiment 1

Experiment 1 in Table 6-9		
Components	Light Fluid	Heavy Fluid
Water [g]	500	500
Xanthan [g]	0,5	0,5
Bentonite [g]	25	25
Mixing time [min]	5	5
Baryte [g]	49	451
Color [g]	10	15
Lignosulfonate [g]	0	0,1
Anti-foam [drops]	10	10
NaOH [ml]	0	5
Mxing time [min]	10	10
PH	8,7	10,3
Measured Data		
Shear rate [rpm]	Dial Readings (Light Fluid)	Dial Readings (Heavy Fluid)
600	40	79,5
300	32	62
200	29,5	55
100	24	48
60	22,5	44
30	20	37
6	15	33
3	13,5	32,5
Rheological & Physical properties		
Properties	Light Fluid	Heavy Fluid
Effective Viscsity [cP]	20	39,75
PV [cP]	8	17,5
Bingham YP(lb/100ft^2)	24	44,5
LSYS (lb/100ft^2)	12,0	32,0
Gel Strength at 10 sec [lb/100ft^2]	16,0	39,0
Gel Strenght at 10 min [lb/100ft^2]	35,0	54,0
Tetthet [ppg]	9,2	13,3
Tetthet [s.g.]	1,10	1,60
Wellbore geometry		
Well ID [cm]	3	
Pipe OD [cm]	2	
Experimental Results Overview		
Rotation speed [rpm]	50-300	
Rotation time [min]	45	
Height of Mixing Zone [cm]	6	

Measured Data [MD] [lb/100ft^2]		
X	Y$_1$	Y$_2$
Shear rate [rpm]	Shear stress Light Fluid [lb/100ft^{t2}]	Shear stres Heavy Fluid [lb/100ft^2]
600	42,71	84,89
300	34,17	66,20
200	31,50	58,73
100	25,63	51,25
60	24,03	46,98
30	21,36	39,51
6	16,02	35,24
3	14,42	34,70
Bigham Model		
X	Y$_1$	Y$_2$
Shear rate [rpm]	Shear stress Light Fluid [lb/100ft^2]	Shear stres Heavy Fluid [lb/100ft^2]
600	42,71	84,89
300	34,17	66,20
0		
Herschel Bulkley Model		
Calculation	Light Fluid	Heavy Fluid
$\Phi_0 = 2 * \Phi_{300} - \Phi_{600}$	12	32
Yield Stress for Φ_0 $(y_0) = 1,0678 * \Phi_0$, [lb/100ft^2]	12,8136	34,1696
n (Φ_{600} and Φ_{300})	0,485	0,663
k (Φ_{600} and Φ_{300}) [lb/100ft^2.s^n]	1,036	0,514
Calculate data for Herschel Bulkley Curve		
X		Y$_1$	Y$_2$
Shear rate [rpm]	Shear rate (Y) [S^{-1}]	Shear stress Light Fluid [lb/100ft^2]	Shear stress Heavy Fluid [lb/100ft^2]
600	1021,38	42,70	84,86
300	510,69	34,16	66,19
200	340,46	30,35	58,65
100	170,23	25,34	49,63
60	102,138	22,59	45,19
30	51,069	19,80	41,13
6	10,2138	16,01	36,57
3	5,1069	15,10	35,68
0	0	12,81	34,17

Figure-3
BH.- Vs HB.- Model
Experiment 1
Table-6-9

Legend:
- Bingham-Light F.
- Bingham-Heavy F.
- MD-Light F.
- MD-Heavy F.
- Herschel B.- Light F.
- Herschel B.- Heavy F.
- Linear (Bingham-Light F.)
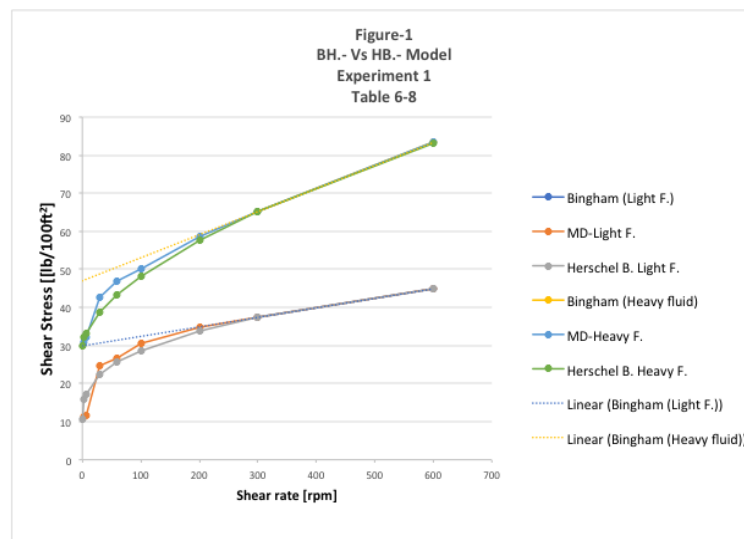- Linear (Bingham-Heavy F.)
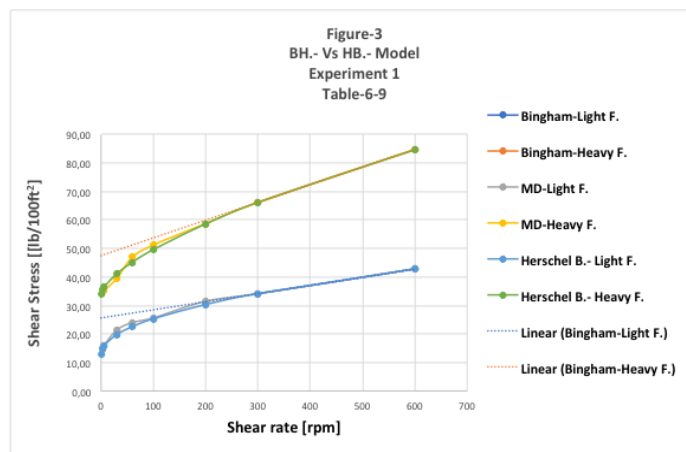
Figure E-3: Rheological analysis of experiment 1 presented in table 6-9

➢ Experiment 4

Experiment 4 in Table 6-9

Components	Light Fluid	Heavy Fluid
Water [g]	500	500
Xanthan [g]	0,5	0,5
Bentonite [g]	25	25
Mixing time [min]	5	5
Baryte [g]	49	451
Color [g]	10	15
Lignosulfonate [g]	0,1	1,5
Anti-foam [drops]	10	15
NaOH [ml]	5	10
Mxing time [min]	10	10
PH	10,1	10,85

Measured Data

Shear rate [rpm]	Dial Readings (Light Fluid)	Dial Readings (Heavy Fluid)
600	34	52
300	25,5	41
200	21	34
100	16	27
60	13	21
30	10	16
6	7	11
3	6,5	9

Rheological & Physical properties

Properties	Light Fluid	Heavy Fluid
Effective Viscsity [cP]	17	26
PV [cP]	8,5	11
Bingham YP(lb/100ft^2)	17	30
LSYS (lb/100ft^2)	6	7
Gel Strength at 10 sec [lb/100ft^2]	10	9
Gel Strenght at 10 min [lb/100ft^2]	19	16
Tetthet [ppg]	9,25	13,25
Tetthet [s.g.]	1,1	1,6

Wellbore geometry

Well ID [cm]	3
Pipe OD [cm]	2

Experimental Results Overview

Rotation speed [rpm]	50-350
Rotation time [min]	40
Height of Mixing Zone [cm]	70

Measured Data [MD] [lb/100ft^2]

X	Y$_1$	Y$_2$
Shear rate [rpm]	Shear stress Light Fluid [lb/100f^{t2}]	Shear stres Heavy Fluid [lb/100ft^2]
600	36,31	55,53
300	27,23	43,78
200	22,42	36,31
100	17,08	28,83
60	13,88	22,42
30	10,68	17,08
6	7,47	11,75
3	6,94	9,61

Bigham Model

X	Y$_1$	Y$_2$
Shear rate [rpm]	Shear stress Light Fluid [lb/100ft^2]	Shear stres Heavy Fluid [lb/100ft^2]
600	36,31	55,53
300	27,23	43,78
0		

Herschel Bulkley Model

Calculation	Light Fluid	Heavy Fluid
Φ_0 =2* Φ_{300} -Φ_{600}	6	7
Yield Stress for Φ_0 (y_0) =1,0678* Φ_0 [lb/100ft^2]	6,4068	7,4746
n (Φ_{600} and Φ_{300})	0,522	0,404
k (Φ_{600} and Φ_{300}) [lb/100ft^2.s^n]	0,805	2,920

Calculate data for Herschel Bulkley Curve

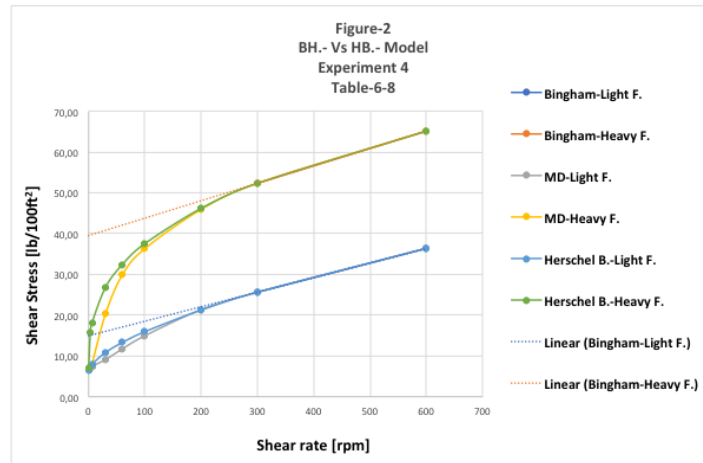| X		Y$_1$	Y$_2$
Shear rate [rpm]	Shear rate (Y) [S^{-1}]	Shear stress Light Fluid [lb/100ft^2]	Shear stress Heavy Fluid [lb/100f^{t2}]
600	1021,38	36,29	55,51
300	510,69	27,22	43,77
200	340,46	23,25	38,28
100	170,23	18,14	30,76
60	102,138	15,40	26,41
30	51,069	12,67	21,79
6	10,2138	9,11	14,94
3	5,1069	8,29	13,12
0	0	6,41	7,47

Figure-4
BH.- Vs HB.- Model
Experiment 4
Table-6-9

Figure E-4: Rheological analysis of experiment 4 presented in Table 6-9

Rheological Analysis Group 3 (Δρ of 0.60 sg)

➤ Experiment 1

Experiment 1 in Table 6-10		
Components	Light Fluid	Heavy Fluid
Water [g]	500	500
Xanthan [g]	0,5	0,5
Bentonite [g]	25	25
Mixing time [min]	5	5
Baryte [g]	49	551
Color [g]	10	15
Lignosulfonate [g]	0	0,15
Anti-foam [drops]	10	15
NaOH [ml]	0	7,5
Mxing time [min]	10	10
PH	8,5	10,02
Measured Data		
Shear rate [rpm]	Dial Readings (Light Fluid)	Dial Readings (Heavy Fluid)
600	43	87
300	35	71
200	30	63
100	26	56
60	21	48
30	17	41
6	13	35
3	12,5	34
Rheological & Physical properties		
Properties	Light Fluid	Heavy Fluid
Effective Viscsity [cP]	21,5	43,5
PV [cP]	8	16
Bingham YP(lb/100ft^2)	27	55
LSYS (lb/100ft^2)	12	33
Gel Strength at 10 sec [lb/100ft^2]	16	35
Gel Strenght at 10 min [lb/100ft^2]	29	62
Tetthet [ppg]	9,15	14,3
Tetthet [s.g.]	1,1	1,7
Wellbore geometry		
Well ID [cm]	3	
Pipe OD [cm]	2	
Experimental Results Overview		
Rotation speed [rpm]	50-350	
Rotation time [min]	45	
Height of Mixing Zone [cm]	10	

Measured Data [MD] [lb/100ft^2]		
X	Y$_1$	Y$_2$
Shear rate [rpm]	Shear stress Light Fluid [lb/100f^{t2}]	Shear stres Heavy Fluid [lb/100ft^2]
600	45,92	92,90
300	37,37	75,81
200	32,03	67,27
100	27,76	59,80
60	22,42	51,25
30	18,15	43,78
6	13,88	37,37
3	13,35	36,31
Bigham Model		
X	Y$_1$	Y$_2$
Shear rate [rpm]	Shear stress Light Fluid [lb/100ft^2]	Shear stres Heavy Fluid [lb/100ft^2]
600	45,92	92,90
300	37,37	75,81
0		
Herschel Bulkley Model		
Calculation	Light Fluid	Heavy Fluid
$\Phi_0 = 2 * \Phi_{300} - \Phi_{600}$	12	33
Yield Stress for Φ_0 $(y_0) = 1,0678 * \Phi_0$ [lb/100ft^2]	12,8136	35,2374
n (Φ_{600} and Φ_{300})	0,430	0,507
k (Φ_{600} and Φ_{300}) [lb/100ft^2.s^n]	1,677	1,722
Calculate data for Herschel Bulkley Curve		

X		Y$_1$	Y$_2$
Shear rate [rpm]	Shear rate (Y) [S^{-1}]	Shear stress Light Fluid [lb/100ft^2]	Shear stress Heavy Fluid [lb/100f^{t2}]
600	1021,38	45,90	92,87
300	510,69	37,37	75,80
200	340,46	33,43	68,27
100	170,23	28,12	58,49
60	102,138	25,10	53,18
30	51,069	21,93	47,87
6	10,2138	17,37	40,83
3	5,1069	16,20	39,17
0	0	12,81	35,24

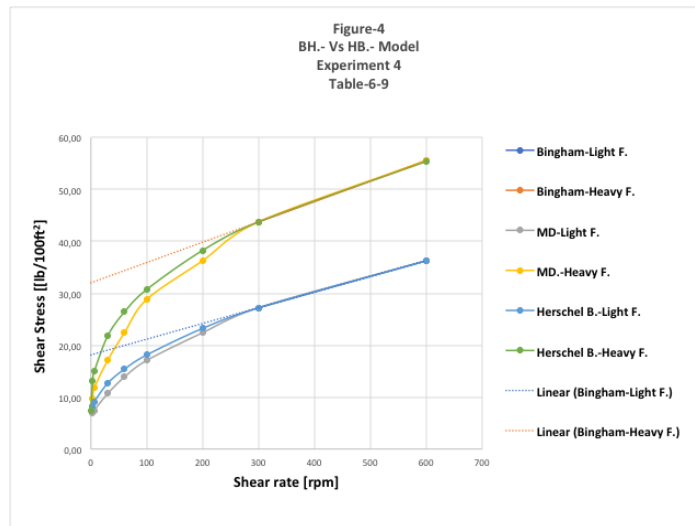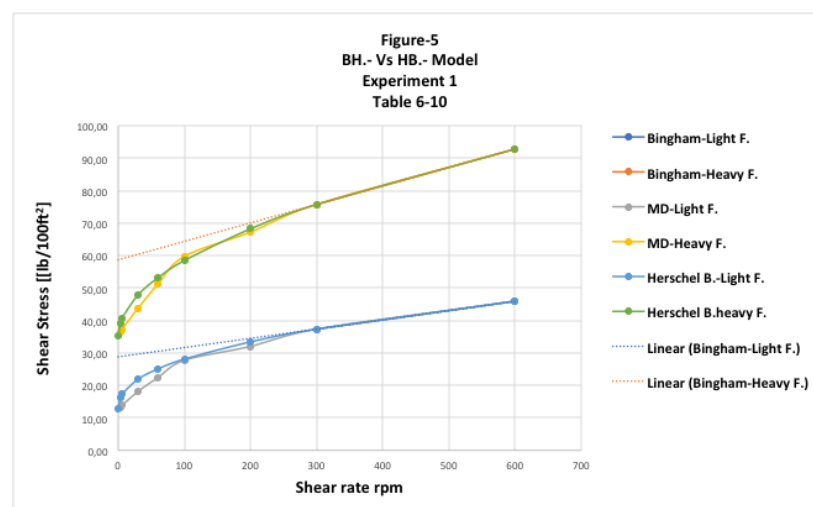Figure E-5: Rheological analysis of experiment 1 presented in Table 6-10

➢ Experiment 2

Experiment 2 in Table 6-10		
Components	Light Fluid	Heavy Fluid
Water [g]	500	500
Xanthan [g]	0,5	0,5
Bentonite [g]	25	25
Mixing time [min]	5	5
Baryte [g]	49	551
Color [g]	10	15
Lignosulfonate [g]	0	0,7
Anti-foam [drops]	10	15
NaOH [ml]	0	10
Mxing time [min]	10	10
PH	8,5	10,12
Measured Data		
Shear rate [rpm]	Dial Readings (Light Fluid)	Dial Readings (Heavy Fluid)
600	43	67
300	35	49
200	30	41
100	26	31
60	21	25
30	17	22
6	13	16
3	12,5	15
Rheological & Physical properties		
Properties	Light Fluid	Heavy Fluid
Effective Viscsity [cP]	21,5	33,5
PV [cP]	8	18
Bingham YP(lb/100ft^2)	12	14
LSYS (lb/100ft^2)	12	14
Gel Strength at 10 sec [lb/100ft^2]	16	17
Gel Strenght at 10 min [lb/100ft^2]	29	32
Tetthet [ppg]	9,15	14,3
Tetthet [s.g.]	1,1	1,72
Wellbore geometry		
Well ID [cm]	3	
Pipe OD [cm]	2	
Experimental Results Overview		
Rotation speed [rpm]	50-350	
Rotation time [min]	60	
Height of Mixing Zone [cm]	18	

Measured Data [MD] [lb/100ft^2]		
X	Y_1	Y_2
Shear rate [rpm]	Shear stress Light Fluid [lb/100f^{12}]	Shear stres Heavy Fluid [lb/100ft^2]
600	45,92	71,54
300	37,37	52,32
200	32,03	43,78
100	27,76	33,10
60	22,42	26,70
30	18,15	23,49
6	13,88	17,08
3	13,35	16,02
Bigham Model		
X	Y_1	Y_2
Shear rate [rpm]	Shear stress Light Fluid [lb/100ft^2]	Shear stres Heavy Fluid [lb/100ft^2]
600	45,92	71,54
300	37,37	52,32
0		
Herschel Bulkley Model		
Calculation	Light Fluid	Heavy Fluid
$\Phi_0 = 2* \Phi_{300} - \Phi_{600}$	12	14
Yield Stress for Φ_0 $(y_0) = 1,0678* \Phi_{0,}$ [lb/100ft^2]	12,8136	14,9492
n (Φ_{600} and Φ_{300})	0,430	0,598
k (Φ_{600} and Φ_{300}) [lb/100ft^2.s^n]	1,677	0,896

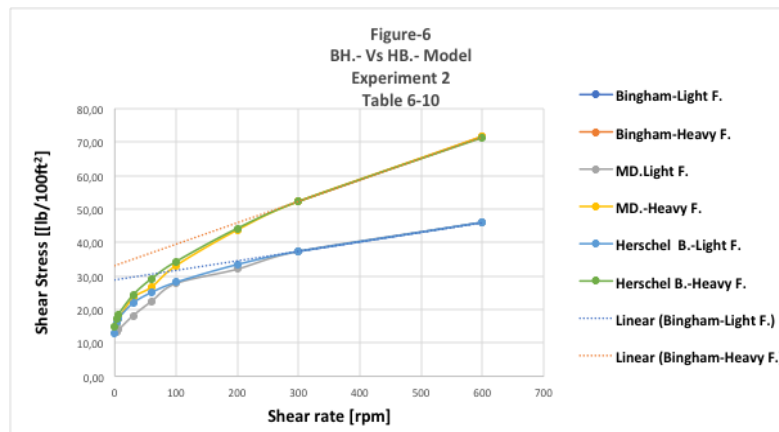| Calculate data for Herschel Bulkley Curve			
X		Y_1	Y_2
Shear rate [rpm]	Shear rate (Y) [S^{-1}]	Shear stress Light Fluid [lb/100ft^2]	Shear stress Heavy Fluid [lb/100f^{12}]
600	1021,38	45,90	71,51
300	510,69	37,37	52,31
200	340,46	33,43	44,26
100	170,23	28,12	34,31
60	102,138	25,10	29,21
30	51,069	21,93	24,37
6	10,2138	17,37	18,55
3	5,1069	16,20	17,33
0	0	12,81	14,95

Figure E-6: Rheological analysis of experiment 2 presented in Table 6-10

Rheological Analysis Group 4 (Δρ of 0.70 sg)

➢ Experiment 1

Experiment 1 in Table 6-11		
Components	Light Fluid	Heavy Fluid
Water [g]	500	500
Xanthan [g]	0,5	0,5
Bentonite [g]	25	25
Mixing time [min]	5	5
Baryte [g]	49	660
Color [g]	10	15
Lignosulfonate [g]	0	0,3
Anti-foam [drops]	10	15
NaOH [ml]	0	7,5
Mxing time [min]	10	10
PH	8,64	10,05
Measured Data		
Shear rate [rpm]	Dial Readings (Light Fluid)	Dial Readings (Heavy Fluid)
600	47,5	83
300	39	67
200	35,5	59
100	28	51
60	23,5	45
30	19	39
6	12	33
3	11	32
Rheological & Physical properties		
Properties	Light Fluid	Heavy Fluid
Effective Viscsity [cP]	23,75	41,5
PV [cP]	8,5	16
Bingham YP(lb/100ft^2)	30,5	51
LSYS (lb/100ft^2)	10,0	31,0
Gel Strength at 10 sec [lb/100ft^2]	14	36
Gel Strenght at 10 min [lb/100ft^2]	26	57
Tetthet [ppg]	9,2	15,1
Tetthet [s.g.]	1,1	1,81
Wellbore geometry		
Well ID [cm]	3	
Pipe OD [cm]	2	
Experimental Results Overview		
Rotation speed [rpm]	50-35	
Rotation time [min]	60	
Height of Mixing Zone [cm]	18	

Measured Data [MD] [lb/100ft^2]		
X	Y$_1$	Y$_2$
Shear rate [rpm]	Shear stress Light Fluid [lb/100ft^2]	Shear stres Heavy Fluid [lb/100ft^2]
600	50,72	88,63
300	41,64	71,54
200	37,91	63,00
100	29,90	54,46
60	25,09	48,05
30	20,29	41,64
6	12,81	35,24
3	11,75	34,17
Bigham Model		
X	Y$_1$	Y$_2$
Shear rate [rpm]	Shear stress Light Fluid [lb/100ft^2]	Shear stres Heavy Fluid [lb/100ft^2]
600	50,72	88,63
300	41,64	71,54
0		
Herschel Bulkley Model		
Calculation	Light Fluid	Heavy Fluid
$\Phi_0 = 2 \cdot \Phi_{300} - \Phi_{600}$	10	31
Yield Stress for Φ_0 (γ_0) =1,0678* Φ_0, [lb/100ft^2]	10,678	33,1018
n (Φ_{600} and Φ_{300})	0,371	0,530
k (Φ_{600} and Φ_{300}) [lb/100ft^2.s^n]	3,070	1,409
Calculate data for Herschel Bulkley Curve			
X		Y$_1$	Y$_2$
Shear rate [rpm]	Shear rate (Y) [S^{-1}]	Shear stress Light Fluid [lb/100ft^2]	Shear stress Heavy Fluid [lb/100f^2]
600	1021,38	50,71	88,60
300	510,69	41,64	71,53
200	340,46	37,32	64,10
100	170,23	31,28	54,56
60	102,138	27,73	49,47
30	51,069	23,87	44,44
6	10,2138	17,94	37,93
3	5,1069	16,30	36,45
0	0	10,68	33,10
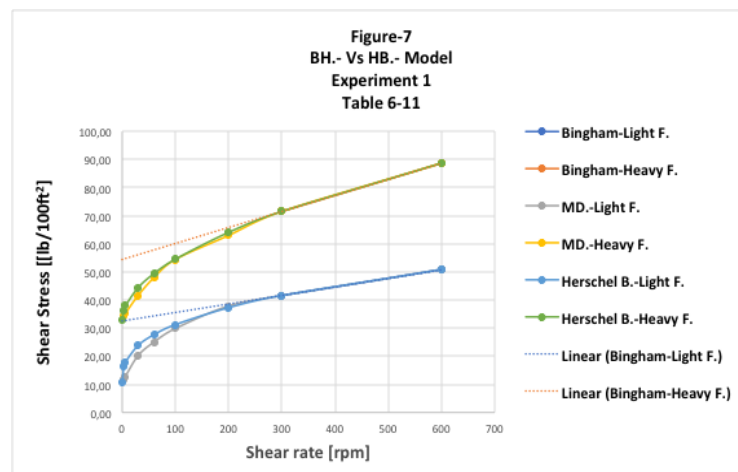
Figure E-7: Rheological analysis of experiment 1 presented in Table 6-11

➢ Experiment 2

Experiment 2 in Table 6-11		
Components	Light Fluid	Heavy Fluid
Water [g]	500	500
Xanthan [g]	0,5	0,5
Bentonite [g]	25	25
Mixing time [min]	5	5
Baryte [g]	49	660
Color [g]	10	15
Lignosulfonate [g]	0,1	1,1
Anti-foam [drops]	10	15
NaOH [ml]	4	8,5
Mxing time [min]	10	10
PH	10,04	10,34
Measured Data		
Shear rate [rpm]	Dial Readings (Light Fluid)	Dial Readings (Heavy Fluid)
600	47,5	87
300	39	69
200	35,5	58
100	28	47
60	23,5	39
30	19	31
6	12	14
3	11	13
Rheological & Physical properties		
Properties	Light Fluid	Heavy Fluid
Effective Viscsity [cP]	23,75	43,5
PV [cP]	8,5	18
Bingham YP (lb/100ft^2)	30,5	51
LSYS (lb/100ft^2)	10	12
Gel Strength at 10 sec [lb/100ft^2]	14	13
Gel Strenght at 10 min [lb/100ft^2]	26	32
Tetthet [ppg]	9,2	14,95
Tetthet [s.g.]	1,1	1,8
Wellbore geometry		
Well ID [cm]	3	
Pipe OD [cm]	2	
Experimental Results Overview		
Rotation speed [rpm]	50-350	
Rotation time [min]	50	
Height of Mixing Zone [cm]	28	

Measured Data [MD] [lb/100ft^2]		
X	Y$_1$	Y$_2$
Shear rate [rpm]	Shear stress Light Fluid [lb/100f^{t2}]	Shear stres Heavy Fluid [lb/100ft^2]
600	50,72	92,90
300	41,64	73,68
200	37,91	61,93
100	29,90	50,19
60	25,09	41,64
30	20,29	33,10
6	12,81	14,95
3	11,75	13,88
Bigham Model		
X	Y$_1$	Y$_2$
Shear rate [rpm]	Shear stress Light Fluid [lb/100ft^2]	Shear stres Heavy Fluid [lb/100ft^2]
600	50,72	92,90
300	41,64	73,68
0		
Herschel Bulkley Model		
Calculation	Light Fluid	Heavy Fluid
$\Phi_0 = 2* \Phi_{300} - \Phi_{600}$	10	12
Yield Stress for Φ_0 (y_0) =1,0678* Φ_0, [lb/100ft^2]	10,678	12,8136
n (Φ_{600} and Φ_{300})	0,371	0,396
k (Φ_{600} and Φ_{300}) [lb/100ft^2.s^n]	3,070	5,160

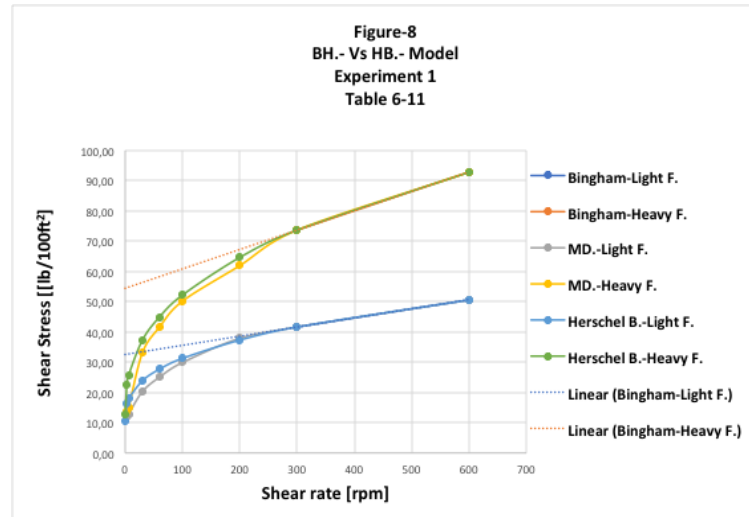| Calculate data for Herschel Bulkley Curve			
X		Y$_1$	Y$_2$
Shear rate [rpm]	Shear rate (ϒ) [S^{-1}]	Shear stress Light Fluid [lb/100ft^2]	Shear stress Heavy Fluid [lb/100ft^2]
600	1021,38	50,71	92,87
300	510,69	41,64	73,66
200	340,46	37,32	64,64
100	170,23	31,28	52,21
60	102,138	27,73	45,00
30	51,069	23,87	37,28
6	10,2138	17,94	25,75
3	5,1069	16,30	22,65
0	0	10,68	12,81

➢

Figure E-8: Rheological analysis of experiment 2 presented in Table 6-11

Appendix F: MATLAB Code For Image Analysis

```matlab
%% Image analysis for Heavy over Light
clear all
clf
clc
file_name = ('DSC01436.JPG')
%  Read image "filename" with format = height x width x color:
<352x1024x3 uint8>
Bilde=imread(x40Min);


%% ************* Original image  ***************************
figure(1)
image(Bilde)
title('Original image in color')



%% ************* Original image converted to gray
********************
%  *****************     figure(2)
******************************
%
*****************************************************************
******



figure(2)
% "Graybilde" er bedre Â bruke enn de splittede ss variantene
for Â se
% detaljer.
Graybilde = rgb2gray(Bilde);


subplot(2,1,1)
hold off
imshow(Graybilde) %Seems to be necessary to enable the hi-res
```

135

```matlab
gray scale
image(Graybilde)
hold on
title('Image with pathlines along pipe and along meter stick')


skyv =[0 180 -180];
nl=3
for il=1:nl
    Lx1=1588-skyv(il);Lx2=1600-skyv(il);Ly1=1;Ly2=5016;
    for i=Ly1:Ly2
        Gadry(il,i)=i; j=round((Lx2-Lx1)*i/(Ly2-Ly1)+Lx1);
        Gadrx(il,i)=j; Gfarge(il,i)= Graybilde(i,j);
    end
end
% Plot inclined lines as paths for pixel intensity
plot(Gadrx(1,:),Gadry(1,:),'-b')
plot(Gadrx(2,:),Gadry(2,:),'-r')
plot(Gadrx(3,:),Gadry(3,:),'-k')



% Plot inclined line along meter stick scale to see cm ticks
Lx1=652;Lx2=980; Ly1=1;Ly2=5016;
    for i=Ly1:Ly2
Ladry(i)=i; j=round((Lx2-Lx1)*i/(Ly2-Ly1)+Lx1);
Ladrx(i)=j; Lfarge(i)= Graybilde(i,j);
plot(Ladrx,Ladry,'-g')
    end


% Plot pixel color intensity along inclined vertical lines
subplot(2,1,2)
hold on
title('Pixel intensities along paths')
plot(Gadry(1,:),Gfarge(1,:),'-b')
```

```matlab
plot(Gadry(2,:),Gfarge(2,:),'-r')
plot(Gadry(3,:),Gfarge(3,:),'-k')

% Plot pixel color intensity along inclined vertical line in
meter stick
plot(Ladry,Lfarge/2+200,'-g')
ylabel('Pixel intensity')
hold off

%% Split imported image into r g and b components and plot
% ***************  figure(3)  ***************************
% ****************************************************

figure(3)
sr = Bilde(:,:,1); % red
sg = Bilde(:,:,2); % green
sb = Bilde(:,:,3); % blue
sall=(sr+sg+sb)/3;

% traditional RGB composition from R, G and B
% sall = 0.2290*sr + 0.5870*sg + 0.1140*sb;


subplot(1,4,1)
colormap autumn
image(sr) %******** red component
%colormap autumn
title('Red')

subplot(1,4,2)
image(sg) %******** green component
colormap summer
title('Green')
```

```matlab
subplot(1,4,3)
image(sb) %******** blue component
colormap winter
title('Blue')


subplot(1,4,4)
%image(sall)
%colormap gray
imshow(Graybilde)
image(Graybilde)
title('Image in grayscale')



%% ********** Scale markers on meter stick **************
%  **********  Figure(4) **************
Lx1=652
Lx2=980
linjalx = [Lx1 Lx2]
Ly1=1
Ly2=5016
linjaly = [Ly1 Ly2]

figure(35)
imshow(Graybilde)
image(sr) %******** red component
%colormap autumn

figure(4)
subplot(2,2,1)
% image(sall)
% colormap bone
%imshow(Graybilde)
image(Graybilde)
hold on
```

```matlab
title('Image with pathline along meter stick')


line(linjalx,linjaly,'Color','k')
tell80=0
for i=Ly1:Ly2
    adry(i)=i;
    j=round((Lx2-Lx1)*i/(Ly2-Ly1)+Lx1);
    adrx(i)=j;
    farge(i)=(sall(i,j)+ sall(i,j-1)+sall(i,j+1))/3;
    indeksf(i)=0;
    indeksf80(i)=0;
    if farge(i)<85
        indeksf(i)=1;
    end
    if farge(i)<80
        tell80=tell80+1;
        indeksf80(i)=2;
    end

end

subplot(2,2,2)
plot(adry,farge)
title('Markers on scale along pathline in image')

subplot(2,2,4) % indexed ticks for cm and mm
%plot(adry,indeksf)
stem(adry,indeksf)
hold on
%plot(adry,indeksf80,'r')
stem(adry,indeksf80,'r')
xmin=Ly1; xmax=Ly2; ymin=0; ymax=4;
axis([xmin xmax ymin ymax])
```

```matlab
ip(1)=1
tell802=1
for i=Ly1:Ly2
    if farge(i)<80
        tell802=tell802+1;
        ip(tell802)=i;
        adryp(tell802)= i-ip(tell802-1);
    end
end
title('"Normalized height" cm and mm ticks ')

subplot(2,2,3)
plot(ip,adryp,'*')
title('Distance between cm markers on scale')
xlabel('Pixel nr')
ylabel('Distance in pixels between clear markers')
hold on
k=0.57
for i=Ly1:Ly2
    Pix(i)=i;
    Fitdist(i)=145 - ((i-1)/3000)^k*60  ;
end
plot(Pix,Fitdist,'-r')
xmin=Ly1; xmax=Ly2; ymin=80; ymax=140;
axis([xmin xmax ymin ymax])
```